The potential benefits of combined heat and power based district energy grids

by

Jean Duquette

B.Eng., McMaster University, 2000

M.Eng., McMaster University, 2003

M.Sc., Zaragoza University, 2008

A Dissertation Submitted in Partial Fulfillment

of the Requirements for the Degree of

DOCTOR OF PHILOSOPHY

in the Department of Mechanical Engineering

University of Victoria

The potential benefits of combined heat and power based district energy grids

by

Jean Duquette

B.Eng., McMaster University, 2000

M.Eng., McMaster University, 2003

M.Sc., Zaragoza University, 2008

Supervisory Committee

Dr. Peter Wild, (Department of Mechanical Engineering)

Co-Supervisor

Dr. Andrew Rowe, (Department of Mechanical Engineering)

Co-Supervisor

Dr. Ned Djilali, (Department of Mechanical Engineering)

Departmental Member

Dr. Pan Agathoklis, (Department of Electrical and Computer Engineering)

Outside Member

Abstract

In this dissertation, an assessment is conducted of the potential benefits of combined heat and power (CHP) based district energy (DE) grids in energy systems of different scale having significant fossil fuel fired electrical generation capacity. Three studies are included in the research.

In the first study, the potential benefits of expanding CHP-based DE grids in a large scale energy system are investigated. The impacts of expanding wind power systems are also investigated and a comparison between these technologies is made with respect to fossil fuel utilization and CO_2 emissions. A model is constructed and five scenarios are evaluated with the EnergyPLAN software taking the province of Ontario, Canada as the case study. Results show that reductions in fuel utilization and CO_2 emissions of up to 8.5% and 32%, respectively, are possible when switching to an energy system comprising widespread CHP-based DE grids.

In the second study, a high temporal resolution numerical model (*i.e.* the SS-VTD model) is developed that is capable of rapidly calculating distribution losses in small scale variable flow DE grids with low error and computational intensity. The SS-VTD model is validated by comparing simulated temperature data with measured temperature data from an existing network. The Saanich DE grid, located near Victoria, Canada, is used as the case study for validation.

In the third study, the potential benefits of integrating high penetrations of renewable energy via a power-to-heat plant in a small scale CHP-based DE grid are investigated. The impacts of switching to a CHP-based DE grid equipped with an electric boiler plant versus a conventional wave power system are compared with respect to fossil fuel utilization and CO_2 emissions. The SS-VTD model is used to conduct the study. The energy system of the Hot Springs Cove community, located on the west coast of Vancouver Island, Canada is used as the case study in the analysis. Results show that relative to the conventional wave power system, reductions in fuel utilization and CO_2 emissions of up to 47% are possible when switching to a CHP-based DE grid.

Table of Contents

List of Tables

List of Figures

Acknowledgments

I would like to thank my supervisors, Dr. Peter Wild and Dr. Andrew Rowe, for their guidance and financial support throughout this academic journey. Their seemingly endless journal article revisions have helped make me a better writer in the end.

I would also like to thank my wife Yanira for her ongoing encouragement, positive spirit, and love that knows no limits.

Finally, I would like to thank my kids, Aydan and Yuna (who came into this world while this thesis was underway), for keeping me in the present moment and teaching me what truly matters in life.

Dedication

To my father whose philosophy, vision, work ethic, and determination have inspired me to take this leap into the unknown.

Chapter 1:

Introduction

A district energy (DE) grid is a centralized energy management system built around a network of buried pipes that permits the distribution of thermal energy from sources to loads. Common DE loads include space heating and cooling, and domestic hot water heating in residential, commercial, and industrial buildings. DE grids are able to make use of a multitude of energy sources, both fossil fuel and renewable based, such as natural gas, oil, coal, solar, geothermal, biomass, and waste/surplus heat. A schematic configuration of a DE grid comprising multiple sources, energy conversion components, and loads is shown in Figure 1. As shown in Figure 1, typical energy conversion components include boilers, chillers, heat pumps, and heat exchangers for providing heating and cooling services; combined heat and power (CHP) units for supplying both heat and power simultaneously [1], and cooling towers for dumping excess heat to the environment. Depending on location, thermal storage infrastructure may also be added to increase overall efficiency [2]. The arrows shown in Figure 1 depict the various energy types (*e.g.* chemical, electrical, thermal) and energy pathways that are present in the system.

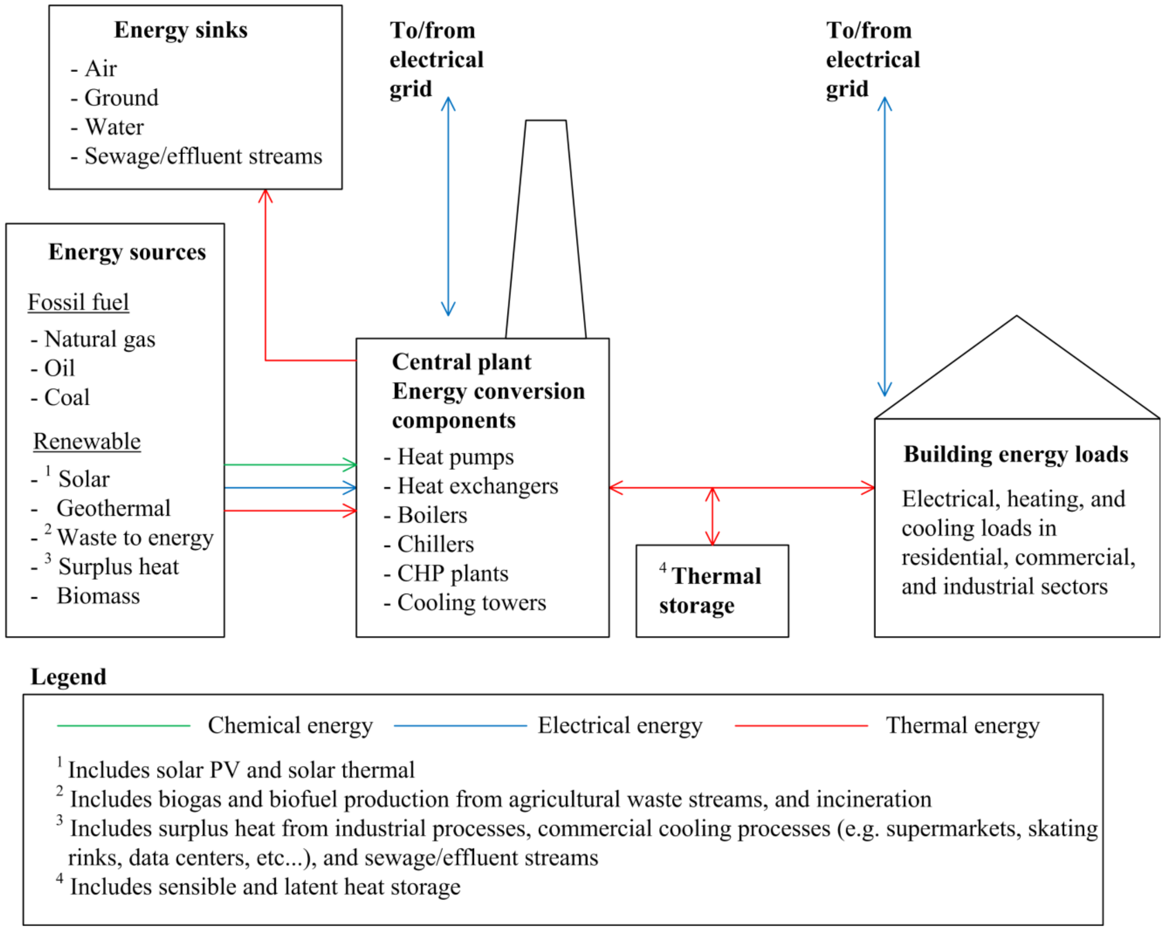

Figure 1: Energy sources, sinks, building loads, and central plant energy conversion components typically found in a DE grid. Arrows show type and direction of energy flows in the system

The main benefits [3] associated with DE grids include:

1. High energy efficiencies are achieved as loads are aggregated and managed simultaneously at a centralized energy plant [4]
2. Decreased fossil fuel utilization
3. Decreased emissions
4. Increased penetration of variable generation sources

5. Increased integration of waste and surplus energy streams
6. Increased system flexibility
7. Reduced energy costs
8. Increased security of energy supply
9. Reduced reliance on large-scale conventional generation and transmission infrastructure.

This dissertation focuses on the first five benefits mentioned above.

1.1 Overview of district energy grid modeling studies

Numerical modeling studies are commonly used to provide insight into DE grid operational performance when one or several system parameters or environmental conditions are varied. Results from these studies can be used for optimally sizing components as well as selecting optimal system control strategies without the risks or costs of conducting tests on a real system [5]. A number of modeling studies found in the literature focus on the following research topics: large-scale expansion of CHP-based district energy grids; renewable energy integration via power-to-heat plants in district energy grids; and heat losses in district energy grids. A review of the literature surrounding each of these topics is provided in the following sections.

1.1.1 Large-scale expansion of CHP-based district energy grids

A number of modeling studies have been conducted to examine the impacts of expanding CHP-based DE grids on a large scale. Danestig et al. [6] incorporate Stockholm's DE network into a broader national scale model which was used to study the potential for CHP capacity growth in the city. This study showed that when CHP plants with high electricity to heat ratios are used, up to 15% of Sweden's total electricity load can be met by CHP resulting in CO_2 emission reductions of up to 5 million tons per year. Lund et al. [7] modelled the Lithuanian national energy system for a scenario in which one of its largest nuclear power plants is decommissioned. To replace the missing generation capacity, they proposed replacing all boilers in the existing district heating systems with CHP plants. Simulation results show that compared to using new thermal power stations, this strategy would lower both fossil fuel consumption and CO_2 emissions by up to 70%. Munster et al. [8] developed a model of the Danish energy system and showed that CHP and district heating can contribute to the sustainability and security of supply of future energy systems and that it is cost effective to increase the district heating share up to 57% of the total national heat demand. Chen et al. [9] constructed a model of the Danish energy system for a scenario in which CHP-based DE power plants are fitted with high efficiency thermoelectric generators. They showed that by integrating thermoelectric technology in the current CHP fleet, reductions in fossil fuel consumption and CO_2 emissions of up to 1.08 PJ/year and 0.08 Mt/year, respectively, can be achieved. Lund and Mathiesen [10] modeled a hypothetical "100% renewable energy" configuration of the Danish energy system to compare the impacts of increasing the generation capacity of three separate biomass powered CHP technologies (i.e. combined cycle gas turbine, circulating fluidized bed, and advanced pulverized fuel technologies) on the annual fuel consumption and cost. They showed that combined cycle gas turbine CHP plants are preferable with regards to both fuel consumption and cost and recommend their implementation in large-scale CHP-based DE grids.

As described above, the majority of studies found in the literature focus on the benefits of expanding CHP-based DE grids in an energy system with regards to decreased fossil fuel consumption and/or decreased CO_2 emissions. No studies have been identified that compare these benefits with those from large-scale wind power systems.

1.1.2 Renewable energy integration via power-to-heat plants in district energy grids

Model-based studies have investigated the impacts of power-to-heat technologies, such as electric boilers, in DE grids for integrating high levels of variable renewable generation. Blarke [11] compared electric boilers and heat pumps for balancing excess wind generation in the Danish energy system for the years 2003 to 2010. Heat and power generation from existing CHP plants and wind energy penetrations were fixed in his analysis, as was the total thermal storage capacity. This study showed that both electric boilers and heat pumps are capable of providing consistent improvements regarding the intermittency-friendliness of the energy system relative to the reference case, however, heat pumps are able to do so in a more cost-effective manner. Böttger et. al. [12] modeled the German energy system for the years 2012 and 2025 to assess the impacts of integrating 1000 MW of electric boiler capacity in district heating grids to be used as a secondary control power reserve for accommodating wind and solar photovoltaic (PV) energy sources in the grid. This study demonstrates that when wind and solar PV penetrations of 23% and 54% are considered, CO_2 emission reductions equivalent to 0.4 and 1.8 million tons, and power generation cost reductions of up to 65 and 158 million Euros are possible for the 2012 and 2025 energy systems, respectively.

Model-based studies have also investigated the impacts of heat pumps in DE grids for integrating high levels of variable renewable generation. Li et. al. [13] developed an energy model of a Chinese city comprising an interconnected electrical and thermal grid to identify optimal dispatch strategies for both a wind farm coupled to a heat pump plant, and a combined heat and power plant. This study showed that, relative to the case where thermal and electrical grids are operating independently, coupling electrical and thermal grids can lead to reductions in daily wind curtailment and network heat loss of up to 50% and 27%, respectively. Pensini et. al. [14] constructed an energy model of the North-Eastern part of the United States to assess the impacts of utilizing excess electricity for heating purposes in an energy system with a high penetration of wind and solar energy. Their analysis was carried out for the years 1999 to 2002 and considered both heat pumps coupled to thermal storage tanks in district heating grids, and electric resistance heaters coupled to high temperature thermal storage units in individual buildings. They found that heat pumps are more cost-effective than electrical resistance heaters and that CO_2 emission reductions of up to 97% in the heating sector are possible, relative to the reference energy system. Hedegaard and Münster [15] modeled the Danish energy system in 2030 with a wind energy penetration of approximately 60% to assess the feasibility of using heat pumps and thermal storage on a large scale to support wind power integration. They demonstrated that heat pumps and thermal storage can reduce system costs, CO_2 emissions, and peak/reserve capacity requirements in the energy system.

As described above, the majority of studies found in the literature focus on the impacts of integrating renewable energy on total CO_2 emissions for a fixed renewable energy penetration scenario in which DE grid distribution losses are assumed to be constant. No studies have been identified that analyze these systems over a range of renewable energy penetration scenarios using a high temporal resolution model that is capable of calculating DE grid distribution losses as a function of time.

1.1.3 Heat losses in district energy grids

A number of modeling studies have been conducted to examine heat losses in DE grids. Grosswindhager et al. [16] modeled the Tannheim DE grid in Tyrol, Austria to calculate temperature and flow characteristics at a number of consumer load points. They showed that heat losses vary throughout the year as a function of network pipe surface area and flow rate and account for approximately 14% of the total annual heat production in the system. Hassine and Eicker [17] constructed a model of a biomass powered CHP-based DE grid in Scharnhauser Park, Germany to assess the impacts of consumer spatial variation and pumping control on energy consumption. They found that reductions in grid heat loss and pumping energy consumption of up to 11% and 40%, respectively, occurred as a result of decreasing the average consumer distance from the heating plant by approximately 20% and switching to a variable flow system. Li and Svendsen [18] developed a model of the Lystrup DE grid in Denmark to assess the impacts of varying the supply temperature (i.e. from low to medium temperature) and adding thermal storage capacity at consumer substations. This study showed that increasing the supply temperature from low to medium causes the annual heat loss to increase by 60.4% and 45.2% in the storage and no-storage cases, respectively. This study also showed that adding storage causes the annual heat loss to decrease by 33.7% and 20.1% in the low and medium supply temperature systems, respectively. Li et al. [19] constructed a detailed model of a hypothetical CHP-based DE grid to assess the impacts of decreasing grid supply temperature on heat loss and pump power consumption. They found that lowering the supply temperature from 70°C to 55°C causes both the annual pump power consumption and heat loss to decrease by approximately 0.5%. However, lowering the supply temperature by the same amount at peak heating load conditions causes these parameters to increase by approximately 1.6% and 5.5%, respectively. Lund and Mohammadi [20] modeled the Studstrup CHP-based DE grid in Denmark to assess the impacts of pipe insulation thickness on heat loss and pipe investment costs. They showed that increasing pipe insulation thickness by a factor of approximately 1.5 causes heat losses to decrease by approximately 30% and pipe network investment costs to increase by approximately 11%.

As described above, the majority of studies found in the literature are conducted at hourly time resolution and focus on the impacts of varying one or more system parameters on heat losses in CHP-based DE grids. Studies conducted at time resolutions of one hour or greater have been shown to underestimate energy use in individual buildings due to the aggregation of high frequency load variations [21]. For example, Hawkes and Leach [22] constructed a model of a residential combined heat and power system using 1-hour and 5-minute resolution energy demand data, respectively, to assess the impacts of time resolution on calculated model outputs. They found that the energy delivered by system components (*i.e.* combined heat and power unit, boiler, electrical grid) varied by up to 40% between demand datasets and that CO_2 emission reductions were overestimated by up to 40% using the hourly demand dataset.

No studies have been identified that examine district energy grid heat losses using a high temporal resolution model. Nor do any studies focus on heat losses in CHP-based DE grids equipped with renewable power-to-heat plants.

1.2 Objectives

The primary objective of this work is to assess the potential benefits of CHP-based DE grids in energy systems having significant fossil fuel fired electrical generation capacity.

This objective is broken down into the following sub-objectives:

1. Determine the conditions under which expanding CHP-based DE grids is preferable to expanding wind power systems with respect to fossil fuel utilization and CO_2 emissions.

Sub-objective 1 is addressed in the context of a large scale energy system (*i.e.* a provincial or national energy system) in which a significant proportion of the electrical generation capacity is fossil fuel fired. The province of Ontario, Canada is chosen as the jurisdiction of study. The current ratio of fossil fuel fired electrical generation capacity to peak load in Ontario is approximately 0.42 [23].

2. Determine the conditions under which CHP-based DE grids equipped with renewable power-to-heat boilers are preferable to conventional renewable power systems with respect to fossil fuel utilization, CO_2 emissions, and overall energy efficiency.
3. Quantify DE grid distribution losses and their impact on the total thermal load that must be supplied at the central generation plant in a CHP-based DE grid equipped with renewable power-to-heat boilers.

Sub-objectives 2 and 3 are addressed in the context of a small scale energy system (*i.e.* a municipal energy system) in which the total electrical generation capacity is fossil fuel fired. The energy system of the Hot Springs Cove community, located on the west coast of Vancouver Island, Canada is chosen as the case study in the analysis. Hot Springs Cove currently does not have a district energy grid. In the analysis, the DE grid is modeled using the SS-VTD model (see Sub-objective 4).

4. Develop and validate a high temporal resolution numerical model (*i.e.* the SS-VTD model) that is capable of calculating distribution losses (*i.e.* heat losses and electrical pumping requirements) in small scale, variable flow DE grids with low error and computational intensity.

Sub-objective 4 is required to address sub-objectives 2 and 3. No existing model could be procured that offers capabilities fitting the description of the SS-VTD model.

1.3 Organization of dissertation

This dissertation is presented in the manuscript style. Details of the research are described in three manuscripts, presented in Appendices A, B, and C. Appendix D contains supplementary materials. Each of these manuscripts has either been published in or submitted to a relevant international journal specialized in energy research. The main body of the dissertation contains four chapters. Chapter 2 provides a technical background of the various components commonly encountered in a DE grid. Chapter 3 describes the motivation, methodology, and contributions of each manuscript in the appendix as well as a unifying commentary. Chapter 4 presents potential avenues for future work.

Chapter 2:

Overview of district energy grids

A DE grid typically comprises three main parts: the DE plant, the pipe network, and the building substations. Each of these parts is described in the following sections.

2.1 DE plant

A DE grid may consist of a single central energy plant, or a series of smaller plants interconnected by pipes that provide steam, hot water, or chilled water to the buildings connected to the network. Energy conversion in the plant is typically achieved using one or several of the following components: CHP units, fossil fuel-fired boilers, electric boilers, heat pumps, heat exchangers, solar thermal collectors, chillers, cooling towers, thermal storage tanks, and pumps. The DE plant components mentioned above are described separately as follows:

2.2.1 CHP units

CHP units generate heat and power simultaneously from a single fuel source, which can vary depending on the CHP technology used. Typical CHP fuels include natural gas, coal, and biomass. Typical CHP technologies used in DE grids include steam turbines, gas turbines, combined cycle gas turbines, microturbines, and reciprocating engines. These systems are characterized by the following three key attributes: overall efficiency, heat-to-power ratio, and thermal quality. The overall energy efficiency is defined as the sum of the electrical efficiency and the thermal efficiency. The heat-to-power ratio is the ratio of the amount of useful thermal energy available to the amount of electricity generated. The thermal quality is typically determined by the temperature of the thermal output. A higher thermal quality is achieved at higher temperatures (*e.g.* 500°C steam) as the output is suited to meet most industrial process needs. A lower thermal quality output (*e.g.* 80°C water), on the other hand, can only be used for a limited number of thermal applications. The overall efficiency, heat-to-power ratio, and thermal quality of various CHP technologies are shown in Table 1.

Table 1: Electrical efficiency, overall efficiency, heat-to-power ratio, and thermal quality by CHP technology type

CHP technology	[1,2] **Electrical efficiency (%)**	[1] **Overall efficiency (%)**	[3] **Heat-to-power ratio**	[1] **Thermal quality**
Non-condensing "back-pressure" steam turbine	14-28	84-92	2-5.5	High
Condensing steam turbine	22-40	60-80	0.5-2.6	High
Gas turbine	24-42	70-85	0.7-2.5	High
Combined cycle gas turbine	34-55	69-83	0.25-1.4	Medium
Microturbines	15-33	60-75	0.8-4	Medium to low
Reciprocating engine	33-53	75-85	0.4-1.6	Low

[1] Obtained from Ref. [24]. Represents data from existing facilities in Canada.
[2] Modern facilities typically operate at higher end of range depicted [25].
[3] Calculated

2.2.2 Fossil fuel-fired boilers

Fossil fuel-fired boilers generate heat through the combustion of fuels such as natural gas, or oil. Most newly built DE plants use condensing boilers that have thermal efficiencies in the range of 85-95% [26]. Although commonly used for backup and/or peaking purposes, fossil fuel-fired boilers can also be used independently for supplying 100% of the DE thermal load.

2.2.3 Electric boilers

Electric boilers generate heat by passing electricity through a series of resistive heating elements. As electricity is fully converted to heat in these systems, the energy efficiency is 100%. Electric boilers can be used as a power-to-heat technology in DE grids for balancing periods of overproduction from intermittent renewable energy sources like solar PV and wind in the electrical grid. As a result, higher renewable energy penetrations can be achieved.

2.2.4 Heat pumps

Heat pumps are electrical devices that transfer heat from one location to another using a vapour-compression cycle. They are similar to electric boilers in that they can be used as a power-to-heat technology in DE grids to accommodate higher penetrations of intermittent renewable energy in the electrical grid. Typical heat sources for DE grid heat pumps include surplus heat from residential and commercial cooling processes (*e.g.* air conditioning, skating rinks, supermarkets, and data centers), effluent and sewage streams, and geothermal bodies. The latter two sources mentioned above are also examples of heat sinks in which heat can be rejected by DE grid heat pumps when the system is in cooling. The energy efficiency of a heat pump is measured by its coefficient of performance (COP). The COP of a heat pump is defined as the ratio of heating or cooling provided by the device to the compressor work required and is highly dependent on the temperatures present at the evaporator and condenser. The higher the COP, the more efficient the heat pump. COP values for DE grid heat pumps can range anywhere between 3 and 8 on an annual basis [26].

2.2.5 Heat exchangers

Heat exchangers transfer heat between one or more fluids. They are commonly used in DE plants to recover surplus heat from a number of sources (*e.g.* CHP units and industrial processes), and as a means to exchange heat between closed loop piping circuits.

2.2.6 Solar thermal collectors

Solar thermal energy is harnessed in DE plants using solar collectors. A solar collector is a device that collects heat by capturing solar radiation. Flat plate and evacuated tube collector designs are typically used in DE plants for this purpose. The solar collectors are either installed on building rooftops or in stand-alone arrays.

2.2.7 Chillers

A chiller is a heat pump that cools water. Chillers are commonly used in DE plants to supply cold water to the DE grid during the cooling season. The two major types of chiller models are vapour-compression chillers and absorption chillers. The former uses an electric motor or mechanical power from an engine or turbine to drive the compressor in a vapour-compression cycle. The latter is heat-driven and uses both a generator and an absorber in an absorption cooling cycle. The efficiency of a chiller, like a heat pump, is measured by its COP. COP values for vapour-compression and absorption chillers range from approximately 3.8-8 and 0.7-1.7, respectively [26].

2.2.8 Cooling towers

Cooling towers remove heat from the cooling water that circulates through chiller condensers and heat exchangers and rejects it to the atmosphere. Depending on the entering air and water temperatures, the cooling water is cooled by either sensible or evaporative cooling processes, or a combination of both. Cooling towers typically require a supply of cooling water, an electric fan to induce airflow and a pump to circulate the cooling water. The COP of a cooling tower is measured as the ratio of heat rejected to the atmosphere to the work required to operate both the fan and the pump. Cooling tower COPs can range from approximately 6-20 [26].

2.2.9 Thermal storage tanks

Thermal storage tanks are commonly located in close proximity to the DE plant and are used to increase system efficiency by lowering the amount of unutilized heat dumped to the environment. They are often used in conjunction with CHP plants as a means for storing hot or chilled water produced by these plants during periods of peak electrical demand. The stored water is subsequently circulated in the DE grid to meet loads during periods of peak thermal demand [27]. A similar storage strategy is used with solar thermal plants when intermittent solar generation is high and both the electrical and thermal demand is low [28].

2.2.10 Pumps

The main pumps used for circulating water through the DE grid are normally located in the DE Plant. DE pumps can either operate at constant speed or variable speed. Most newly built DE plants use variable speed pumps as they offer superior energy efficiency, reliability, and life cycle costs, relative to constant speed pumps [29].

2.2 Pipe network

The pipe network connects the primary DE plant to the various building substations located throughout the system. In larger systems, secondary DE plants are used to connect the larger diameter transmission pipes to the smaller diameter distribution pipes. A secondary DE plant typically contains energy conversion components such as boilers and chillers to adjust the fluid temperature, and booster pumps to adjust the fluid pressure.

The DE pipe network can be characterized by the parameters discussed in the following subsections:

2.2.1 Supply temperature

The pipe network can carry steam, and water over a range of different temperatures. Most newly built DE grids are water-based systems as steam systems are expensive and difficult to maintain. Water-based systems can be classified into the following five groups based on supply temperature: Chilled water (< 5°C); ambient temperature (~ 10-25°C); low temperature (~ 40-50°C); medium temperature (~ 70-90°C); and high temperature (> 90°C). The main advantage associated with using lower temperature water in DE grids is that heat losses to the ground are reduced. The main disadvantage is that annual pumping energy requirements are increased.

2.2.2 Pipe material

Pipe materials typically vary based on the DE grid supply temperature. Medium and high temperature water-based systems commonly use insulated steel pipes, whereas ambient and low temperature systems commonly use high density polyethylene (HDPE) pipes. HDPE pipes are preferable to steel pipes as they are inexpensive and in certain cases do not require insulation.

2.2.3 Pipe number

DE grids typically require an independent 2-pipe distribution system for providing heating or cooling services [30]. One pipe supplies heating/cooling water to the DE grid from the DE plant and the other pipe returns heating/cooling water to the DE plant from the DE grid. The majority of systems that provide both heating and cooling services are constructed as 4-pipe systems (*i.e.* a separate 2-pipe system is used for the heating loop and the cooling loop). Ambient temperature DE grids (see Section 2.2.1), however, are an exception as they are able to provide heating and cooling in the same 2-pipe system.

2.2.4 Flow pattern

A DE grid is typically operated as a supply-return system, reverse-return system, or parallel-flow system, as shown in Figure 2 for a simplified DE grid comprising two separate loads. In supply-return systems, the pressure difference between supply and return pipes can decrease significantly with distance from the DE plant, potentially causing service interruptions to customers located further away from the DE plant. To avoid this issue, differential pressure control valves are commonly installed at various load points in the network. Differential pressure control valves provide hydraulic balance to the DE grid. In reverse-return systems, the pressure difference between supply and return pipes is automatically balanced throughout the system due to the geographical layout of the pipes. Differential pressure control valves are therefore not required in reverse-return systems. In parallel-flow systems, the pressure difference between supply and return pipes remains relatively constant throughout the entire piping network.

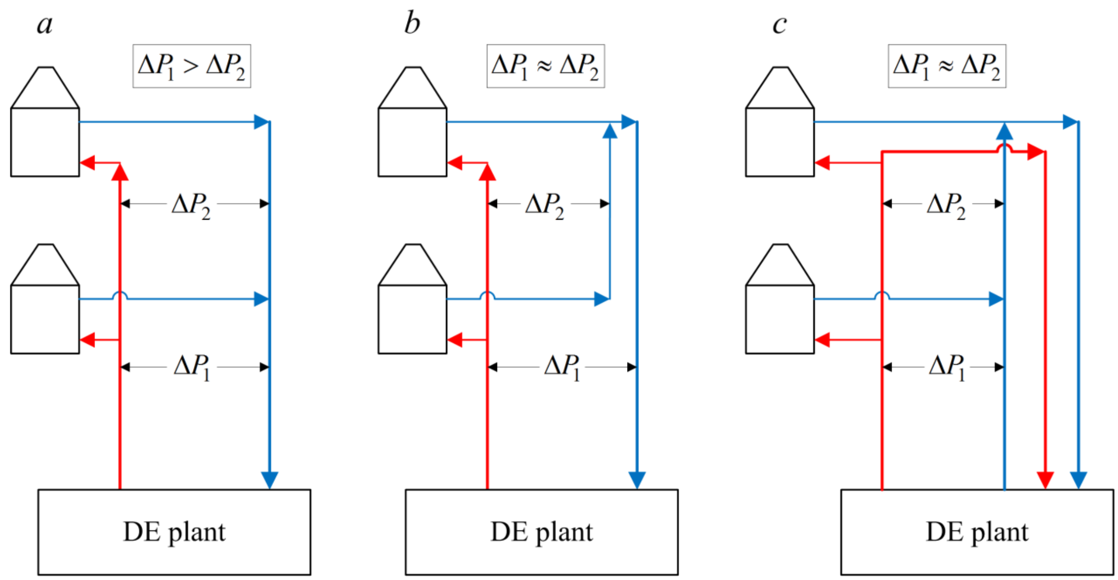

Figure 2: Typical DE grid fluid flow patterns: (*a*) supply-return, (*b*) reverse-return, and (*c*) parallel-flow. Red and blue arrows represent supply and return pipes, respectively

2.2.5 Flow control method

DE grids can operate either at constant flow or variable flow. Variable flow systems can be pressure and/or temperature controlled. In pressure controlled systems, pump speed is varied in order to maintain a set point pressure differential across a predefined control valve (usually located at the furthest extremity of the piping network). In temperature controlled systems, pump speed is varied in order to maintain a set point temperature differential across a predefined heat exchanger or heat pump unit (usually located in close proximity to a building substation).

2.3 Building substations

In a building substation, a connection is made between the DE grid and the individual building heating and/or cooling system. The connection can be direct or indirect. In a direct connection, fluid from the DE grid circulates directly into the building heating or cooling loop. In an indirect connection, fluid from the DE grid is isolated from the building loop and energy is exchanged via a heat exchanger or heat pump.

In this chapter, a technological overview of district energy grids has been presented. The next chapter focuses on the methods and contributions of the studies included in this dissertation.

Chapter 3:

Contributions

This chapter is divided into three sections, which provide an overview of the motivation, methodology, and contributions for the three studies undertaken in this research. Full details of each study are presented as manuscripts and are included as Appendices A through C.

3.1 The potential benefits of widespread combined heat and power based district energy networks in the province of Ontario[1]

In this study, the impacts of expanding CHP-based DE grids versus expanding wind power systems are investigated with respect to fossil fuel utilization and CO_2 emissions in an energy system having significant fossil fuel fired electrical generation capacity.

Various national level modeling studies have been conducted to examine the impacts of expanding these two technologies independently [6–8,31–35]. However, no studies have been identified that compare them in the context of a large-scale system (*i.e.* a provincial or national energy system). Comparing these systems from a cost-benefit perspective can provide valuable information to policy makers interested in adopting policies that incent energy technologies that provide better return on investment. The current study is the first to compare these systems from a technological standpoint. The province of Ontario, Canada is chosen as the jurisdiction of study.

[1] Manuscript published in Energy

Models corresponding to a reference energy system and a widespread district energy (WDE) system are constructed. Reference year (*i.e.* 2007) energy system components and capacities are considered in the reference model. Natural gas boilers and absorption chillers are used in the WDE model for heating and cooling in DE grids, respectively. Three WDE scenarios (*i.e.* Scenarios II to IV) are constructed and compared with the reference scenario (*i.e.* Scenario I) on the basis of CO_2 emissions and fossil fuel utilization. An additional scenario (*i.e.* Scenario V) is constructed to assess the impacts of expanded wind generation capacity relative to the expanded DE infrastructure scenarios. For each scenario, Table 1 of Appendix A summarizes total heating/cooling loads, conversion technologies, component efficiencies, and fuel types for individual buildings and DE grids.

Scenarios II to IV (*i.e.* the widespread district energy scenarios) represent hypothetical configurations of the Ontario energy system. These differ from the reference scenario in that approximately 60% of the total residential and commercial heating and cooling load is transferred from individual building systems to DE networks. In Scenario II, DE heat is supplied entirely using natural gas boilers and total CHP installed capacity is zero. In Scenario III, back pressure steam turbine (BPST) CHP plants are used. In Scenario IV, combined cycle gas turbine (CCGT) CHP plants are used instead of BPST CHP plants. The CHP technologies in Scenarios III and IV are selected as they represent two extremes on the scale of heat-to-power ratio. Scenario V is identical to Scenario I but with increased wind capacity. Both the total CHP capacity in Scenarios III and IV and the total wind capacity in Scenario V are set to approximately 25% of the total power plant installed capacity in the reference year.

The EnergyPLAN analysis tool is used to construct all models and to conduct the simulations. EnergyPLAN is capable of optimizing an energy system based solely on the technical operation of its components. A technical dispatch strategy is applied to Scenarios I to V with the objective of minimizing fossil fuel utilization. For all scenarios, a stable electrical grid is maintained at all times since at least 60% of all generation is supplied by generators capable of providing ancillary services such as frequency support, voltage support, and operating reserves [36]. For the 2007 Ontario system, these are nuclear, hydro, CHP, or large thermal power plants (LTPPs). The EnergyPLAN technical dispatch strategy is depicted in Figure 2 of Appendix A.

The main contributions of this study are summarized as follows:

1. <u>Replacing combined cycle gas turbine (CCGT) plants with back pressure steam turbine (BPST) plants in an energy system comprising widespread CHP-based DE grids causes a large increase in heat production and a small decrease in electrical capacity factor.</u> Relative to Scenario IV (CCGT CHP plants), switching to Scenario III (BPST CHP plants) causes a 600% increase in heat production and a 37% decrease in electrical capacity factor. This increase in heat production and associated decrease in capacity factor is attributed to the lower electrical efficiencies common to BPST CHP plants. Differences between Scenario III and Scenario IV are directly related to the heat to power ratio of the distinct CHP technologies used in each scenario.
2. <u>Switching to an energy system comprising widespread CHP-based DE grids causes a large decrease in the minimum installed capacity of large fossil fuel fired electrical generation plants.</u> In this study, large fossil fuel fired electrical

generation plants are referred to as large thermal power plants (LTPPs). Relative to the reference energy system (Scenario I), switching to widespread BPST CHP-based DE grids (Scenario III) and CCGT CHP-based DE grids (Scenario IV) causes the minimum installed LTPP capacity required for balancing the electrical load to decrease by 50% and 87%, respectively. Switching to large-scale wind power systems (Scenario V), however, causes no change in the minimum installed LTPP capacity relative to the reference energy system.

3. <u>Switching to an energy system comprising widespread CHP-based DE grids causes a large decrease in fossil fuel utilization and CO_2 emissions</u>. Reductions of 8.5% and 32% are observed for Scenario IV relative to Scenario I, respectively. In Scenario V, fossil fuel utilization and CO_2 emissions are 8.7% and 21% lower than in Scenario I. Since these reductions are nearly equivalent to those achieved in Scenario IV, one may question the value of investing in an energy system comprised of WDE over maintaining a conventional system and investing in large-scale wind power. To answer this question, a sensitivity analysis is performed over a large installed capacity range. The sensitivity analysis reveals that widespread CHP-based DE grids have lower fossil fuel utilization and CO_2 emissions than large-scale wind systems for relative installed capacities below approximately 30% of the peak electrical load. Since wind power capacity to peak load ratios greater than 30% are seldom exceeded in electrical grids due to grid stability issues, this point can be treated as an upper limit to wind penetration in the energy system. Therefore, if a choice were to be made between expanding CHP-based DE systems or wind systems solely based on reduced fossil fuel

utilization and reduced CO_2 emissions, CCGT CHP-based DE systems are the preferred option.

Although economics are not covered, this study demonstrates the potential impacts of introducing widespread DE networks comprised of natural gas-fired CHP plants and wind systems in the province of Ontario. The results of this study are applicable to other jurisdictions with similar energy mix who are faced with decisions on how to best proceed with future energy infrastructure investments. The results also bring to light the importance of accounting for heat to power ratio in large-scale energy planning studies that incorporate CHP generation.

A more complete description of this study is presented in [23]. The manuscript is included in Appendix A of this dissertation.

Results included in this manuscript are based on an aggregated study that is conducted on a large scale energy system using a commercial hourly resolution model. As the findings of the study reveal CHP-based DE grids to be an attractive technology for large scale energy systems, it was felt that further analysis of these systems was merited at a more refined scale; hence work was undertaken to develop a model that is capable of analyzing small scale DE grids at high temporal resolution (see sub-objective 4, listed in Section 1.2).

3.2 Thermal performance of a steady state physical pipe model for simulating district heating grids with variable flow[2]

In the context of this dissertation, this study was undertaken to develop a model that can be used to address sub-objectives 2 and 3 described in Section 1.2. The primary objective of this study is to construct and validate a high temporal resolution numerical model (*i.e.* the SS-VTD model) that is capable of calculating distribution losses (*i.e.* heat losses and electrical pumping requirements) in small scale, variable flow district heating (DH) grids. A small scale DH grid is defined as a thermal energy distribution network that is used for servicing loads in an independent municipality. As described in Section 1.1.3, a high temporal resolution model is needed to account for the high frequency variations in generation and load present in such systems, and estimate the total thermal load that must be supplied at the central generation plant with low error. A secondary objective of this study is to assess the SS-VTD model for error and computational intensity.

Temperature dynamics in variable flow DH grids are difficult to model due to the challenges of tracking transport delays in the network pipes [16]. A number of modeling studies have been conducted that focus on temperature dynamics in variable flow DH grids [17,18,37–45]. The majority of these studies are conducted using physical pipe models that are classified as either transient, steady state, or pseudo-transient models. In transient models, the pipe energy equation is presented as a one-dimensional partial differential equation (1D-PDE). Transient models provide relatively accurate results for

---

[2] Manuscript published in Applied Energy

variable flow systems and do not require tracking of transport delays. However, the computational intensity of these models can be high [40]. In steady state models, each pipe is typically represented as a series of lumped masses. Although computational intensity is low for steady state DH grid models, these models are limited in their capacity to track transport delays in variable flow systems [46]. In pseudo-transient models, the steady state (SS) lumped mass model is combined with a variable transport delay (VTD) model to enable the progress of the fluid to be tracked in time as the flow rate varies [47]. The combination of both of these models results in the SS-VTD model. No studies have been identified that assess the SS-VTD model numerically for error and computational intensity.

In the current study, the SS-VTD model is assessed both experimentally and numerically. The experimental assessment serves to validate the SS-VTD model and is conducted by comparing simulated temperature data with measured temperature data from an existing network. The Saanich DE grid, located near Victoria, Canada, is used as the case study for validation. The Saanich DE grid is simulated in Simulink® using the SS-VTD model with a time step of 60 seconds. A time period of 6 hours is simulated from 9:00 am to 3:00 pm on December 2nd, 2012. Results show that the simulated dataset fits closely with the measured dataset. However, the following inconsistencies were found: the two datasets are offset in time by approximately 2 minutes and the simulated temperature dataset overestimates temperature by approximately 0.2°C on average.

The numerical assessment is conducted by applying the SS-VTD model to a variable flow DH pipe model and comparing fluid outlet temperatures with those obtained using a transient model (*i.e.* the 1D-PDE model). Results from the 1D-PDE model are used as a reference for the comparison and are used to assess the error of the SS-VTD model. The computational intensity of the SS-VTD model is assessed in a similar manner by comparing CPU run times for all simulations. Simulations of the 1D-PDE and SS-VTD models are conducted for a period of 30 minutes. The inlet water temperature used in the analysis is selected arbitrarily and fluctuates between 40°C and 80°C in a sinusoidal waveform with a period of 1200 seconds. The mass flow rate used in the analysis is also selected arbitrarily and fluctuates between 150 kg/s and 750 kg/s in a sinusoidal waveform with a period of 600 seconds.

The 1D-PDE model is simulated in the Matlab® partial differential equation (PDE) toolbox™ environment with a time step of 1 second. The SS-VTD model is simulated in Simulink® over a range of time steps, Δt, and pipe segment lengths, Δx. Two sets of simulations are conducted: In the first set, the impact of varying Δt while holding Δx constant is assessed. In the second set, the impact of varying Δx while holding Δt constant is assessed. By varying Δx, the effect of increased pipe discretization can be observed. Fifteen scenarios with time steps and pipe segment lengths ranging from 1 s to 150 s and 3 m to 500 m are considered in the analysis, respectively. Model error in the analysis is determined by the standard deviation of a probability density function (PDF) representing the percent difference between the 1D-PDE and SS-VTD fluid outlet temperature time series datasets. The PDF is evaluated using a sample of 100 equally spaced bins. Model computational intensity is determined by the CPU simulation time. Simulations are performed using Simulink® version R2015a on a computing platform equipped with an Intel Core i5 2.67 GHz processor and 8 GB of RAM.

The main contributions of this study are summarized as follows:

1. <u>A novel approach is developed for simulating small scale district energy grids</u>. This approach, called the steady state variable transport delay (SS-VTD) approach, is based on the discretization of a pipe into many segments to account for varying transverse thermal resistance and surrounding soil surface temperature variations. Benefits of this approach include low error, low computational intensity, the ability to calculate network distribution losses, and the ability to track variable transport delays in the pipe network. A method is proposed for selecting stable simulation parameters (*i.e.* Δx and Δt) to be used in the SS-VTD model. Stable simulation parameters for a given scenario are selected based on the calculated peak Courant number, which must have a value that is lesser or equal to one.
2. <u>The benefit of using the SS-VTD simulation approach relative to a transient approach is significant with respect to computational intensity</u>. When compared with the 1D-PDE model at the same fixed time step of 1 s, the CPU simulation time of the SS-VTD model is approximately 4000 times shorter. This benefit increases as larger time steps are used in the SS-VTD model, but at the cost of increased error. With respect to reproducibility of results, the SS-VTD model is nearly equivalent to the 1D-PDE model at the same fixed time step of 1 s.
3. <u>The impact of decreasing the discretized pipe segment length on the error of the SS-VTD model is minimal</u>. Reducing the pipe segment length, Δx, from 500 m to 3 m causes no observable change in the standard deviation. This result is not surprising as the total thermal resistance per unit length of pipe, R', is assumed

to be constant as a function of distance in both the 1D-PDE and SS-VTD models considered. The impact of pipe segment length on the computational intensity of the SS-VTD model, however, is considerable. Increasing Δx from 3 m to 500 m causes a decrease in CPU simulation time for all time step sizes considered.

4. The impact of decreasing the time step size on the error and computational intensity of the SS-VTD model is significant. Reducing Δt from 150 s to 10 s causes a decrease in standard deviation, from 23.5 % to 2.3 %. Corresponding to this decrease in standard deviation is a relatively small increase in CPU simulation time, from 0.23 s to 0.33 s. This result shows that there is a clear benefit associated with reducing the time step size with regards to decreasing the error of the SS-VTD model. Between Δt =10 s to Δt =1 s, however, there is a significant increase in CPU simulation time, from 0.33 s to 0.78 s. The decrease in error, from Δt =10 s to Δt =1 s, on the other hand, is less significant as the standard deviation decreases only from 2.3 % to 1.2 %. This relatively small gain in accuracy comes with a high computational cost.

The main limitation of this study is that the total thermal resistance per unit length of pipe, R' , is assumed to be constant as a function of distance in the models considered. Assuming constant R' in the SS-VTD model can provide satisfactory results for small DH grids, as demonstrated by the Saanich DE grid model. However, significant error may arise when modeling larger DH grids, since thermal interactions between the pipe and the soil surface can vary considerably with distance.

The results of this study bring to light the importance of assessing the trade-offs between error and computational intensity before selecting suitable values of Δx and Δt for a particular pipe flow problem. The SS-VTD model's ability to handle variable transport delays makes it a valuable tool for simulating variable speed pumping systems, a common addition in today's modern DH grids. Potential uses of the model include the design and operational optimization of DH grids [48].

A more complete description of this study is presented in [49]. The manuscript is included in Appendix B of this dissertation. The SS-VTD model developed in this study has been validated and can therefore be used as a high temporal resolution DE grid modeling tool for analyzing small scale DE grids (see sub-objectives 2 and 3 from Section 1.2).

3.3 Coupled electrical-thermal grids to accommodate high penetrations of renewable energy in an isolated system[3]

The primary objective of this study in the context of this dissertation is to determine the conditions under which small scale CHP-based DE grids equipped with wave power-to-heat boilers are preferable to conventional wave power systems with respect to fossil fuel utilization, CO_2 emissions, and overall energy efficiency. A secondary objective is to assess the impacts of DE grid distribution losses on the total thermal load that must be supplied at the central generation plant (*i.e.* the powerhouse) in a small scale CHP-based DE grid equipped with wave power-to-heat boilers.

---

[3] Manuscript submitted to Renewable Energy

Model-based studies have investigated the impacts of power-to-heat technologies, such as heat pumps and electric boilers, in DE grids for integrating high levels of variable renewable generation [11–15,50–53]. The majority of these studies focus on the impacts of integrating renewable energy on total CO_2 emissions for a fixed renewable energy penetration scenario. The majority of these studies are also conducted using hourly resolution models in which DE grid distribution losses (*i.e.* heat losses and electrical pumping requirements) are assumed to be constant. No studies have been identified that analyze a CHP-based DE grid using a high temporal resolution model that is capable of calculating DE grid distribution losses with a high level of accuracy. Nor do any studies examine a range of different renewable energy penetration scenarios. The current study is the first to do so. The energy system of the Hot Springs Cove community, located on the west coast of Vancouver Island, Canada is used as the case study in the analysis.

Hot Springs Cove is an isolated community (*i.e.* not grid connected) with a population that varies from approximately 50 to 80 from winter to summer, respectively. There are 44 buildings in the community. Building types include residential buildings, commercial buildings, and a school. All buildings have an electrical and auxiliary heating load, and an electrical appliance load. The electrical heating and appliance load is met using a centralized diesel generator plant. The auxiliary heating load is met using propane heaters in all buildings except the school which also uses a ground source heat pump.

Models are constructed in the Matlab/Simulink™ environment corresponding to three scenarios: a reference scenario, a wave energy scenario and a DH-wave energy scenario. The reference scenario represents the community in the year 2011.

The wave energy scenario represents the community with wave energy integration and includes a wave energy converter (WEC) plant and a dump load. Wave energy penetration varies from 0-45% in the wave energy scenario. Wave energy penetration (WEP) is defined as the total annual electricity generated from wave energy divided by the total annual fossil fuel consumption in the reference year.

The DH-wave energy scenario represents the community with wave energy integration and a DE grid. The DE grid is modeled using the steady state - variable transport delay (SS-VTD) model. The SS-VTD model is a load driven pipe flow model that allows rapid computation of grid heat losses, grid pumping energy requirements, and pipe outlet temperatures. The model also tracks time delays in the pipes as the flow rate varies. A thorough description and validation of the SS-VTD model is provided in Ref. [49]. The DH-wave energy scenario includes a diesel CHP plant, a diesel boiler plant, an electric boiler plant, a cooling tower, and a number of heat exchangers and variable speed pumps. The electrical and thermal grids are coupled in the DH-wave energy scenario as wave energy is used to meet electrical loads directly, via the electrical grid, and heating loads indirectly, via the electric boiler plant.

The Simulink® software is used to conduct time series simulations on the three scenarios described above using an explicit fixed step continuous solver based on Euler's method [54]. A technical dispatch strategy is used to allocate electricity and heat generation at each 30 second time step for a period of one year for all scenarios with the objective of minimizing fossil fuel consumption. The Simulink technical dispatch strategy is depicted in Figures A.1 and A.2 of Appendix C.

The main contributions of this study are summarized as follows:

1. Adding a CHP-based DE grid with an electric boiler plant to a high penetration wave power system causes a significant increase in wave energy utilization. Relative to the wave energy scenario, switching to the DH-wave energy scenario causes the wave energy utilization ratio to increase by a factor of up to 1.5. The wave energy utilization ratio (r_{WEU}) is defined as

$$r_{WEU} = \frac{\text{Annual useful electrical energy generation derived from wave energy}}{\text{Annual electrical energy generation derived from wave energy}}$$

   where useful electrical energy represents energy that is used to do work and/or generate heat in the community. This result demonstrates the gains in overall system efficiency that can be achieved when using an electric boiler plant to convert excess wave power to heat.

2. Adding a CHP-based DE grid with an electric boiler plant to a high penetration wave power system causes a significant decrease in fossil fuel consumption and CO_2 emissions. Relative to the wave energy scenario, switching to the DH-wave energy scenario causes fossil fuel consumption and CO_2 emissions to decrease by up to 47 % over the range of wave energy penetration set points analyzed.

3. DE grid heat losses vary considerably throughout the year as a function of the total thermal load that is supplied at the central generation plant. Heat losses account for and vary between 7% and 25% of the total thermal load that is supplied at the central generation plant in the CHP-based DE grid. On an annual

basis, distribution heat losses account for approximately 12% of the total heat supplied to the DE grid.

The current study compares the technical impacts of wave powered CHP-based DE grids and wave power systems. Economics are not considered. This is one of the main limitations of this study. Additional consideration of capital costs and lifetimes for system components is needed to assess economic viability. A second limitation of the study is that the analysis is conducted using a DE grid model that comprises a number of fixed input parameters such as the supply temperature, the thermal conductivity of pipe materials and soil, the pipe burial depth, the grid size, and the pumping control method. It is unclear what impacts varying these parameters may have.

The current study demonstrates that there are clear advantages to integrating wave energy in a CHP-based DE grid relative to a conventional electrical grid. The results of this study are applicable to other jurisdictions with significant installed thermal power capacity who are considering transitioning to a higher efficiency, low carbon energy system. Although this work focuses on wave energy integration, the findings from this study may also be broadly applicable to other similar systems comprising intermittent variable renewable generation sources such as wind and solar energy.

A more complete description of this study is presented in Appendix C of this dissertation.

Chapter 4:

Future work

This dissertation demonstrates the potential benefits of CHP-based DE grids. Although extensive research has been carried out in meeting the objectives stated in Section 1.2, certain limitations exist.

The main limitation of the study presented in Section 3.1, *The potential benefits of widespread combined heat and power based district energy networks in the province of Ontario*, is that economics are not considered. Energy and infrastructure costs are an important consideration when assessing the feasibility of an energy system. Future work stemming from this study could include a scenario in which these costs are incorporated in the model. Another scenario could account for rising energy loads in the near future.

The main limitation of the study presented in Section 3.2, *Thermal performance of a steady state physical pipe model for simulating district heating grids with variable flow*, is that the total thermal resistance per unit length of pipe used in the SS-VTD model scenarios is constant as a function of distance. Although this assumption can provide satisfactory results for small DE grids, significant error may arise when modeling larger DE grids since thermal interactions between the pipe and the soil surface can vary considerably with distance. Potential future work could include modeling a large DE grid using the SS-VTD model to confirm this hypothesis.

One limitation of the study presented in Section 3.3, *Coupled electrical-thermal grids to accommodate high penetrations of renewable energy in an isolated system*, is that the analysis is conducted using a DE grid model that comprises a number of fixed input parameters such as the supply temperature, the thermal conductivity of pipe materials and soil, the pipe burial depth, the grid size, and the pumping control method. A future study could be conducted to assess the impacts of varying these parameters. Another limitation is that economics are not covered. Consideration of capital costs and lifetimes for system components is needed to fully assess the feasibility of the scenarios considered. This is therefore a topic for future research.

Other potential areas for future work include assessing the impacts of hot water storage, building demand side management measures, alternative power to heat technologies (*e.g.* heat pumps), and spatial variation of heating loads in CHP-based DE grids.

Bibliography

[1] Skagestad B, Mildenstein P. IEA - District Heating and Cooling Connection Handbook. International Energy Agency; 2000.

[2] Andersen A. DESIRE - CHP plants with big thermal stores balancing fluctuating productions from wind turbines. 2007.

[3] CDEA. Canadian District Energy Association, District Energy - A National Survey Report. Toronto: Canadian District Energy Association; 2008.

[4] Joelsson A, Gustavsson L. District heating and energy efficiency in detached houses of differing size and construction. IGEC III Spec Issue Third Int Green Energy Conf (IGEC-III), June 18–20, 2007, Västerås, Sweden 2009;86:126–34. doi:10.1016/j.apenergy.2008.03.012.

[5] Wernstedt F, Davidsson P, Johansson C. Simulation of District Heating Systems for Evaluation of Real-Time Control Strategies. Proc. 1st Eur. Simul. Model. Conf., 2003.

[6] Danestig M, Gebremehdin A, Karlsson B. Stockholm CHP potential—An opportunity for CO2 reductions? Energy Policy 2007;35:4650–60. doi:10.1016/j.enpol.2007.03.024.

[7] Lund H, Šiupšinskas G, Martinaitis V. Implementation strategy for small CHP-plants in a competitive market: the case of Lithuania. Appl Energy 2005;82:214–27. doi:10.1016/j.apenergy.2004.10.013.

[8] Münster M, Morthorst PE, Larsen H V, Bregnbæk L, Werling J, Lindboe HH, et al. The role of district heating in the future Danish energy system. Energy 2012;48:47–55. doi:10.1016/j.energy.2012.06.011.

[9] Chen M, Lund H, Rosendahl LA, Condra TJ. Energy efficiency analysis and impact evaluation of the application of thermoelectric power cycle to today ' s CHP systems. Appl Energy 2010;87:1231–8. doi:10.1016/j.apenergy.2009.06.009.

[10] Lund R, Mathiesen BV. Large combined heat and power plants in sustainable energy systems. Appl Energy 2015;142:389–95. doi:10.1016/j.apenergy.2015.01.013.

[11] Blarke MB. Towards an intermittency-friendly energy system: Comparing electric boilers and heat pumps in distributed cogeneration. Appl Energy 2012;91:349–65. doi:10.1016/j.apenergy.2011.09.038.

[12] Böttger D, Götz M, Theofilidi M, Bruckner T. Control power provision with power-to-heat plants in systems with high shares of renewable energy sources –

An illustrative analysis for Germany based on the use of electric boilers in district heating grids. Energy 2015;82:157–67. doi:10.1016/j.energy.2015.01.022.

[13] Li J, Fang J, Zeng Q, Chen Z. Optimal operation of the integrated electrical and heating systems to accommodate the intermittent renewable sources. Appl Energy 2015. doi:10.1016/j.apenergy.2015.10.054.

[14] Pensini A, Rasmussen CN, Kempton W. Economic analysis of using excess renewable electricity to displace heating fuels. Appl Energy 2014;131:530–43. doi:10.1016/j.apenergy.2014.04.111.

[15] Hedegaard K, Münster M. Influence of individual heat pumps on wind power integration – Energy system investments and operation. Energy Convers Manag 2013;75:673–84. doi:10.1016/j.enconman.2013.08.015.

[16] Grosswindhager S, Voigt A, Kozek M. Efficient Physical Modelling of District Heating Networks. Model. Simul., vol. Calgary, A, 2011.

[17] Hassine BI, Eicker U. Simulation and Optimization of the District Heating Network in Scharnhauser Park. Proc. 2nd Polygeneration Conf., vol. Tarragona, 2011.

[18] Li H, Svendsen S. Energy and exergy analysis of low temperature district heating network. Energy 2012;45:237–46. doi:10.1016/j.energy.2012.03.056.

[19] Li P, Nord N, Ståle I, Ge Z, Yang Z, Yang Y. Integrated multiscale simulation of combined heat and power based district heating system. Energy Convers Manag 2015;106:337–54. doi:10.1016/j.enconman.2015.08.077.

[20] Lund R, Mohammadi S. Choice of insulation standard for pipe networks in 4 th generation district heating systems. Appl Therm Eng 2016;98:256–64. doi:10.1016/j.applthermaleng.2015.12.015.

[21] Wright A, Firth S. The nature of domestic electricity-loads and effects of time averaging on statistics and on-site generation calculations. Appl Energy 2007;84:389–403. doi:10.1016/j.apenergy.2006.09.008.

[22] Hawkes A, Leach M. Impacts of temporal precision in optimisation modelling of micro-Combined Heat and Power. Energy 2005;30:1759–79. doi:10.1016/j.energy.2004.11.012.

[23] Duquette J, Wild P, Rowe A. The potential benefits of widespread combined heat and power based district energy networks in the province of Ontario. Energy 2014;67:41–51. doi:10.1016/j.energy.2013.12.038.

[24] Nyboer J, Groves S. Canadian Industrial Energy End-use Data and Analysis Centre - A review of Existing Cogeneration Facilities In Canada. 2012.

[25] Energinet.dk. Technology data for energy plants. 2012. doi:ISBN: 978-87-7844-940-5.

[26] Harvey LDD. A handbook on low-energy buildings and district-energy systems. Earthscan; 2006.

[27] King M, Bradford B. COMMUNITY ENERGY: PLANNING , DEVELOPMENT & DELIVERY – STRATEGIES FOR THERMAL NETWORKS. 2013.

[28] Bauer D, Marx R, Drück H. Solar District Heating Systems for Small Districts with Medium Scale Seasonal Thermal Energy Stores. Energy Procedia 2016;91:537–45. doi:10.1016/j.egypro.2016.06.195.

[29] US Department of Energy. Variable Speed Pumping - A Guide to Successful Applications. Washington, D.C.: U.S. Department of Energy Industrial Technologies Program; 2004.

[30] American Society of Heating, Refrigeration and Air-Conditioning Engineers I. 2012 ASHRAE Handbook - Heating, Ventilating, and Air-Conditioning Systems and Equipment (I-P Edition), 2012, p. 12.1-12.40.

[31] Connolly D, Lund H, Mathiesen B V, Leahy M. Modelling the existing Irish energy-system to identify future energy costs and the maximum wind penetration feasible. Energy 2010;35:2164–73. doi:10.1016/j.energy.2010.01.037.

[32] Batas Bjelić I, Rajaković N, Ćosić B, Duić N. Increasing wind power penetration into the existing Serbian energy system. Energy 2013;57:30–7. doi:http://dx.doi.org/10.1016/j.energy.2013.03.043.

[33] Le NA, Bhattacharyya SC. Integration of wind power into the British system in 2020. Energy 2011;36:5975–83. doi:http://dx.doi.org/10.1016/j.energy.2011.08.018.

[34] Liu W, Lund H, Mathiesen BV. Large-scale integration of wind power into the existing Chinese energy system. PRES 2010 2011;36:4753–60. doi:http://dx.doi.org/10.1016/j.energy.2011.05.007.

[35] Hong L, Lund H, Möller B. The importance of flexible power plant operation for Jiangsu’s wind integration. 23rd Int Conf Effic Cost, Optim Simul Environ Impact Energy Syst ECOS 2010 2012;41:499–507. doi:http://dx.doi.org/10.1016/j.energy.2012.02.038.

[36] NRCan. Natural Resources Canada - Office of Energy Efficiency, Comprehensive Energy Use Database, 1990-2008 2011;http://oee.

[37] Gabrielaitiene I, Bohm B, Sunden B. Dynamic Temperature Simulation in District Heating Systems in Denmark Regarding Pronounced Transient Behaviour. J

Environ Manage 2011;17:79–87.

[38] Gabrielaitiene I, Bøhm B, Sunden B. Modelling temperature dynamics of a district heating system in Naestved, Denmark—A case study. Energy Convers Manag 2007;48:78–86. doi:10.1016/j.enconman.2006.05.011.

[39] Gabrielaitiene I, Kacianauskas R, Sunden B. Application of the Finite Element Method for Modelling of District Heating Networks. vol. 9. University of Ljubljana: Digital Library of Construction Informatics and Information Technology in Civil Engineering and Construction; 2001.

[40] Gabrielaitiene I, Kacianauskas R, Sunden B. Thermo-Hydraulic Finite Element Modelling of District Heating Network by the Uncoupled Approach. J Civ Eng Manag 2012;9:153–62.

[41] Stevanovic VD, Zivkovic B, Prica S, Maslovaric B, Karamarkovic V, Trkulja V. Prediction of thermal transients in district heating systems. Energy Convers Manag 2009;50:2167–73. doi:http://dx.doi.org/10.1016/j.enconman.2009.04.034.

[42] Haiyan L, Valdimarsson P. District Heating Modelling and Simulation. Thirty fourth Work. Geotherm. Reserv. Eng., vol. Stanford, 2009.

[43] Hassine I Ben, Eicker U. Control Aspects of Decentralized Solar Thermal Integration into District Heating Networks. Proc 2nd Int Conf Sol Heat Cool Build Ind (SHC 2013) 2014;48:1055–64. doi:http://dx.doi.org/10.1016/j.egypro.2014.02.120.

[44] Sener AC. Modelling of Balcova Geothermal District Heating System, Turkey. vol. 13. Reykjavik, Iceland: The United Nations University, Geothermal Training Programme; 2002.

[45] Liu X, Wu J, Jenkins N, Bagdanavicius A. Combined analysis of electricity and heat networks. Appl Energy 2015:1–13. doi:10.1016/ j.apenergy.2015.01.102.

[46] Heller A. Demand Modelling for Central Heating Systems. vol. R-040. Lyngby, Denmark: Department of Buildings and Energy, Technical University of Denmark; 2000.

[47] Yan A, Zhao J, An Q, Zhao Y, Li H, Huang YJ. Hydraulic performance of a new district heating system with distributed variable speed pumps. Appl Energy 2013;112:876–85. doi:http://dx.doi.org/10.1016/j.apenergy.2013.06.031.

[48] Pini Prato A, Strobino F, Broccardo M, Parodi Giusino L. Integrated management of cogeneration plants and district heating networks. Appl Energy n.d. doi:10.1016/j.apenergy.2012.02.038.

[49] Duquette J, Rowe A, Wild P. Thermal performance of a steady state physical pipe

model for simulating district heating grids with variable flow. Appl Energy 2016;178:383–93. doi:10.1016/j.apenergy.2016.06.092.

[50] Hedegaard K, Mathiesen BV, Lund H, Heiselberg P. Wind power integration using individual heat pumps – Analysis of different heat storage options. Energy 2012;47:284–93. doi:10.1016/j.energy.2012.09.030.

[51] Østergaard PA. Wind power integration in Aalborg Municipality using compression heat pumps and geothermal absorption heat pumps. Energy 2013;49:502–8. doi:10.1016/j.energy.2012.11.030.

[52] Yang Y, Wu K, Long H, Gao J, Yan X, Kato T, et al. Integrated electricity and heating demand-side management for wind power integration in China. Energy 2014;78:235–46. doi:10.1016/j.energy.2014.10.008.

[53] Zwaenepoel B, Vansteenbrugge J, Vandoorn TL, Van Eetvelde G, Vandevelde L. Ancillary services for the electrical grid by waste heat. Appl Therm Eng 2014;70:1–6. doi:10.1016/j.applthermaleng.2014.04.010.

[54] Mathworks. Simulink - Simulation and model-based design 2014. http://www.mathworks.com/products/simulink/.

Appendix A:

The potential benefits of widespread combined heat and power based district energy grids in the province of Ontario

Duquette J, Wild P, Rowe A. The potential benefits of widespread combined heat and power based district energy networks in the province of Ontario. Energy 2014;67:41–51. doi:10.1016/j.energy.2013.12.038.

Energy 67 (2014) 41–51

Contents lists available at ScienceDirect

Energy

journal homepage: www.elsevier.com/locate/energy

The potential benefits of widespread combined heat and power based district energy networks in the province of Ontario

Jean Duquette*, Peter Wild [1], Andrew Rowe [2]

Institute for Integrated Energy Systems, Department of Mechanical Engineering, University of Victoria, PO Box 1700, Stn. CSC, Victoria, BC V8W 2Y2, Canada

ARTICLE INFO

Article history:
Received 28 July 2013
Received in revised form
13 December 2013
Accepted 16 December 2013
Available online 24 January 2014

Keywords:
CHP
Wind
District energy
EnergyPLAN
Ontario

ABSTRACT

In this work, an assessment is conducted of the potential primary energy savings and CO_2 reductions associated with converting a conventional energy system comprising high thermal power plant penetration to one of two configurations. The first configuration consists of widespread DE (District Energy) grids equipped with CHP (Combined Heat and Power) plants, and the second includes wind energy. A model is constructed and five scenarios are evaluated with the EnergyPLAN software taking the province of Ontario, Canada as the case study. Scenario optimization results show that reductions in fuel utilization and CO_2 emissions of up to 8.5% and 32%, respectively, are possible when switching to an energy system comprising widespread CHP based DE grids. A sensitivity analysis reveals that widespread CHP based DE systems have lower fuel utilization and CO_2 emissions than large-scale wind systems for relative installed capacities below approximately 25% of the total generation mix. Differences in fuel utilization and CO_2 emissions of up to 6.4% and 10%, respectively, are observed when comparing outputs from energy systems made up of two distinct CHP technologies, demonstrating the importance of accounting for heat to power ratio in large-scale energy planning studies that incorporate CHP generation.

1. Introduction

DE (District Energy) and wind power are both capable of reducing fossil fuel utilization and CO_2 emissions. The efficiency of wind conversion depends on the wind resource at the site as well as the turbine equipment used [1]. As wind power is intermittent, ancillary services must be provided to the electricity grid at all times to stabilize potential imbalances between supply and demand and maintain voltage and frequency to acceptable levels [2,3]. This is especially true for energy systems with high levels of wind energy penetration. A DE system is an integrated system in which energy is generated locally and is distributed to individual buildings within a network. High energy efficiencies can be achieved in DE systems as loads are aggregated and managed simultaneously, thereby, reducing waste energy streams [4]. Other advantages of DE include increased flexibility, reduced energy costs, increased security of energy supply, and reduced reliance on large-scale conventional generation and transmission infrastructure [5]. A DE system may consist of a single central energy plant, or a series of smaller plants interconnected by pipes that provide steam, hot water, or chilled water to the clients connected to the network. Typical DE system components include boilers, chillers and/or heat pumps for providing heating and cooling services, as well as CHP (Combined Heat and Power) units for supplying both heat and power simultaneously [6]. Depending on location, thermal storage infrastructure may also be added to increase overall efficiency [7].

Various national level modeling studies have been conducted to examine the impacts of expanding CHP-based DE grids on a large scale. Danestig et al. [8] incorporate Stockholm's DE network into a broader national scale model which was used to study the potential for CHP capacity growth in the city. This study showed that when CHP plants with high electricity to heat ratios are used, up to 15% of Sweden's total electricity load can be met by CHP resulting in CO_2 emission reductions of up to 5 million tons per year. Lund et al. [9] modeled the Lithuanian national energy system for a scenario in which one of its largest nuclear power plants is decommissioned. To replace the missing generation capacity, they proposed replacing all boilers in the existing district heating systems with CHP plants. Simulation results show that compared to using new thermal power stations, this strategy would lower both fossil fuel consumption and CO_2 emissions by up to 70%. Münster et al. [10] developed a model of the Denmark energy system and showed that CHP and district heating can contribute to the sustainability and security of supply of future energy systems and that it is cost effective to

* Corresponding author. Tel.: +1 250 853 3180.
E-mail addresses: duquette@uvic.ca (J. Duquette), pwild@uvic.ca (P. Wild), arowe@uvic.ca (A. Rowe).
[1] Tel.: +1 250 721 8901.
[2] Tel.: +1 250 721 8920.

0360-5442/$ – see front matter © 2013 Elsevier Ltd. All rights reserved.
http://dx.doi.org/10.1016/j.energy.2013.12.038

increase the district heating share up to 57% of the total national heat demand.

A number of national level modeling studies have also been conducted to assess the impacts of high penetrations of wind energy. Connolly et al. [11] constructed a model of the Irish energy system to identify maximum feasible levels of wind penetration. They found that a wind penetration of approximately 30% was optimal from both a technical and economic standpoint. Bjelic et al. [12] assessed the large-scale integration of wind power in the Serbian energy system for a number of scenarios. They demonstrated that 2500 MW of installed wind capacity is feasible given that the existing pumped storage hydro capacity is used for balancing purposes. Le and Bhattacharyya [13] modeled the British energy system to assess the optimal wind power integration in 2020 based on the total cost of supply. For the two scenarios considered, they concluded that integrating 80 TWh of wind is preferable from both a technical and economic perspective. Liu et al. [14] developed a model of the Chinese energy system and showed that the maximum feasible wind power penetration is approximately 26%. A similar type large-scale wind integration study was conducted by Hong et al. [15] focusing on the province of Jiangsu in China. The study presents impacts with respect to technical limitations, total fossil fuel consumption, and total emissions from implementing a number of different regulation strategies to the province's energy system.

As described above, the majority of case studies found in the literature focus on the impacts of expanding a particular technology solution (i.e. CHP-based DE grids or wind energy generation) on a nation's energy system. No studies have been identified that compare these two technologies in the context of a large-scale system.

The objective of this research is to compare the impacts from widespread switching to CHP-based DE grids versus widespread switching to wind power in an energy system having significant installed thermal power capacity. The province of Ontario, Canada is chosen as the jurisdiction of study. The current ratio of thermal power plant capacity to peak load in Ontario is approximately 0.42. Models corresponding to a reference scenario and a WDE (Widespread District Energy) scenario are constructed. Reference year energy system components and capacities are considered in the reference model. Boilers, and absorption chillers are considered in the WDE model. Data from 2007 (the reference year) is used to formulate the reference scenario primarily because this is the most recent year for which Canada census data is available. Three WDE scenarios are constructed and compared with the reference scenario on the basis of CO_2 emissions and fossil fuel consumption. An additional scenario is constructed to assess the impacts of expanded wind generation capacity relative to the expanded DE infrastructure scenarios.

The EnergyPLAN analysis tool is used to construct all models and to conduct the simulations. EnergyPLAN was specifically developed for the purpose of planning and designing energy systems consisting of intermittent energy sources and DE networks. The main advantage of EnergyPLAN relative to other energy modeling tools is that it is capable of optimizing an energy system based solely on the technical operation of its components. The model has been used extensively for case studies of large scale wind integration and CHP for Denmark, Ireland, Italy, Germany, Spain, Serbia, China, and the UK [7,11–20].

2. Methodology

2.1. The EnergyPLAN model

EnergyPLAN was originally developed by the Sustainable Energy Planning Research group at Aalborg University, Denmark in 1999. The latest version (i.e. V-10.0) is programmed in Delphi Pascal and provides a user friendly interface consisting of tab sheets. The model utilizes a deterministic, bottom-up approach and incorporates hourly distributions of energy generation and loads for a one year period. If longer time horizons are required, multiple one year blocks may be combined to shape a desired scenario. Model input data comprises energy loads, energy sources, power plant and transmission capacities and related economic data. Outputs are energy balances, fuel consumption, imports/exports as well as total costs including income from the exchange of electricity. The primary purpose of the model is to assist in the design of national or regional energy planning strategies. It is also appropriate for analyzing future energy systems in which the integration of fluctuating energy sources may be an issue [21].

EnergyPLAN encompasses the three primary sectors of an energy system; electricity, heat and transportation. This allows technologies such as CHP, heat pumps, electric vehicles, and hydrogen to be used to balance electricity production and load [22]. The model can be used to optimize an energy system from a technical perspective or from a market perspective. The technical analysis utilizes an optimization algorithm aimed at lowering CO_2 emissions while balancing loads and maintaining a stable electricity grid. The market analysis considers individual generator marginal production costs, internal market prices as well as trade opportunities with neighboring electricity markets. The optimization is based on the fundamental assumption that each plant will generate to maximize profit, taking into consideration any taxes and CO_2 emission costs.

In the current study, EnergyPLAN is used to model the 2007 Ontario energy system from a technical perspective. The energy pathways considered in the model are shown in Fig. 1. All energy flows are load-driven and stem from multiple generation sources. Among the end-use technologies, buildings whose heating and cooling needs are met by DE systems and buildings whose needs are met by individual systems are identified separately.

2.2. Scenario description

Five scenarios are developed in EnergyPLAN, independent of any existing provincial energy plan or strategy. As the focus of the study is purely technical, political and economic constraints are not considered. For each scenario, Table 1 summarizes total heating/cooling loads, conversion technologies, component efficiencies and fuel types for individual buildings and DE grids. Identical conversion technologies and fuel types are used in all scenarios for heating and cooling in individual buildings. Relative contributions and efficiencies of individual building conversion technologies are assumed to follow the distribution shown in Table 2 for all scenarios. Table 2 shows heating/cooling system efficiencies by fuel type as well as the heating to cooling load ratio for individual buildings. In all scenarios, district CHP plants and district boilers run solely on natural gas. All district boilers are assumed to have thermal efficiencies of 85%.

Scenario I is the reference scenario and is based on historical data from 2007 for all sources and loads. Hourly electricity system generation data by type (i.e. Wind, Hydro, Nuclear, Thermal) is obtained from the IESO (Independent Electricity System Operator) [23]. Power plant efficiencies, fuel mix ratios, and CO_2 fuel intensities are procured from Statistics Canada [24]. Electricity generation data is summarized in Table A.1 of the Appendix. Total individual building and DE heating/cooling loads are estimated to be 161 TWh and 6 TWh, respectively. No cooling takes place in the DE networks. The total CHP installed capacity is estimated to be 441 $MW_{(e)}$ with an average thermal efficiency, average electrical efficiency, and a heat-to-power ratio of 50%, 40%, and 1.25,

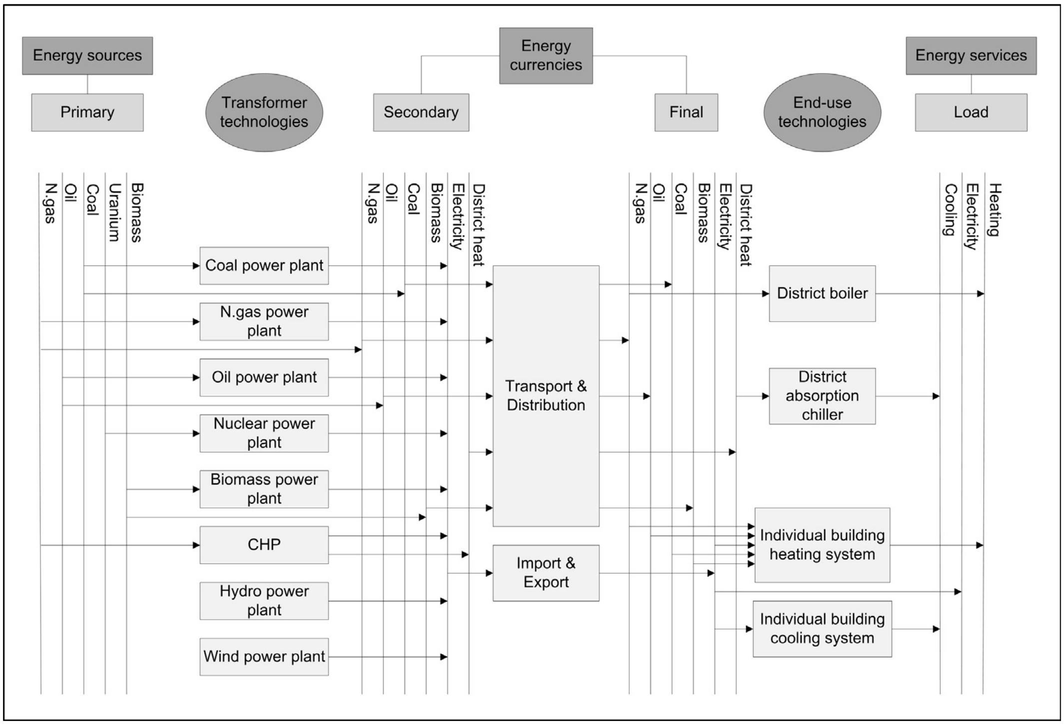

Fig. 1. Energy chains considered in the 2007 Ontario EnergyPLAN model (figure adapted from Refs. [21,43,44]).

respectively. These values are representative of the gas turbine CHP plants typically used by utilities for electricity generation in the province [25].

Scenarios II to IV represent hypothetical configurations of the Ontario energy system. These differ from the reference scenario in that approximately 60% of the total residential and commercial heating and cooling load is transferred from individual building systems to DE networks. A value of 60% is chosen since it is equivalent to the percentage of buildings in the province located in areas with population densities greater or equal to 400 inhabitants per km^2 [26]. The total individual building and DE heating/cooling loads are estimated to be 67 TWh and 100 TWh, respectively, in Scenarios II to IV. It is assumed that the heating to cooling load ratio for individual buildings shown in Table 2 applies to DE grids in Scenarios II to IV. In these scenarios, cooling takes place in the DE networks via single-effect absorption chillers with a COP (Coefficient of Performance) of 0.7 [27]. In Scenario II, total CHP installed capacity is zero. In Scenario III, total CHP installed capacity is 6800 $MW_{(e)}$ with average thermal efficiency, average electrical efficiency, and heat-to-power ratio of 70%, 14%, and 5, respectively. In Scenario IV, total CHP installed capacity is 6800 $MW_{(e)}$ with average thermal efficiency, average electrical efficiency, and heat-to-power ratio of 27.5%, 55%, and 0.5, respectively. Efficiency and heat-to-power ratios for Scenarios III and IV are representative of BPST (Back Pressure Steam Turbine) CHP plants and CCGT (Combined Cycle Gas Turbine) CHP plants, respectively. These are selected as they represent two extremes on the scale of heat-to-power ratio. For each CHP technology, installed capacity is set to 6800 $MW_{(e)}$, equivalent to 25% of the total power plant installed capacity in the reference year (see Table A.1 in Appendix).

Table 1
Annual heating/cooling (H/C) loads for Reference, Widespread District Energy (WDE), and Wind scenarios (IB, BPST, CCGT, NG, η_{th}, η_e, and htp refer to individual buildings, back pressure steam turbine, combined cycle gas turbine, natural gas, thermal efficiency, electrical efficiency, and heat-to-power ratio, respectively).

Scenario			I	II	III	IV	V
			Reference	WDE – No CHP	WDE – BPST	WDE – CCGT	Wind
Total H/C loads (TWh)	IB		161	67	67	67	161
	DE		6	100	100	100	6
Conversion technologies	IB	Heating	Boiler, furnace, radiator	Boiler, furnace, radiator	Boiler, furnace, radiator	Boiler, furnace, radiator	Boiler, furnace, radiator
		Cooling	Air conditioner	Air conditioner	Air conditioner	Air conditioner	Air conditioner
	DE	Heating	Boiler (η_{th} = 85%), CHP (η_{th} = 50%, η_e = 40%, htp = 1.25)	Boiler (η_{th} = 85%)	Boiler (η_{th} = 85%), BPST-CHP (η_{th} = 70%, η_e = 14%, htp = 5)	Boiler (η_{th} = 85%), CCGT-CHP (η_{th} = 27.5%, η_e = 55%, htp = 0.5)	Boiler (η_{th} = 85%), CHP (η_{th} = 50%, η_e = 40%, htp = 1.25)
		Cooling	None	Absorption chiller (COP = 0.7)	Absorption chiller (COP = 0.7)	Absorption chiller (COP = 0.7)	None
Fuel type	IB	Heating	NG, electric, oil, biomass	NG, electric, oil, biomass	NG, electric, oil, biomass	NG, electric, oil, biomass	NG, electric, oil, biomass
		Cooling	Electric	Electric	Electric	Electric	Electric
	DE	Heating	NG	NG	NG	NG	NG
		Cooling	None	NG	NG	NG	None

Table 2
2007 Total annual Individual Building (IB) Heating and Cooling (H/C) loads by fuel type (η_{th} and α refer to thermal efficiency and fuel consumption, respectively).

IB H/C fuel type	[a]α (TWh)	η_{th} (%) [34]	[b]Heating load (TWh)	[b]Cooling load (TWh)
Oil	8.3	83	6.9	0
Natural gas	106.7	91	97.1	0
Biomass	5.3	70	3.7	0
Electricity for heating	33.7	100	33.7	0
Electricity for cooling	6.5	3 (COP)	0	19.5
Totals	160.5	–	141.5	19.5

[a] Based on Table A.2, Appendix.
[b] Calculated.

Scenario V is identical to Scenario I but with increased wind capacity. Total wind capacity is set to 6800 $MW_{(e)}$ in Scenario V to enable comparison of results with those of Scenarios III and IV.

2.3. Scenario dispatch strategy

A technical dispatch strategy is used to reallocate hourly energy generation by generator type for Scenarios I to V with the objective of minimizing fossil fuel consumption. For all cases, hourly changes in generation mixtures are permitted but the hourly electrical demand profile is constant. Hourly outputs from LTPP (Large Thermal Power Plants), CHP and wind are variable in the model. Generation from hydro and nuclear plants is set at their 2007 hourly values, as are imports and exports. All CHP systems in the model require a thermal (i.e. heating/cooling) load to operate. Therefore, at times when no thermal load is present, the CHP units cannot be dispatched. EnergyPLAN meets the hourly thermal load by dispatching available CHP plants first, followed by boilers to make up the thermal balance. CHP installed capacity is set as described in Section 2.2 whereas boiler installed capacity is selected by the model.

The technical dispatch strategy is depicted in Fig. 2. Scenario input data is comprised of hourly distributions of sources and loads and installed capacities of wind and CHP, as shown in the “Scenario input data” box, in Fig. 2. Hourly available wind power distributions are computed by scaling the 2007 hourly wind power data based on installed wind capacity. The hourly distributions and capacities vary by scenario. Fig. 2 shows an iterative dispatch algorithm that is repeated at each hourly time step for a year, as follows:

1) Set hourly values for hydro, nuclear, imports, and exports are dispatched;
2) DE heating/cooling loads are met (i). CHP is either dispatched until the heating/cooling load is met, at which point the process goes on, or until either CHP capacity is reached or the electricity load is met. If the latter is the case, boilers are dispatched accordingly to satisfy the condition;
3) Electricity loads are met (ii). If wind power is available (iii), it will either be dispatched until the electricity load is met, at which point the process continues, or until wind capacity is reached. In the latter case or if no wind power is available (iii), LTPP is dispatched to meet the load;

Hourly outputs from the technical dispatch are shown in the “Scenario output data” box, in Fig. 2.

2.4. Estimation of hourly heating and cooling load distributions

2.4.1. Space heating

The hourly space heating load distribution is estimated for the province of Ontario using the HDD (Heating Degree Day) analysis

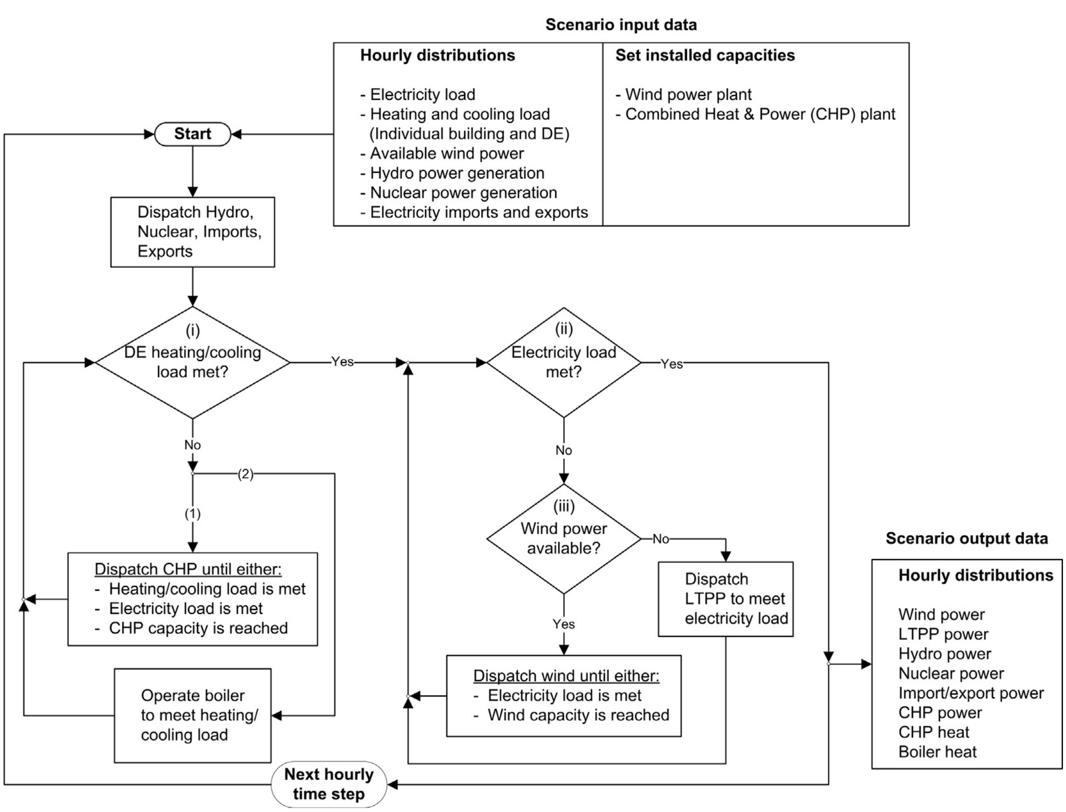

Fig. 2. EnergyPLAN technical dispatch algorithm.

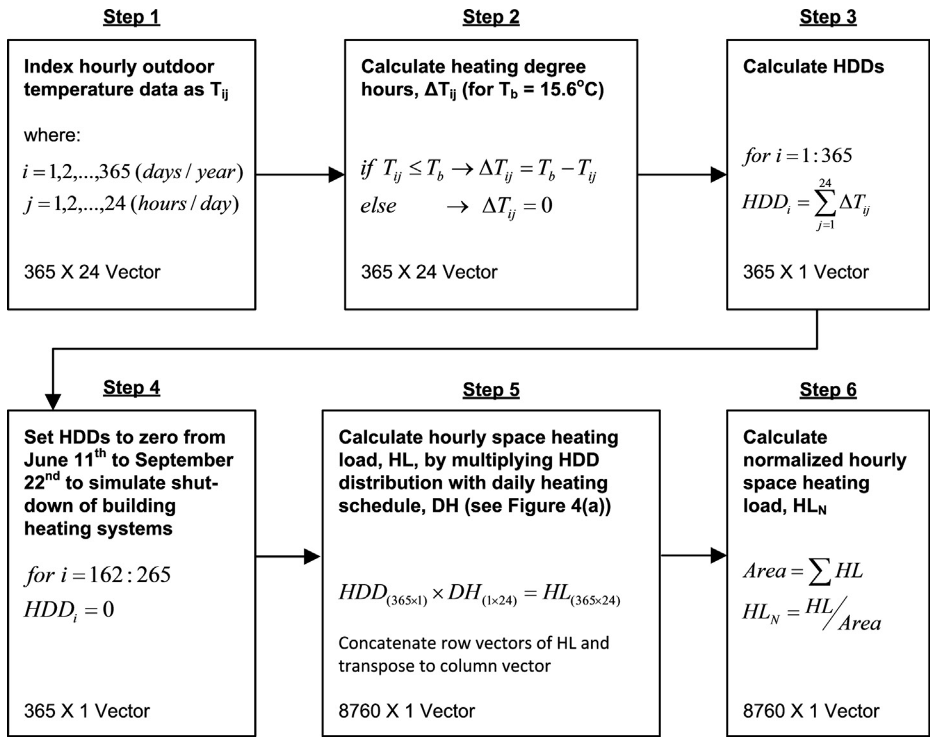

Fig. 3. Steps taken to estimate hourly space heating load over the period of a year.

method outlined by Connoly in Refs. [28] [29], [22]. HDDs quantify the variation in outdoor temperature, T, relative to a predetermined base temperature, T_b, and are indicative of the amount of heating required on a given day. More information on HDD analysis can be obtained from Ref. [30]. Following local design practice, a base temperature of 15.6 °C is used in the present study [30]. As it is difficult to account for outdoor temperature variations over the entire province, data from the city of Toronto is chosen to represent the whole of Ontario in the study. The choice is based on the fact that a large proportion of the province's population and buildings are located in or near this city. Hourly recorded outdoor temperatures for Toronto are acquired from the Environment Canada online database for the reference year [31]. The steps taken and equations used [22,28,29] to estimate the space heating load distribution over the year, HL_N, are illustrated in Fig. 3.

In step 5, an average daily heating schedule (Fig. 4(a)) is introduced into the dataset to estimate periods of time in which home heating systems are likely to be on due to thermostat regulation [32]. The schedules illustrated in Fig. 4(a) and (b) are normalized to the peak daily heating and cooling loads, respectively. Consequently, Fig. 4(a) and (b) is unitless. In step 6, a normalized hourly space heating load distribution is obtained for the province.

2.4.2. Water heating

Unlike space heating, water heating loads are not assumed to be proportional to HDDs [33]. Rather, the water heating load is assumed to be constant as a result of the smoothing effects of the aggregation of many individual loads [28] [29], [22]. Table A.2 of the Appendix shows residential and commercial secondary energy use for space heating and water heating, respectively. These values correspond to a total water heating to space heating load ratio of approximately 1:3.

2.4.3. Space cooling

The estimated hourly space cooling load distribution is based on CDD (Cooling Degree Days), which is a variation on the HDD method [22]. This method is illustrated in Fig. 5.

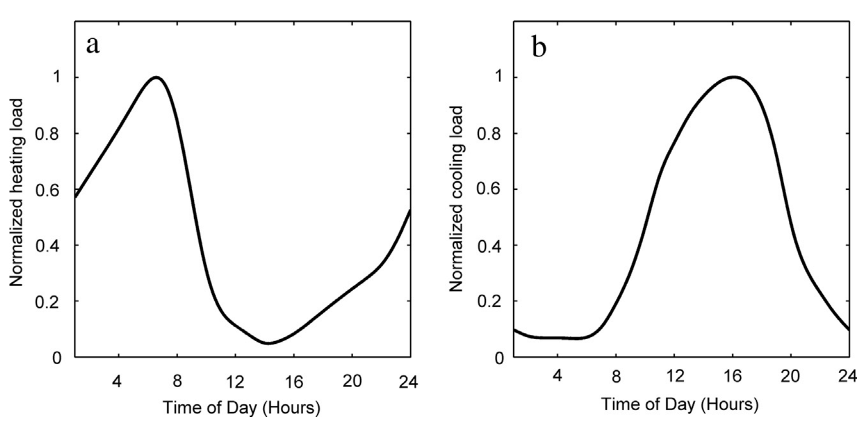

Fig. 4. a. Average daily heating schedule. b. Average daily cooling schedule.

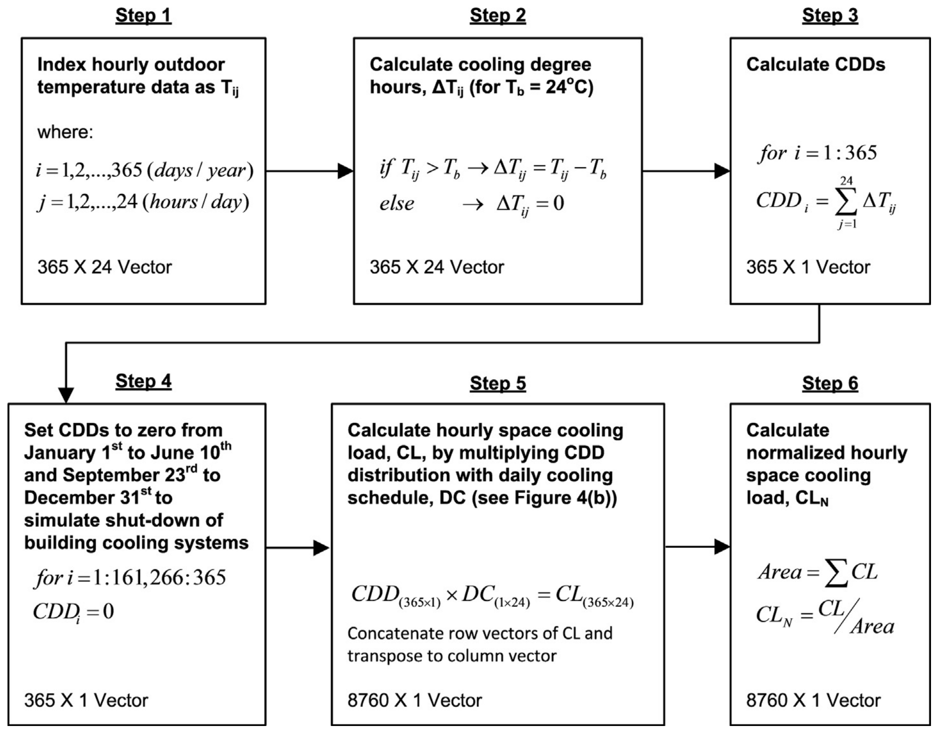

Fig. 5. Steps taken to estimate hourly space cooling load over the period of a year.

2.4.4. Scaling factors for individual buildings

Total annual heating and cooling loads for individual buildings are calculated for the residential and commercial sectors. The industrial sector is not included in the analysis due to lack of available data. These loads are estimated by attributing either a thermal efficiency or a COP (Coefficient of Performance) to fuel consumption rates (Table 2). The thermal efficiencies for each heating system type are obtained from the Ontario Ministry of Energy [34] and it is assumed that the entire space cooling load is met using electrical devices (i.e. air conditioners) with an average COP of 3.0 [27]. The resulting loads, shown in Table 2, (141.5 TWh and 19.5 TWh) are used to scale the normalized hourly heating and cooling load distributions estimated in Sections 2.4.1 to 2.4.3. The scaling is accomplished by setting the area under the normalized distribution equal to the total annual load.

2.5. Estimation of annual district energy load

The total heating load met by DE systems in the reference year is based on data obtained from a HLDC (Heating Load Duration Curve). The steps taken to obtain the HLDC are as follows: (1) the normalized space and water heating loads (Section 2.4) are summed for each time step; (2) a histogram is constructed from the data; (3) a cumulative distribution is plotted and displayed with largest load on the left and smallest load on the right [35]; (4) the cumulative distribution is scaled to obtain the HLDC. The amount by which the cumulative distribution is scaled is determined from a commonly used design guideline for sizing CHP systems [36]. This guideline specifies that the heating load should be met by CHP systems for at least 5000 h of the year. Ontario's total CHP capacity for the reference year is estimated to be 441 $MW_{(e)}$. This is equivalent to a thermal capacity of 551 $MW_{(th)}$ assuming an electrical efficiency of 40% and a thermal efficiency of 50%. The HLDC is found by increasing the area under the cumulative distribution up to the point where the total CHP thermal capacity (i.e. 551 $MW_{(th)}$) meets all heating loads for 5000 h of the year.

The calculated HLDC is shown in Fig. 6. Important design parameters are also labeled in Fig. 6. All loads below 551 MW are met with CHP while all loads above are met with boilers. A total annual DE heating load of approximately 6 TWh is estimated by summing the area under the curve in Fig. 6. Additional heat distribution losses of 10% are added to this total in the EnergyPLAN model.

3. Model validation

A twofold approach is used to verify that the reference scenario is representative of the 2007 Ontario energy system for the sectors considered. First, documented hourly LTPP outputs for the reference year are compared with those calculated by the EnergyPLAN model. A comparison of the datasets reveals a high degree of overlap. The average hourly difference between datasets is

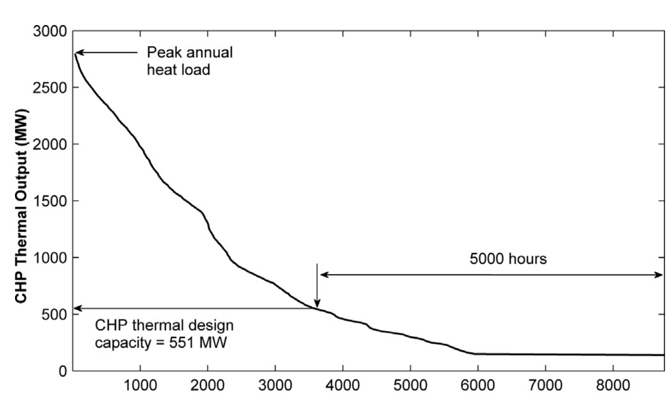

Fig. 6. Estimated 2007 Ontario DE heating load-duration curve.

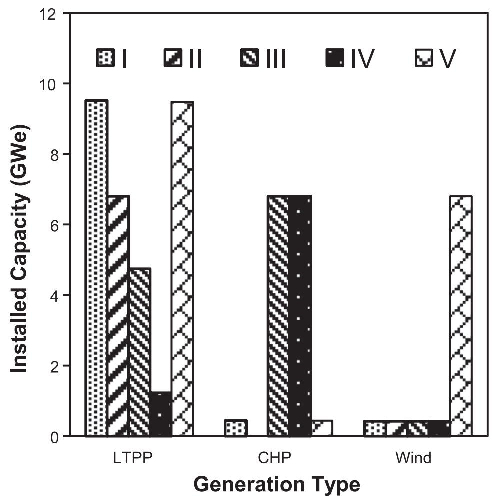

Fig. 7. Minimum installed capacity by scenario required for system balance.

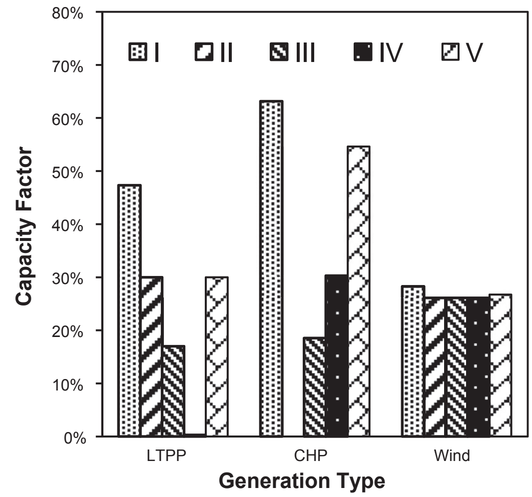

Fig. 9. Capacity factor by scenario.

calculated to be 1.6% indicating a close match between the reference scenario and the actual electrical system. Secondly, documented CO_2 emissions from the reference year are compared with those calculated by the EnergyPLAN model for the residential, commercial, and electricity sectors combined. Total CO_2 emissions in Ontario for 2007 are 63 $MtCO_{2(e)}$ [37] while EnergyPLAN calculates CO_2 emissions of 59 $MtCO_{2(e)}$ for the reference scenario. As these modeled emissions are within 7% of the documented emissions, the reference scenario is considered to be an acceptable basis for comparison in the study.

4. Results and discussion

A technical dispatch strategy is applied to Scenarios I to V. For all scenarios, a stable electrical grid is maintained at all times since at least 60% of all generation is supplied by generators capable of providing ancillary services such as frequency support, voltage support, and operating reserves [38]. For the 2007 Ontario system, these are nuclear, hydro, CHP, or LTPP generators. Wind generators cannot provide ancillary services.

The main results of the study are illustrated in Figs. 7–11. Fig. 7 shows the minimum installed capacity by generator type required for balancing the electricity load in each of the five scenarios. LTPP installed capacity is highest in Scenario I (9.5 $GW_{(e)}$) and lowest (1.2 $GW_{(e)}$) in Scenario IV. The drop in LTPP capacity from Scenario I to Scenario II is attributed to DE boilers displacing electrical heating and cooling devices previously installed in individual buildings. Further reductions in LTPP capacity in Scenarios III and IV are related to the respective increases in efficiency brought on by a larger installed capacity of BPST-CHP and CCGT-CHP plants in the system.

Scenario IV has the lowest LTPP capacity due to the high electrical efficiencies associated with CCGT-CHP plants. Most of this capacity is required to meet the high peak power loads encountered during the hot summer months. During the summer, there is a significant mismatch between daily DE peak loads and electrical peak loads. This effect is illustrated in Fig. 8(a) and (b), which show electrical power and DE thermal load time series data, respectively, for Scenario IV during a three day period in August. Data used for

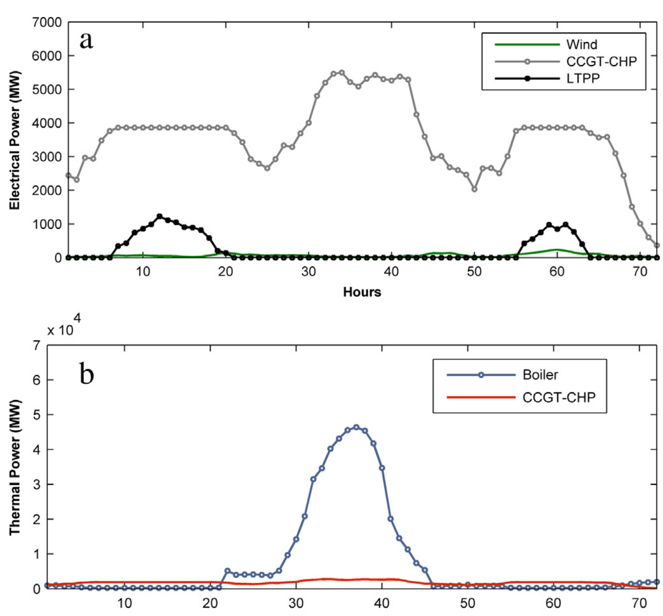

Fig. 8. a: Scenario IV Hourly electricity output for three days in August. b: Scenario IV Hourly DE heating output for three days in August.

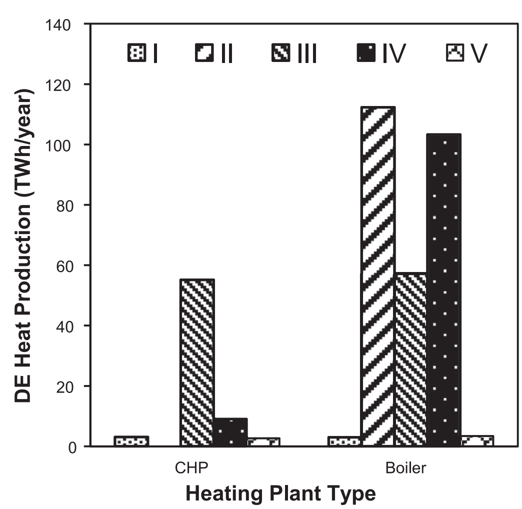

Fig. 10. DE heat production by scenario.

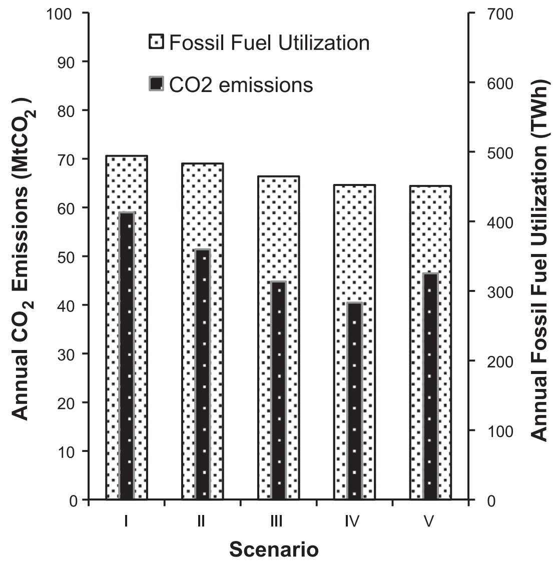

Fig. 11. Total fossil fuel utilization and CO_2 emissions by scenario.

Fig. 8(a) and (b) are taken over a 72 h period from August 23rd, 2007 at 5 am to August 26th, 2007 at 5 am. Since imports, exports, hydro and nuclear outputs are fixed, these are omitted from the figures for clarity. Fig. 8(a) shows LTPPs coming online at hours 6 to 20 and hours 55 to 64. Although sufficient CCGT-CHP capacity is available to meet the electrical load during these periods, these units cannot operate due to the low DE thermal load requirement at these times (Fig. 8(b)). Similarly, Fig. 8(b) shows boilers coming online at hours 21 to 46 primarily to meet the cooling load via absorption chillers. The cooling load is particularly high on August, 24th relative to neighboring days due to the outdoor temperature being well above 24 °C, the base temperature used for calculating CDDs (Fig. 5), for the majority of the day. CCGT-CHP plants are unable to meet a larger share of the DE thermal load during this period since their operation is limited by the electrical load (Fig. 8(a)). As a consequence of the peak load mismatch portrayed in Fig. 8(a) and (b), CHP plants are not always able to operate at full capacity when needed and, as a result, LTPP capacity is required.

Since Scenario V builds on to Scenario I only with respect to increased wind capacity (no WDE network is present), the LTPP installed capacities (Fig. 7) are equivalent (i.e. 9.5 $GW_{(e)}$). The high LTPP capacity requirement in Scenario V is primarily due to: (1) the absence of a WDE network which creates a need for electrical heating and cooling in individual buildings; (2) the need for backup generation for intermittent wind generation.

Fig. 9 shows the capacity factors in each scenario by generation type. Capacity factor is the ratio of the electrical energy generated to the electrical energy generated for operation at full capacity. The capacity factor for LTPPs drops progressively from 48% in Scenario I to approximately 0.5% in Scenario IV. The LTPP capacity factor in Scenario V is 30%. The capacity factors for CHP in Scenarios I and V are relatively high at 63% and 55%, respectively. In Scenario IV, a small increase occurs from 19% to 30% relative to Scenario III due to the higher electrical efficiencies common to CCGT-CHP plants. The lower CHP capacity factors for Scenarios III and IV can be explained by the fact that CHP units are being dispatched solely to displace LTPPs. In a scenario where electricity exports are permitted, higher CHP penetration in the grid would occur.

The increase in CHP capacity factor from Scenario III to Scenario IV, shown in Fig. 9, is directly proportional to the increase in total annual electricity production between scenarios. The total annual heat production in Scenario IV is, however, less than in Scenario III. Fig. 10 illustrates the annual DE heat production for CHP plants and boilers by scenario. In Scenario II, the full DE thermal load (i.e. 110 TWh) is met by boilers. In Scenario III, CHP heat production is greater than in Scenario IV (57 TWh relative to 9 TWh, respectively) due to the higher thermal efficiencies common to BPST-CHP plants.

The results for Scenarios III and IV (Figs. 9 and 10) demonstrate that electricity and heat outputs vary widely depending on the CHP technology used, bringing to light the importance of CHP heat to power ratio in the design of WDE systems.

Fig. 11 illustrates total fossil fuel utilization and CO_2 emissions by scenario. All WDE scenarios in Fig. 11 show reduced fossil fuel utilization and CO_2 emissions, relative to Scenario I. Reductions of 8.5% and 32% are observed for Scenario IV relative to Scenario I, respectively. Reductions of 6.4% and 10% are observed for Scenario IV relative to Scenario III, respectively. Reductions from Scenario III to Scenario IV are directly related to the heat to power ratio of the distinct combined heat and power technologies used in each scenario. Lower fossil fuel utilization occurs as a result of overall system efficiency improvements and lower CO_2 emissions are attributed to natural gas CHP plants displacing thermal plants that use high carbon intensity fuels.

In Scenario V, fuel use and emissions are 8.7% and 21% lower than in Scenario 1 (Fig. 11). Since these reductions are nearly equivalent to those achieved in Scenario IV, one may question the value of investing in an energy system comprised of WDE over maintaining a conventional system and investing in large-scale wind power. To answer this question, a sensitivity analysis is performed. Fossil fuel utilization and CO_2 emission reductions are calculated for Scenarios III to V using the EnergyPLAN technical dispatch algorithm and plotted as a function of installed CHP capacity (Scenarios III and IV) and installed wind capacity (Scenario V) in Figs. 12 and 13. Previously, only a single installed capacity set point of 6800 $MW_{(e)}$ was considered in the analysis.

Fig. 12 shows that Scenarios III and IV achieve lower fossil fuel utilization than Scenario V for all installed capacity set points lower than approximately 4500 $MW_{(e)}$ and 6500 $MW_{(e)}$, respectively. This effect is due to the reduced electricity load from displacing electrical heating and cooling in individual buildings with DE services and the increase in overall system efficiency from adding CHP plants.

Fig. 13 shows that Scenarios III and IV achieve lower CO_2 emissions than Scenario V for all installed capacity set points lower than approximately 8000 $MW_{(e)}$ and 12000 $MW_{(e)}$,

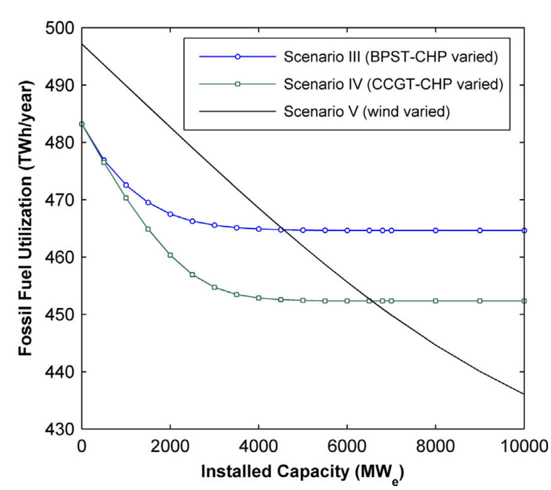

Fig. 12. Optimized fossil fuel utilization as a function of installed CHP/wind capacity.

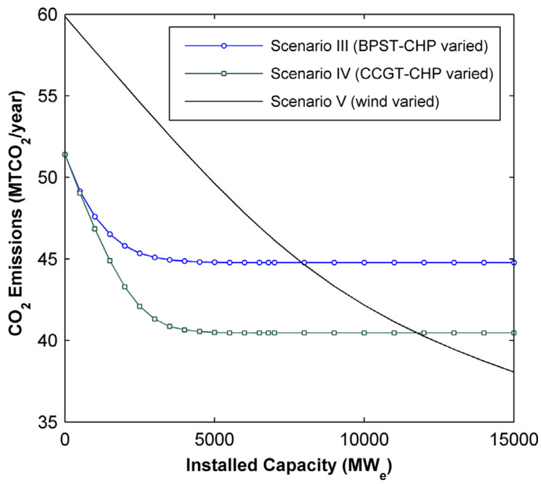

Fig. 13. Optimized CO_2 emissions as a function of installed CHP/wind capacity.

respectively. As in Fig. 12, this effect is due to the reduced electricity load from displacing electrical heating and cooling in individual buildings with DE services. This effect is also due to natural gas CHP plants displacing thermal plants that use high carbon intensity fuels. Approximately 70% of the total annual LTPP electricity generation in Scenario I is fueled from coal and oil, both highly carbon intensive fuels. Although large reductions in CO_2 emissions are possible in the current energy system by fuel switching, the same may not hold true for a different jurisdiction with a different energy mix.

The current analysis shows that there are clear advantages and disadvantages to expanding either CHP based DE systems or wind systems on a large scale. If a choice were to be made between these technologies solely based on reduced fossil fuel utilization and reduced CO_2 emissions, CCGT-CHP based DE systems would clearly be the preferred option. This is demonstrated in Fig. 12, which shows that CCGT – CHP based DE systems have lower fossil fuel utilization than wind for all installed capacity values below approximately 6500 $MW_{(e)}$, the point where both curves intersect. Since at 6500 $MW_{(e)}$, the wind power capacity to peak load ratio is approximately 0.3, a relatively high value that is seldom exceeded due to grid stability issues, this intersection point can be treated as an upper limit to wind penetration in the energy system.

In a more realistic context however, many other factors would need to be taken into account when choosing between technologies. For example, even though reductions in fossil fuel utilization are significant with conventional large-scale wind (Scenario V), high LTPP installed capacities are required for back-up generation. Conversely, CCGT-CHP based DE requires little LTPP back-up (Scenario IV). However, low thermal efficiencies in Scenario IV mean that a higher boiler capacity is needed. These factors need consideration as they play into the economic feasibility of the system. Although economics are not covered, this study demonstrates the potential impacts of introducing widespread DE networks comprised of natural gas-fired CHP plants and wind systems in the province of Ontario. Rising energy loads in the near future could potentially be met by increasing the installed capacity of such technologies without needing to eliminate the existing LTPP capacity.

5. Conclusions

The 2007 Ontario reference energy system was constructed in the EnergyPLAN environment. Three WDE (Widespread District Energy) scenarios as well a large-scale wind scenario were analyzed. A technical dispatch was performed on all scenarios with the objective of minimizing total system fossil fuel utilization when the total hourly electricity generation is fixed in all scenarios. Reductions in fossil fuel utilization and CO_2 emissions of up to 8.5% and 32%, respectively, were found to take place when switching to an energy system comprising widespread combined heat and power based district energy grids. A sensitivity analysis was performed showing that widespread CHP-based DE systems have lower fossil fuel utilization and CO_2 emissions than large-scale wind systems for relative installed capacities below approximately 25% of the total generation mix. CCGT plants are favored relative to BPST plants with respect to savings in fossil fuel utilization and CO_2 emissions as reductions of up to 6.4% and 10%, respectively, were observed. This is directly due to the high electrical efficiency and low heat to power ratio of CCGT-CHP plants. The results of this study are applicable to other jurisdictions with similar energy mix who are faced with decisions on how to best proceed with future energy infrastructure investments. The results also bring to light the importance of accounting for heat to power ratio in large-scale energy planning studies that incorporate CHP generation.

Appendix

Table A.1
Ontario 2007 electricity system data [23,24].

Power plant data

Power Plant Type	Installed Capacity (MW)	Total Annual Generation (TWh)	Efficiency (%)	Peak Load (MW)
Wind	420	1.04	-	21400
Hydro	6050	32.8	-	
Nuclear	10820	80.3	32	
Thermal	9558	41.3	34	
Total	26850	156		

Thermal plant data

Thermal Plant Fuel Type	Total Annual Generation (GWh)	CO_2 Intensity of Fuel (kg/GJ)
Coal	27932	93
Oil	270	78
Natural Gas	12532	56
Biomass	518	0

Electricity imports & exports to neighbouring provinces and the US

Total Annual Exports (TWh)	Total Annual Imports (TWh)
12.2	7.2

Table A.2
Ontario 2007 energy use data [37,39–41].

<table>
<tr><td colspan="2">Total secondary energy use</td><td colspan="5">739 TWh</td></tr>
<tr><td colspan="7">Secondary energy use by sector</td></tr>
<tr><td>Sector</td><td>Residential</td><td>Commercial</td><td>Industrial</td><td>Agricultural</td><td>Transportation</td><td>Other</td></tr>
<tr><td>%</td><td>19</td><td>10</td><td>27</td><td>2</td><td>33</td><td>9</td></tr>
<tr><td colspan="7">Residential secondary energy use by end use</td></tr>
<tr><td>End use</td><td>Space Heating</td><td>Water Heating</td><td>Space Cooling</td><td>Lighting</td><td colspan="2">Appliances</td></tr>
<tr><td>%</td><td>59</td><td>22</td><td>2</td><td>4</td><td colspan="2">13</td></tr>
<tr><td colspan="7">Commercial secondary energy use by end use</td></tr>
<tr><td>End use</td><td>Space Heating</td><td>Water Heating</td><td>Space Cooling</td><td>Lighting</td><td colspan="2">Other</td></tr>
<tr><td>%</td><td>48</td><td>8</td><td>5</td><td>12</td><td colspan="2">27</td></tr>
<tr><td colspan="7">Principal heating fuels in residential sector</td></tr>
<tr><td>Type</td><td>Electricity (%)</td><td colspan="2">Natural gas (%)</td><td>Oil (%)</td><td colspan="2">Wood & other (%)</td></tr>
<tr><td>Space Heating</td><td>19</td><td colspan="2">68</td><td>7</td><td colspan="2">6</td></tr>
<tr><td>Water Heating</td><td>26</td><td colspan="2">70</td><td>4</td><td colspan="2">2</td></tr>
<tr><td colspan="7">Principal heating fuels in commercial sector</td></tr>
<tr><td>Type</td><td colspan="2">Electricity (%)</td><td colspan="2">Natural gas (%)</td><td colspan="2">Other (%)</td></tr>
<tr><td>Space Heating</td><td colspan="2">20</td><td colspan="2">73</td><td colspan="2">7</td></tr>
<tr><td>Water Heating</td><td colspan="2">51</td><td colspan="2">49</td><td colspan="2">0</td></tr>
</table>

Table A.3
Ontario 2007 grid-tied CHP penetration [25,42].

<table>
<tr><td>Total installed grid-tied CHP</td><td colspan="2">2741 $MW_{(e)}$</td></tr>
<tr><td colspan="3">Grid-tied CHP distribution by sector</td></tr>
<tr><td>Sector</td><td>Industrial</td><td>Commercial</td></tr>
<tr><td>%</td><td>84</td><td>16</td></tr>
<tr><td>Total CHP capacity considered in analysis</td><td colspan="2">441 $MW_{(e)}$</td></tr>
</table>

References

[1] de Prada Gil M, Gomis-Bellmunt O, Sumper A, Bergas-Jané J. Power generation efficiency analysis of offshore wind farms connected to a SLPC (single large power converter) operated with variable frequencies considering wake effects. Energy 2012;37:455–68.
[2] Lund H. Large-scale integration of wind power into different energy systems. Energy 2005;30:2402–12.
[3] Lund H. Electric grid stability and the design of sustainable energy systems. Int J Sustain Energy 2005;24:45–54.
[4] Joelsson A, Gustavsson L. District heating and energy efficiency in detached houses of differing size and construction. Appl Energy 2009;86:126–34.
[5] CDEA. District energy – a national survey report. Canadian District Energy Association; 2008.
[6] Skagestad B, Mildenstein P. IEA – district heating and cooling connection handbook; 2000.
[7] Andersen A. DESIRE – CHP plants with big thermal stores balancing fluctuating productions from wind turbines; 2007.
[8] Danestig M, Gebremehdin A, Karlsson B. Stockholm CHP potential—an opportunity for CO_2 reductions? Energy Policy 2007;35:4650–60.
[9] Lund H, Šiupšinskas G, Martinaitis V. Implementation strategy for small CHP-plants in a competitive market: the case of Lithuania. Appl Energy 2005;82:214–27.
[10] Münster M, Morthorst PE, Larsen HV, Bregnbæk L, Werling J, Lindboe HH, et al. The role of district heating in the future Danish energy system. Energy 2012;48:47–55.
[11] Connolly D, Lund H, Mathiesen BV, Leahy M. Modelling the existing Irish energy-system to identify future energy costs and the maximum wind penetration feasible. Energy 2010;35:2164–73.
[12] Batas Bjelić I, Rajaković N, Ćosić B, Duić N. Increasing wind power penetration into the existing Serbian energy system. Energy 2013;57:30–7.
[13] Le NA, Bhattacharyya SC. Integration of wind power into the British system in 2020. Energy 2011;36:5975–83.
[14] Liu W, Lund H, Mathiesen BV. Large-scale integration of wind power into the existing Chinese energy system. Energy 2011;36:4753–60.
[15] Hong L, Lund H, Möller B. The importance of flexible power plant operation for Jiangsu's wind integration. Energy 2012;41:499–507.
[16] Lund H. Large-scale integration of optimal combinations of PV, wind and wave power into the electricity supply. Renew Energy 2006;31:503–15.
[17] Henrik L. Large-scale integration of wind power into different energy systems. Energy 2005;30:2402–12.
[18] Lund H, Münster E. Management of surplus electricity-production from a fluctuating renewable-energy source. Appl Energy 2003;76:65–74.
[19] Lund H, Münster E. Modelling of energy systems with a high percentage of CHP and wind power. Renew Energy 2003;28:2179–93.
[20] Franco A, Salza P. Strategies for optimal penetration of intermittent renewables in complex energy systems based on techno-operational objectives. Renew Energy 2011;36:743–53.
[21] Lund H. EnergyPLAN – advanced energy systems analysis computer model – documentation version 9.0; 2011.
[22] Connolly DA. User's guide to EnergyPLAN; 2010.
[23] IESO. Generator reports. Independent Electricity System Operator; 2011.
[24] StatsCan. Statistics Canada. Electric power generation, transmission and distribution; 2007.
[25] Strickland C, Nyboer J. A review of existing cogeneration facilities in Canada; 2004.
[26] HRSDC. Human Resources and Skills Development Canada. Indicators of well-being in Canada; 2011.
[27] ASHRAE. Thermodynamics and refrigeration cycles. USA. In: Anonymous ASHRAE fundamentals handbook (SI) 1997. 1.14–20.
[28] Connolly D, Lund H, Mathiesen BV. Developing a model of the Irish energy-system. In: Proceedings of the joint action on climate change, Aalborg 2009.
[29] Connolly D, Lund H, Mathiesen BV, Leahy M. The first step towards a 100% renewable energy-system for Ireland. Appl Energy 2011;88:502–7.
[30] ASHRAE. Energy estimating and modeling methods. USA. In: American Society of Heating, Refrigeration and Air-Conditioning Engineers, Inc, editor. ASHRAE fundamentals handbook (SI) 1997. 30.1–30.30.
[31] Environment Canada. Weather office – historical weather; 2012.
[32] Bouchelle MP, Parker DS, Anello MT, Richardson KM. Factors influencing space heat and heat pump efficiency from a large-scale residential monitoring study; 2000.
[33] Aguilar C, White DJ, Ryan DL. Domestic water heating and water heater energy consumption in Canada; 2005.
[34] OME. Ontario Ministry of Energy. Heating & cooling guide: comparing energy costs; 2011.
[35] RETScreen International. RETScreen software – online user manual – combined heat & power project model; 2005.
[36] Salehi GR, Taghdiri E, Deldadeh D. Examining the effect of heat storage in a cogeneration system; 2011. pp. 780–7.
[37] NRCan. Natural Resources Canada – Office of Energy Efficiency. Comprehensive energy use database, 1990-2008; 2011.
[38] Stoft S. Power system economics – designing markets for electricity. New York: Wiley-Interscience; 2002.

[39] NRCan. Natural Resources Canada. Survey of household energy use 2007—a summary report; 2007.
[40] NRCan. Natural Resources Canada. 2008 commercial & institutional consumption of energy survey – summary report; 2011.
[41] CME. Advancing opportunities in energy management in Ontario industrial and manufacturing sector; 2010.
[42] IESO. Independent Electricity System Operator. September monthly generator disclosure report; 2007.
[43] IAEA. MESSAGE – model for energy supply strategy alternatives and their general environmental impacts – user manual; 2003.
[44] Scott DS. Smelling land – the hydrogen defense against climate catastrophe. Canadian Hydrogen Association; 2007.

Appendix B:

Thermal performance of a steady state physical pipe model for simulating district heating grids with variable flow

Duquette J, Rowe A, Wild P. Thermal performance of a steady state physical pipe model for simulating district heating grids with variable flow. Appl Energy 2016;178:383–93. doi:10.1016/j.apenergy.2016.06.092.

Applied Energy 178 (2016) 383–393

Contents lists available at ScienceDirect

Applied Energy

journal homepage: www.elsevier.com/locate/apenergy

Thermal performance of a steady state physical pipe model for simulating district heating grids with variable flow

Jean Duquette *, Andrew Rowe, Peter Wild

Institute for Integrated Energy Systems, Department of Mechanical Engineering, University of Victoria, PO Box 1700, Stn. CSC, Victoria, BC V8W 2Y2, Canada

HIGHLIGHTS

- A steady state variable transport delay (SS-VTD) pipe model is constructed.
- The SS-VTD model is used for simulating variable flow district heating grids.
- A transient model is used to assess the error and speed of the SS-VTD model.
- Simulation results from the SS-VTD model are highly sensitive to varying time step size.
- The SS-VTD model is roughly 3 orders of magnitude faster than the transient model.

ARTICLE INFO

Article history:
Received 15 October 2015
Received in revised form 2 June 2016
Accepted 18 June 2016

Keywords:
District heating
Physical pipe model
Variable flow
Variable transport delay
Simulation

ABSTRACT

Modern district heating grids are typically operated using variable flow control. Challenges arise when modeling thermal interactions in variable flow networks as tracking of transport delays is required. In this work, a pipe model is constructed using a steady state heat transfer model combined with a variable transport delay model. The resulting model (*i.e.* the SS-VTD model) is validated experimentally using measured data from a district energy grid located in Saanich, Canada. Modeling error and computational intensity of the SS-VTD model are assessed numerically by comparing simulation outputs with those obtained using a transient model (*i.e.* the 1D-PDE model). Matlab®/Simulink® software is used to construct the models and conduct the simulations. Fifteen scenarios are simulated over a range of time step sizes and pipe segment lengths. In all scenarios, decreasing pipe segment length and/or time step size results in greater computational intensity. Varying pipe segment length is found to have a minimal impact on the error of the SS-VTD model, whereas varying time step size is found to have a significant impact. Results show that when compared with the 1D-PDE model at the same fixed time step of 1 s, the computational intensity of the SS-VTD model is approximately 4000 times less.

1. Introduction

A District Heating (DH) grid is a centralized energy management system built around a network of pipes that permits the distribution of thermal energy from sources to loads. These systems have been used for over a century to provide both space and hot water heat [1]. Benefits of DH grids include high energy efficiency, fuel flexibility, and low greenhouse gas emissions [2,3]. In recent years, the number of DH grids worldwide has grown significantly [4]. Driving this growth are geopolitical and environmental factors such as rising energy demands, increasing energy insecurity, rising energy costs, and increasing concerns about greenhouse gas emissions [5].

Key elements of state-of-the-art DH grids are operation with medium and low temperature water [6] and variable speed pumping [7]. Variable speed pumping offers superior energy efficiency, reliability, and life cycle costs, relative to constant speed pumping [8]. However, DH grids that utilize variable speed pumping are difficult to model due to the challenges of tracking transport delays in the network pipes [9]. The transport delay in a pipe is defined as the time taken for fluid to flow from pipe inlet to outlet. When flow is constant in a numerical simulation model, the transport delay is constant at each time step and fluid propagation in the pipe can easily be tracked by implementing a constant time lag at the pipe outlet. However, when flow varies, the transport delay varies from time step to time step and tracking fluid propagation is

* Corresponding author.
E-mail addresses: duquette@uvic.ca (J. Duquette), arowe@uvic.ca (A. Rowe), pwild@uvic.ca (P. Wild).

http://dx.doi.org/10.1016/j.apenergy.2016.06.092
0306-2619/

Nomenclature

Symbols

r_a	inner wall radius of pipe (m)
r_b	outer wall radius of pipe (m)
r_c	outer insulation radius of pipe (m)
r_d	outer casing radius of pipe (m)
d	centerline burial depth of pipe relative to soil surface (m)
T_s	soil surface temperature (°C)
T	mean pipe water temperature (°C)
ρ_w	density of water (kg/m^3)
$C_{p,w}$	specific heat capacity of water (kJ/kg K)
A	area (m^2)
$\dot{m}$	mass flow rate (kg/s)
k_w	thermal conductivity of water (W/m K)
R'	total thermal resistance per unit length of pipe (m K/W)
$\bar{h}$	average convection heat transfer coefficient (W/m^2 K)
k_{ab}	thermal conductivity of pipe wall (W/m K)
k_{bc}	thermal conductivity of pipe insulation (W/m K)
k_{cd}	thermal conductivity of pipe outer casing (W/m K)
k_s	thermal conductivity of soil (W/m K)
S	conduction shape factor (m)
$\overline{Nu}$	local Nusselt number
Re	Reynolds number
D_h	pipe hydraulic diameter (m)
L	pipe length (m)
Pr	Prandtl number
ν_w	kinematic viscosity of water (m^2/s)
α_w	thermal diffusivity of water (m^2/s)
f	friction factor
ε	pipe roughness (m)
T_o	mean fluid temperature at pipe outlet (°C)
T_i	mean fluid temperature at pipe inlet (°C)
T_{i_ps}	mean fluid temperature at pipe segment inlet (°C)
τ	transport delay (s)
τ_d	variable transport delay (s)
θ	placeholder variable
t	time (s)
t_o	time at start of simulation (s)
$T_{o,\tau}$	mean fluid temperature at pipe outlet considering the transport delay (°C)
T_{o,τ_ps}	mean fluid temperature at pipe segment outlet considering the transport delay (°C)
Δx	pipe segment length (m)
C_o	courant number
$C_{o,p}$	peak courant number
Δt	simulation time step (s)
$\Delta x_{\min}$	minimum allowable pipe segment length (m)
$\dot{m}_p$	peak mass flow rate (kg/s)
n	number of pipe segments in model
$n_{\max}$	maximum allowable number of pipe segments in model
$\dot{q}_{ps}$	heat loss from pipe segment (W)
$\dot{q}_T$	total heat loss from multi-segment pipe (W)
Ø	diameter
$\dot{m}_{HP}$	secondary piping circuit mass flow rate (kg/s)
$\dot{m}_{HEX}$	primary piping circuit mass flow rate (kg/s)
$\dot{m}_{EFF}$	effluent piping circuit mass flow rate (kg/s)
T_{HP}	recreation center heat exchange plant supply temperature (°C)
T_{HEX}	effluent heat recovery plant supply temperature (°C)
$\dot{Q}_L$	heat transferred from recreation center heat exchange plant to swimming pool (W)
$\dot{Q}_S$	heat transferred from effluent water to the district energy grid (W)
σ	standard deviation (%)
t_{CPU}	CPU simulation time (s)

Acronyms and abbreviations

SS	steady state
VTD	variable transport delay
1D	one-dimensional
PDE	partial differential equation
ODE	ordinary differential equation
DH	district heating
DE	district energy
HDPE	high density polyethylene
CSP	constant speed pump
VSP	variable speed pump
CFL	Courant-Friedrichs-Levy
SCADA	supervisory control and data acquisition
CPU	central processing unit
PDF	probability density function
RAM	random-access memory

cumbersome as consideration must be given to the time history of the flow rate in the pipe [10].

A number of modeling studies have been conducted that focus on temperature dynamics in variable flow DH grids. Gabrielaitiene et al. [11,12] constructed a model of the Naestved DH grid in Denmark to analyze temperature variations in the system for a scenario where large and sudden changes in supply temperature were present. The same authors [13,14] modeled the Vilnius DH grid in Lithuania using two different modeling tools to compare temperature variations and heat loss at defined points in the system. Stevanovic et al. [15] developed a model of the Zemun DH grid in Serbia to investigate thermal transients and fluid propagation time delays from source to consumers in the system. A similar type study was conducted by Grosswindhager et al. [9] focusing on the Tannheim DH grid in Austria. The study presents a fully dynamic physical model that is capable of tracking variable transport delays in the network pipes. Li and Svendsen [16] constructed a hypothetical model of a low temperature DH grid in Lystrup, Denmark to assess the impacts of using one of two configurations of in-house substation on distribution heat losses and overall system exergy efficiency. Haiyan and Valdimarsson [17] developed a model of the Tianjin DH grid in China to assess the impacts of building radiator size on system return temperature and mass flow rate. Hassine and Eicker [18] developed a model of the Sonnenberg solar assisted DH grid in Germany to investigate temperature and pressure variations in the system using two distinct pump control methods. The same authors [19] modeled the Scharnhauser Park DH grid in Germany to assess the impacts of spatial distribution and pump control method on heat losses and electrical energy consumption, respectively. Sener [20] modeled the Balcova geothermal DH grid in Turkey to determine optimal pump operation strategies under various heat demand scenarios. Liu et al. [21] modeled the Barry Island DH grid in South Wales to investigate scenarios in which both heat and power demands can be met fully in the region by linking electricity and heat networks via combined heat and power plants, heat pumps, and electric boilers.

The temperature dynamics in the DH grid studies described above are modeled using physical pipe models based on advection transport [22] and formulated as finite difference problems. These DH grid models can be classified into three groups: transient, steady state, and pseudo-transient.

In transient models, the pipe energy equation is presented as a one-dimensional partial differential equation (1D-PDE). The pipe is divided into segments along the direction of flow and the total heat loss from the pipe is the sum of heat losses of the segments. Transient models provide relatively accurate results for variable flow systems and do not require tracking of transport delays. However, the computational intensity of these models can be high [14].

In steady state models, each pipe is typically represented as a series of lumped masses. Each component of the pipe (*e.g.* fluid, pipe, insulation, casing, etc.) is assigned a mass whose temperature is equal to the average temperature of that component over the length of the pipe [23]. Rates of radial heat transfer between lumped masses are determined by the thermal conductivities of pipe components. By eliminating spatial discretization along the length of the pipe, the pipe energy equation is reduced to an ordinary differential equation (ODE). Although computational intensity is low for steady state DH grid models, these models are limited in their capacity to track transport delays in variable flow systems [24].

In pseudo-transient models, the steady state (SS) lumped mass model is combined with a variable transport delay (VTD) model to enable the progress of the fluid to be tracked in time as the flow rate varies [7]. VTDs are modeled using delay differential equations [10,25]. From this point forward, pseudo-transient models will be referred to as SS-VTD models. No studies have been identified that assess the SS-VTD method numerically for error and computational intensity.

The objectives of this research are to apply the SS-VTD method to a variable flow DH pipe model and to assess error and computational intensity by comparing simulation results with those obtained using the 1D-PDE method. The impacts of pipe length discretization and varying time step size on the SS-VTD simulation results are investigated. Matlab®/Simulink® software (MathWorks, USA) is used to construct both SS-VTD and 1D-PDE pipe models and conduct all simulations. An experimental validation of the SS-VTD model is conducted by comparing simulated data with measured data from an existing network. The Saanich DE grid, located near Victoria, Canada, is used as the case study for validation.

2. Methodology

2.1. Thermal pipe models

Two thermal pipe models are developed: a one-dimensional PDE model, and a SS-VTD model. A schematic depicting the main elements of a buried piping system is shown in Fig. 1. Fig. 1a shows the pipe wall, insulation, and outer casing. Variables r_a, r_b, r_c, and r_d in Fig. 1a represent the radii of the inner pipe wall, outer pipe wall, outer insulation layer, and outer casing, respectively. Fig. 1b shows the buried pipe, where d, T_s, and T are the centerline burial depth of the pipe relative to the soil surface, soil surface temperature, and mean pipe water temperature, respectively. The following assumptions are used in formulating the models:

(1) Water is the working fluid
(2) Fluid flow is one-dimensional and incompressible
(3) Fluid flow is fully developed
(4) Convective heat transfer from the fluid to the surroundings is in the radial direction only
(5) Resistance to heat loss from the pipe is independent of the fluid flow direction
(6) Conduction heat transfer is considered through the pipe, insulation, casing and soil
(7) Material properties of the pipe, insulation, casing, and soil are constant in time and uniform in space and temperature independent
(8) Two-dimensional conduction in the soil is in the y and z directions (see Fig. 1)
(9) Thermal interaction between the supply and return pipes is not included
(10) Bends are treated as straight pipes of equivalent length
(11) The effects of fittings are not included

2.1.1. One-dimensional PDE model

The energy balance in the fluid for the one-dimensional PDE pipe model is defined by

$$\overbrace{\rho_w C_{p,w} A \frac{\partial T}{\partial t}}^{1} + \overbrace{\dot{m} C_{p,w} \frac{\partial T}{\partial x}}^{2} = \overbrace{k_w A \frac{\partial^2 T}{\partial x^2}}^{3} + \overbrace{\frac{(T_s - T)}{R'}}^{4} \quad (1)$$

where ρ_w, $C_{p,w}$, A, and $\dot{m}$ are the density, specific heat capacity, area, and mass flow rate of water in the pipe, respectively; and k_w and R' are the thermal conductivity of water and total thermal resistance per unit length of pipe [26], respectively. Terms 1 to 4 in Eq. (1) (shown schematically in Fig. 2) make up the energy balance for water across a differential segment of the model domain. The terms, in the order stated, represent the gains due to internal energy of the fluid, the enthalpy flux of the fluid, the rate of conductive heat transfer within the fluid, and the convective heat transfer from the soil surface to the fluid.

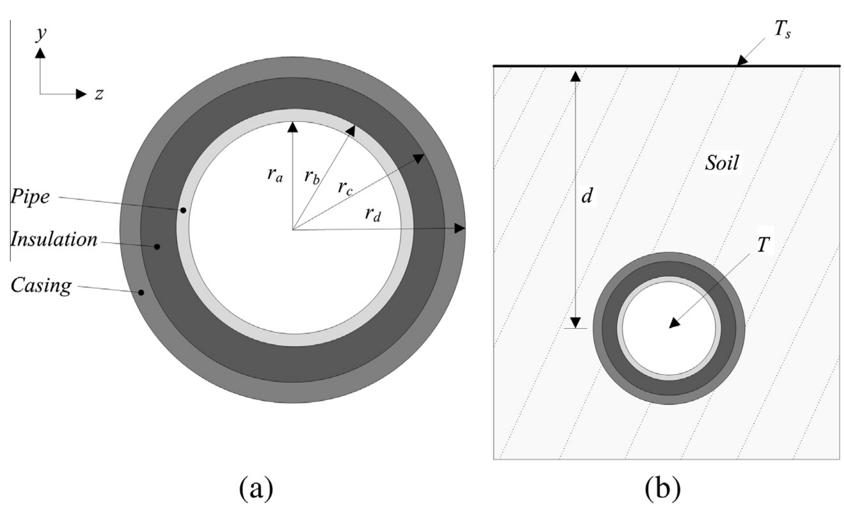

Fig. 1. (a) Schematic of pipe cross section; (b) buried pipe schematic.

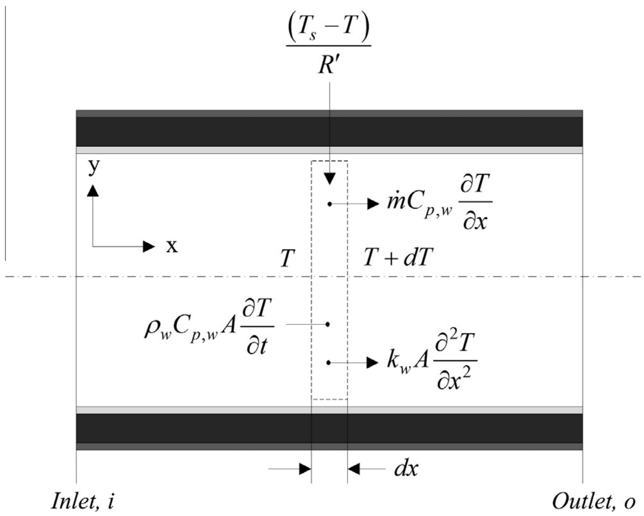

Fig. 2. Energy balance for water across a differential pipe segment.

As conductive heat transfer within the fluid is negligible relative to the other components in Eq. (1) [11], term 3 is assumed to be zero. The total thermal resistance per unit length of pipe is given by:

$$R' = \frac{1}{2\pi r_a \bar{h}} + \frac{\ln\left(\frac{r_b}{r_a}\right)}{2\pi k_{ab}} + \frac{\ln\left(\frac{r_c}{r_b}\right)}{2\pi k_{bc}} + \frac{\ln\left(\frac{r_d}{r_c}\right)}{2\pi k_{cd}} + \frac{1}{Sk_s}, \tag{2}$$

where $\bar{h}$ is the average convection heat transfer coefficient in the pipe; k_{ab}, k_{bc}, k_{cd}, and k_s are the thermal conductivities of the pipe, insulation, casing, and soil, respectively, as shown in Fig. 1; and S is the conduction shape factor. The conduction shape factor per unit length for an isothermal buried, horizontal pipe can be approximated as [26]

$$S = \frac{2\pi}{\cos^{-1}\left(\frac{d}{r_a}\right)}. \tag{3}$$

The average convection heat transfer coefficient is

$$\bar{h} = \frac{\overline{Nu} k_w}{2r_a}, \tag{4}$$

where $\overline{Nu}$ is the local Nusselt number, assuming a constant pipe surface temperature condition with a thermal entry length. Under laminar flow conditions (*i.e.* Reynolds number, Re, $\leqslant 2300$), the local Nusselt number is determined from the Kays and Hausen correlation [26]:

$$\overline{Nu} = 3.66 + \frac{0.0668\left(\frac{D_h}{L}\right)RePr}{1 + 0.04\left[\left(\frac{D_h}{L}\right)RePr\right]^{2/3}}, \tag{5}$$

where D_h, L, and Pr are the pipe hydraulic diameter, pipe length, and Prandtl number, respectively. The Prandtl number and Reynolds number can be expressed by the following relations:

$$Pr = \frac{\nu_w}{\alpha_w}, \tag{6}$$

$$Re = \frac{4\dot{m}}{\pi D_h \rho_w \nu_w}, \tag{7}$$

where ν_w and α_w represent the kinematic viscosity and thermal diffusivity of water, respectively. Under turbulent flow conditions ($2300 \leqslant Re \leqslant 5 \times 10^6$), the local Nusselt number is obtained from the Gnielinski correlation [26]:

$$\overline{Nu} = \frac{\left(\frac{f}{8}\right)(Re - 1000)Pr}{1 + 12.7\left(\frac{f}{8}\right)^{1/2}(Pr^{2/3} - 1)}. \tag{8}$$

The friction factor, f, in Eq. (8) is obtained from the Haaland relation [27]:

$$\frac{1}{\sqrt{f}} = -1.8 \log\left[\frac{6.9}{Re} + \left(\frac{\varepsilon/D_h}{3.7}\right)^{1.11}\right], \tag{9}$$

where ε/D_h is the relative pipe roughness. More information on the 1D-PDE model can be obtained from Refs. [28,29].

2.1.2. SS-VTD model

The SS-VTD model combines a steady state physical pipe model with a variable transport delay model. The steady state model allows rapid computation of heat loss and pipe outlet temperature. The variable transport delay model tracks time delays in the pipe as the flow rate varies, as is the case for variable speed pumping systems. The steady state model is derived by applying an energy balance to the water contained in a pipe, considering only enthalpy and convection effects (*i.e.* terms 2 and 4 from Eq. (1)). The steady state model is expressed as

$$\dot{m}C_{p,w}\frac{dT}{dx} = \frac{(T_s - T)}{R'}. \tag{10}$$

Defining $(T - T_s)$ in Eq. (10) as T^*, rearranging, and integrating between inlet and outlet conditions yields the following expression [26]:

$$\int_{T_i}^{T_o} \frac{dT^*}{T^*} = -\int_0^L \frac{dx}{\dot{m}C_{p,w}R'}, \tag{11}$$

which can be simplified to

$$T_o = T_s + \left[(T_i - T_s)\exp\left(-\frac{L}{\dot{m}C_{p,w}R'}\right)\right]. \tag{12}$$

Eq. (12) describes the mean fluid temperature at the pipe outlet, T_o, assuming constant values of mean fluid temperature at the pipe inlet, T_i, soil surface temperature, T_s, and mass flow rate, $\dot{m}$ [30]. The time required for fluid to travel the length of the pipe is defined as the transport delay, τ.

The relationship between transport delay, pipe diameter, pipe length, and mass flow rate at any instant in time is expressed as

$$L = \int_{t-\tau}^{t} \frac{4\dot{m}(\theta)}{\pi D_h^2 \rho_w} d\theta. \tag{13}$$

The transport delay is calculated by solving Eq. (13). For constant mass flow, τ is constant and is represented as

$$\tau = \frac{\pi D_h^2 \rho_w L}{4\dot{m}}. \tag{14}$$

The transport delay is needed to accurately simulate fluid flow in a pipe using a numerical time series model. At each time step, a new estimate is made of the time required for the fluid that left the pipe inlet at the start of the simulation to reach the pipe outlet. This estimate is based on the transport delay calculated at every time step and is defined as the variable transport delay, τ_d. Fluid propagation in a pipe can easily be modeled when mass flow is constant since τ is constant at every time step and τ_d can be solved by linear interpolation. Modeling the fluid propagation is more difficult when mass flow is variable since τ varies at every time step. The variable transport delay can be calculated by rewriting Eq. (13) as

$$1 = \int_{t-\tau}^{t} \frac{4\dot{m}(\theta)}{\pi D_h^2 \rho_w L} d\theta. \tag{15}$$

Moreover, by defining

$$\tau(\theta) = \frac{\pi D_h^2 \rho_w L}{4\dot{m}(\theta)} \tag{16}$$

and substituting τ for τ_d in Eq. (15), gives

$$1 = \int_{t-\tau_d}^{t} \frac{1}{\tau(\theta)} d\theta. \tag{17}$$

Eq. (17) can be rewritten as

$$1 = \int_{t_o}^{t} \frac{1}{\tau(\theta)} d\theta - \int_{t_o}^{t-\tau_d} \frac{1}{\tau(\theta)} d\theta, \tag{18}$$

where t_o is the time at the start of the simulation. Eq. (18) is represented schematically in Fig. 3, which depicts a snapshot in time during a simulation where $\frac{1}{\tau(\theta)}$ varies from time, t_o, to time, t. At time, t, τ_d can be found by determining the time, $t - \tau_d$, where the area under the curve from $t - \tau_d$ to t equals 1.

Simulink® is used to compute the value of τ_d in the SS-VTD model at each time step during a simulation. This is accomplished using a Simulink® algorithm that stores the time histories of the transport delay, the simulation clock time, the time step index, and the mean fluid temperature at the pipe outlet (see Eq. (12)) in an internal buffer that is capable of growing as the simulation proceeds [31]. The mean fluid temperature at the pipe outlet considering the transport delay, $T_{o,\tau}(t)$, is then calculated at every time step using stored values from the internal buffer [10]:

$$T_{o,\tau}(t) = T_o(t - \tau_d) \tag{19}$$

Once $T_{o,\tau}(t)$ is known, the pipe heat loss, $\dot{q}(t)$, is calculated as follows:

$$\dot{q}(t) = \dot{m}(t) c_p [T_i(t) - T_{o,\tau}(t)], \tag{20}$$

where $\dot{m}(t)$, $T_i(t)$, and $T_{o,\tau}(t)$ are fixed at each time step but can vary from time step to time step.

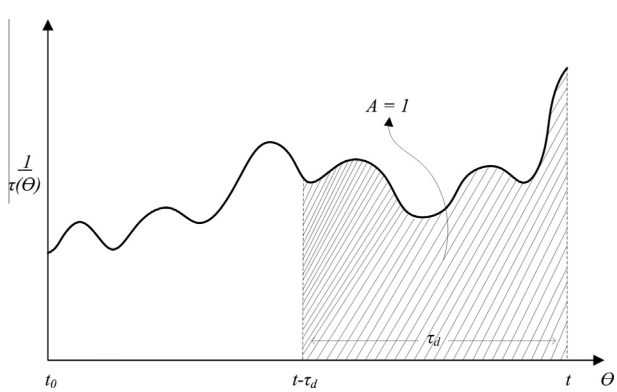

Fig. 3. Schematic representation of Eq. (18).

2.1.3. SS-VTD model simulation approach

To account for varying transverse thermal resistance, $R'(x)$, and surrounding soil surface temperature variations, $T_s(x)$, a pipe of length L is discretized into many segments, Δx, as shown in Fig. 4.

The maximum number of segments, n, of length Δx that can be used in the model is limited by the Courant-Friedrichs-Levy (CFL) stability criterion [24]. For a one dimensional pipe, the CFL criterion can be expressed as

$$C_o(t) = \frac{4\dot{m}(t)\Delta t}{\pi D_h^2 \rho_w \Delta x} \leqslant 1, \tag{21}$$

where $C_o(t)$ is the dimensionless Courant number, $\dot{m}(t)$ is the fluid mass flow rate, and Δt is the simulation time step. The Courant number represents the ratio of the flow distance to the element size in the space domain. By rearranging Eq. (21), it can be seen that the model becomes unstable during a simulation if at any time the ratio

$$\frac{\pi D_h^2 \rho_w \Delta x}{4\dot{m}(t)} < \Delta t. \tag{22}$$

Eq. (16) shows that the relationship shown on the left side of Eq. (22) is equivalent to the transport delay, $\tau(t)$. When $\tau(t) < \Delta t$, numerical diffusion can occur, leading to inaccurate results [22]. Eq. (21) can be rearranged to provide a criterion for selecting the minimum allowable pipe segment length in the pipe model:

$$\Delta x_{\min} \geqslant \frac{4\dot{m}_p \Delta t}{\pi D_h^2 \rho_w}. \tag{23}$$

The peak mass flow rate, $\dot{m}_p$, is used in Eq. (23) to ensure that stability is maintained at all times during a simulation. Once $\Delta x_{\min}$ is known, the maximum allowable number of pipe segments, $n_{\max}$, can be calculated as follows:

$$n_{\max} = \frac{L}{\Delta x_{\min}}, \tag{24}$$

where $n_{\max}$ is rounded to the nearest integer.

Fig. 5 describes the SS-VTD model simulation algorithm for a pipe of length, L, discretized into n pipe segments of length Δx. In the simulation algorithm, inputs are loaded into the SS-VTD model at the start of each time step. The SS-VTD thermal submodels are activated in series and variable transport delays are calculated in each submodel. The temperature output from one submodel is used as an input for the next submodel (*e.g.* the mean fluid temperature output, T_{o,τ_ps1}, from pipe segment $ps1$ is used as the mean fluid temperature input, T_{i_ps2}, for pipe segment $ps2$). The total rate of heat transfer from the pipe, $\dot{q}_T$, is calculated as the sum of all $\dot{q}_{ps}$ outputs:

$$\dot{q}_T(t) = \sum_{i=1}^{n} \dot{q}_{psi}(t), \tag{25}$$

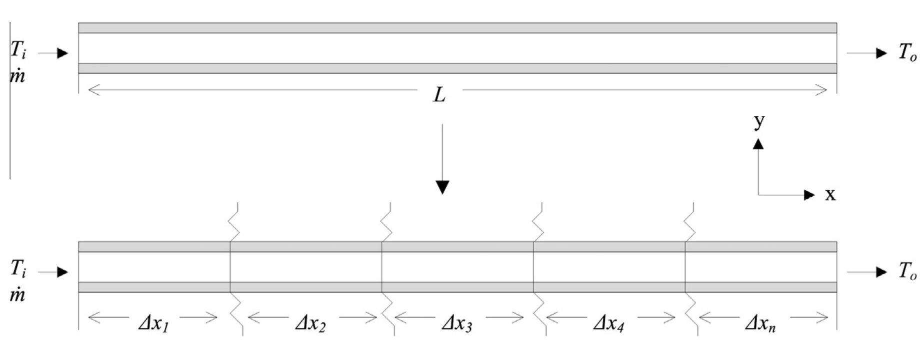

Fig. 4. Pipe of length L discretized into n equivalent segments of length Δx.

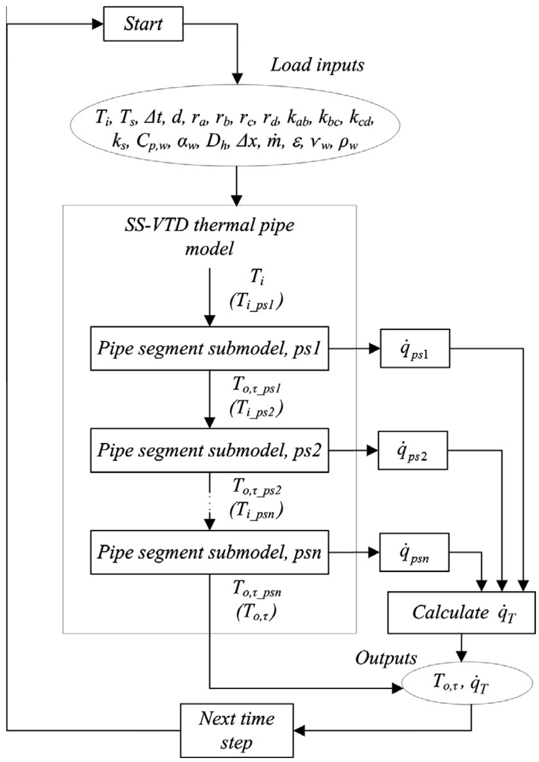

Fig. 5. SS-VTD simulation algorithm for a pipe of length L discretized into n equivalent pipe segments of length Δx.

where n represents the number of pipe segment submodels. The summation described in Eq. (25) is represented by the block labeled 'Calculate $\dot{q}_T$' in Fig. 5. The Simulink® software is used for carrying out the simulation using an explicit fixed step continuous solver based on Euler's method [32].

2.2. SS-VTD model validation

The SS-VTD model is validated experimentally using recorded historical data from the Saanich district energy (DE) grid, located on Vancouver Island near Victoria, Canada [33]. The Saanich DE grid is an ambient temperature, effluent heat recovery system that uses water as the flow medium. Operation at ambient temperature allows for simultaneous heating and cooling to take place at multiple load points in the DE grid using distributed heat pumps. Currently, the Saanich DE grid is at its initial phase of construction and provides service to a single load: a recreation center swimming pool. However, plans are underway to connect several additional loads in the near future.

The layout of the Saanich DE grid is shown schematically in Fig. 6. The DE grid connects the effluent heat recovery plant to the recreation center heat exchange plant using a supply-return piping topology. A tee junction separates the primary piping circuit from the secondary piping circuit. A valve chamber is located at the furthest extremity of the primary piping circuit. DE supply and return pipes are depicted as solid and dashed lines, respectively, in Fig. 6. The piping network in the Saanich DE grid consists of uninsulated high density polyethylene (HDPE) pipes, buried at an approximate depth of 1.1 m. The total distance between the

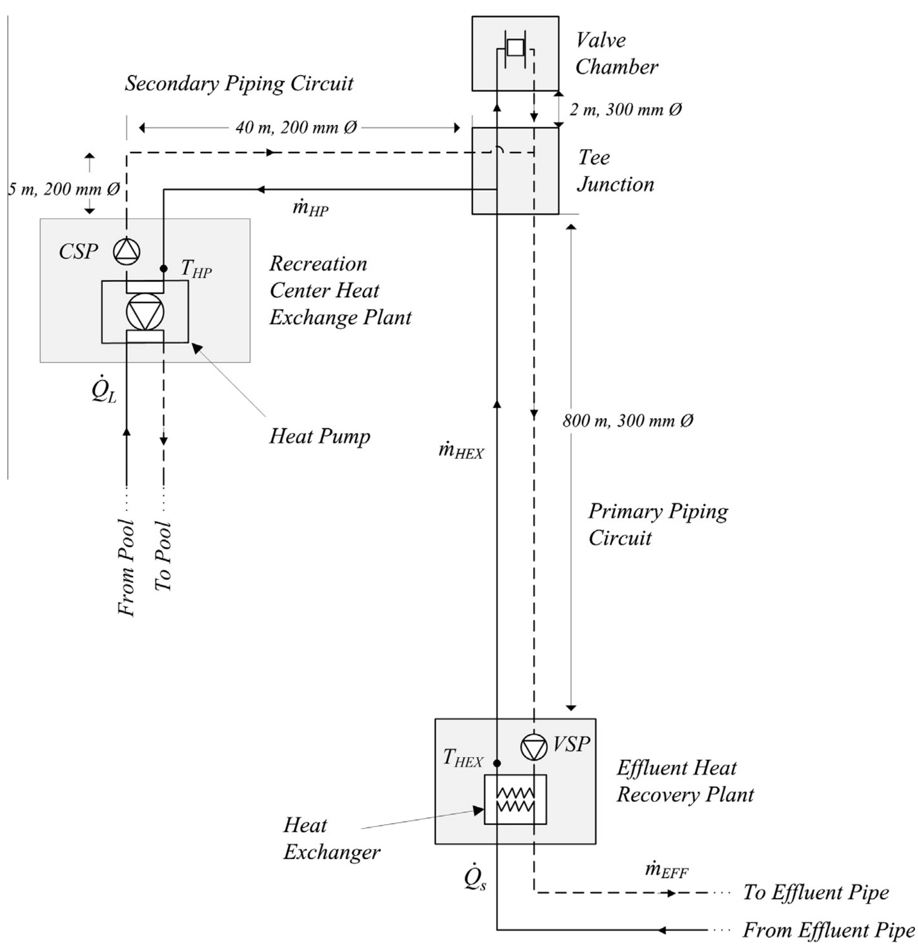

Fig. 6. Saanich DE grid schematic.

effluent heat recovery plant and the heat exchange plant is approximately 845 m. The nominal pipe diameter is reduced over this distance from 300 mm to 200 mm, as shown in Fig. 6.

The Saanich system operates as follows: Heat from the effluent water, shown as $\dot{Q}_s$ in Fig. 6, is transferred to the DE grid via a heat exchanger bank located in the effluent heat recovery plant. The effluent water temperature varies between approximately 10 °C and 20 °C annually. The DE grid is connected to a heat pump located in the recreation center heat exchange plant that is used to heat a swimming pool facility. The swimming pool facility includes two 25 m length pools which have a combined nominal heat load of approximately 390 kW. The recreation center heat pump provides water at a temperature of approximately 50 °C to the swimming pool facility via a separate piping circuit. The average DE grid supply water temperature varies between approximately 12 °C and 21 °C annually. The return water temperature is roughly equivalent to the supply water temperature plus or minus 5 °C, depending on whether the DE grid is providing cooling or heating services to the swimming pool facility, respectively. Heat transferred from the recreation center heat exchange plant to the swimming pool facility is depicted as $\dot{Q}_L$ in Fig. 6.

If the temperature leaving the heat exchanger bank in the effluent heat recovery plant, T_{HEX}, drops below its lower design setpoint value, the mass flow rate in the effluent pipe, $\dot{m}_{EFF}$, is increased to provide more heat to the DE primary piping circuit. Water in the primary piping circuit is distributed via a variable speed pump (VSP) located in the effluent heat recovery plant. The nominal flow rate in the primary piping circuit is approximately 24 kg/s. The secondary piping circuit uses a constant speed pump (CSP) to circulate water in the pipes. The nominal flow rate in the secondary piping circuit is approximately 20 kg/s. The VSP is pressure-controlled and responds to the pressure differential signal measured between supply and return pipes in a bypass valve located in the valve chamber. A pressure differential setpoint value is programmed into the automated DE grid control sequence for control purposes. When the measured pressure differential deviates from the setpoint value, the VSP responds by either increasing or decreasing the primary piping circuit mass flow rate, $\dot{m}_{HEX}$, in an attempt to retain system equilibrium. For example, if the CSP were to suddenly turn on due to a load at the recreation center heat exchange plant, the pressure differential in the valve chamber would decrease and the VSP would react by increasing $\dot{m}_{HEX}$ to compensate for the pressure loss.

The Saanich DE grid is simulated in Simulink® using the SS-VTD model with a time step of 60 s. A time step of 60 s is used to generate outputs that coincide in time with measured system data. A time period of 6 h is simulated from 9:00 am to 3:00 pm on December 2nd, 2012. Table 1 shows a breakdown of select input parameters, defined in Section 2.1, utilized in the Saanich model. Pipe characteristics, shown in Table 1, are based on standard specifications for commercially available HDPE pipe [34]. The peak Courant number, $C_{o,p}$, is calculated for each pipe length in the model to ensure values do not exceed the maximum threshold defined by the CFL stability criterion. Rearranging Eq. (21), the peak Courant number is calculated from the following expression:

$$C_{o,p} = \frac{4\dot{m}_p \Delta t}{\pi \rho_w D_h^2 \Delta x} \tag{26}$$

where $\dot{m}_p$ is the peak mass flow rate attained at any time during the simulation. $C_{o,p}$ values obtained in the primary and secondary piping circuits are 0.93 and 0.91, respectively.

Other inputs to the model include the swimming pool heat load, effluent heat recovery plant supply temperature, primary piping circuit mass flow rate, and secondary piping circuit mass flow rate; shown as $\dot{Q}_L$, T_{HEX}, $\dot{m}_{HEX}$, and $\dot{m}_{HP}$, respectively, in Fig. 6. The soil surface temperature, T_s, in the SS-VTD model is assumed to be equal to the outside air temperature. All measured inputs for the system are obtained from an online SCADA system, which is used to monitor and log data from remote sensors located throughout the DE grid. The measured recreation center heat exchange plant supply temperature, T_{HP} (depicted in Fig. 6), is used as a validation parameter in the analysis.

Table 1
SS-VTD model input parameters used in Saanich DE grid simulation.

Parameter name	Symbol	Value	
		Primary piping circuit	Secondary piping circuit
Pipe length	L	800 m	45 m
Pipe segment length	Δx	80 m	45 m
Peak mass flow rate	$\dot{m}_p$	80 kg/s	20 kg/s
Centerline burial depth of pipe relative to soil surface	d	1.1 m	1.1 m
Pipe hydraulic diameter	D_h	0.286 m	0.193 m
Inner wall radius of pipe	r_a	0.143 m	0.097 m
Outer wall radius of pipe	r_b	0.162 m	0.109 m
Thermal conductivity of pipe wall	k_{ab}	0.51 W/m K	0.51 W/m K
Thermal conductivity of soil	k_s	0.6 W/m K	0.6 W/m K

Measured and simulated data for T_{HP} are shown in Fig. 7 for a six hour period on December 2nd, 2012 between 9:00 am and 3:00 pm. The average outside air temperature recorded during the indicated six hour period is 8.7 °C. Fig. 7 shows that the simulated dataset fits closely with the measured dataset. The two datasets are offset in time by approximately 2 min. Potential causes for the offset are the time step sensitivity in the SS-VTD model, and/or the lack of thermal mass in the SS-VTD model and/or the flow sensor error, specified as ±1% by the manufacturer [35].

The simulated temperature dataset depicted in Fig. 7 overestimates temperature by approximately 0.2 °C on average. This difference is potentially due to the error in estimating the thermal resistance between the buried pipe and the soil surface and/or the temperature sensor error, specified as ±0.15 °C by the manufacturer [35]. The thermal resistance between the pipe and the soil surface is best defined by the total thermal resistance per unit length of pipe, R', in the SS-VTD model. The value of R' is dependent on a number of input variables in the SS-VTD model. In the SS-VTD model, R', is assumed to be constant. In reality, R' varies significantly throughout the year at different points throughout the DE

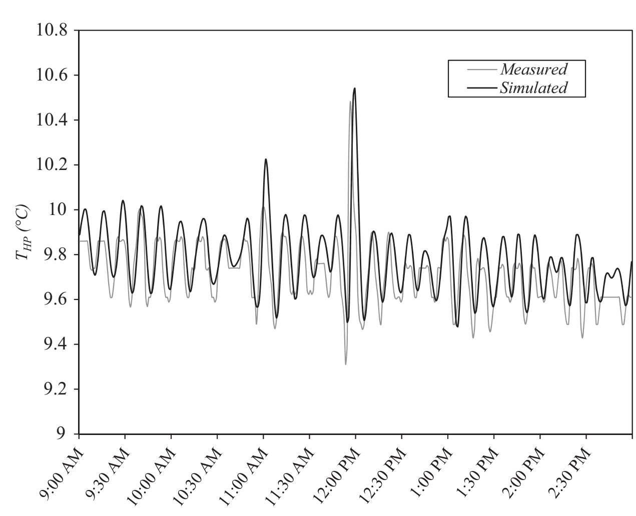

Fig. 7. Measured and simulated datasets for the recreation center heat exchange plant supply temperature, T_{HP}, for a 6 h period on December 2nd, 2012.

grid. R' is affected by a number of factors such as local soil conditions (*e.g.* soil type, density, moisture content), natural ground cover phenomena (*e.g.* snow, flooding), and civil works (*e.g.* paved roads, buildings).

2.3. SS-VTD model performance

In Section 2.2, the SS-VTD model thermal performance is assessed experimentally. In the current section, the SS-VTD model's thermal performance is assessed numerically. Water flowing in a buried pipe is simulated using the SS-VTD model and fluid outlet temperatures are compared with values obtained using the 1D-PDE model. A full description of the 1D-PDE model is provided in Section 2.1.1. Results from the 1D-PDE model are used as a reference for the comparison and are used to assess the error of the SS-VTD model. The computational intensity of the SS-VTD model is assessed in a similar manner by comparing CPU run times for all simulations. Simulations of the 1D-PDE and SS-VTD models are conducted for a period of 30 min. The input parameters used in the models are shown in Table 2. The parameters shown in Table 2 are defined in Section 2.1.1. Table 2 values are based on standard specifications for commercially available insulated steel pipe [34].

The inlet water temperature, T_i, used in the analysis is selected arbitrarily and fluctuates between 40 °C and 80 °C in a sinusoidal waveform with a period of 1200 s, according to Eq. (27).

$$T_i = 60\ ^\circ\mathrm{C} + 20\ ^\circ\mathrm{C} \cdot \sin\left(\frac{\pi}{600} t\right) \tag{27}$$

The mass flow rate used in the analysis is also selected arbitrarily and fluctuates between 150 kg/s and 750 kg/s in a sinusoidal waveform with a period of 600 s, according to Eq. (28).

$$\dot{m} = 450\ \mathrm{kg/s} + 300\ \mathrm{kg/s} \cdot \sin\left(\frac{\pi}{300} t\right) \tag{28}$$

Table 2
Input parameters used in 1D-PDE and SS-VTD models.

Parameter name	Symbol	Value
Pipe length	L	500 m
Centerline burial depth of pipe relative to soil surface	d	1 m
Pipe hydraulic diameter	D_h	0.575 m
Inner wall radius of pipe	r_a	0.288 m
Outer wall radius of pipe	r_b	0.305 m
Outer insulation radius of pipe	r_c	0.355 m
Outer casing radius of pipe	r_d	0.36 m
Thermal conductivity of pipe wall	k_{ab}	43 W/m K
Thermal conductivity of pipe insulation	k_{bc}	0.025 W/m K
Thermal conductivity of pipe outer casing	k_{cd}	0.45 W/m K
Thermal conductivity of soil	k_s	0.6 W/m K
Soil surface temperature	T_s	−40 °C

The 1D-PDE model is simulated in the Matlab® partial differential equation (PDE) toolbox™ environment with a time step of 1 s. The PDE toolbox™ provides functions for solving PDEs in time using finite element analysis. More information on the PDE toolbox™ can be obtained from Ref. [36]. The SS-VTD model is simulated in Simulink® over a range of time steps, Δt, and pipe segment lengths, Δx. Two sets of simulations are conducted: In the first set, the impact of varying Δt while holding Δx constant is assessed. In the second set, the impact of varying Δx while holding Δt constant is assessed. By varying Δx, the effect of increased pipe discretization, as discussed in Section 2.1.3, can be observed.

Thirty scenarios are initially considered in the analysis. A description of each scenario is provided in Table 3. Values of Δx and Δt ranging from 3 m to 500 m and 1 s to 300 s, respectively, are assigned to each scenario. Table 3 also shows the corresponding peak Courant number, $C_{o,p}$, for each scenario (see Eq. (26)). In the current analysis, $\dot{m}_p$ is equivalent to 750 kg/s. The upper bound pipe length is 500 m and corresponds to the full length of the pipe being modeled. The upper bound time step size is determined by the Nyquist sampling criterion. In the current analysis, the maximum input frequency is equivalent to the reciprocal of the period of the mass flow rate in Eq. (28). The minimum Nyquist sampling frequency is obtained by multiplying this value by two. The upper range time step value (*i.e.* 300 s) is then found by taking the reciprocal of the minimum Nyquist sampling frequency. Cells in Table 3 that contain values that fall below the CFL stability limit (see Eq. (21)) are shaded in grey. The grey region in Table 3 defines the simulation stability domain for the analysis. To avoid errors and maintain accuracy in the simulations, only scenarios within the stability domain are considered in the analysis.

Model error in the analysis is determined by the standard deviation of a probability density function (PDF) representing the percent difference between the 1D-PDE and SS-VTD fluid outlet temperature time series datasets. The PDF is evaluated using a sample of 100 equally spaced bins.

Model computational intensity is determined by the CPU simulation time. Simulations are performed using Simulink® version R2015a on a computing platform equipped with an Intel Core i5 2.67 GHz processor and 8 GB of RAM.

3. Results

Fifteen scenarios, from the stability domain defined in Table 3, are considered in the analysis. For each scenario, fluid outlet temperatures, $T_{o,\tau}$, from the SS-VTD model are compared with outlet temperatures obtained from the corresponding 1D-PDE model. Two sets of simulations are conducted.

In the first set of simulations, the impact of varying Δt while holding Δx constant is assessed. Fig. 8 shows the results of the SS-VTD simulation at fixed Δx and five values of Δt for a period of 30 min. The results of the 1D-PDE model for Δx = 500 m and

Table 3
SS-VTD model scenarios with corresponding peak Courant numbers, $C_{o,p}$. Shaded cells are considered in the analysis and represent scenarios that are within the simulation stability domain.

	$C_{o,p}$				
	Δx = 3 m	Δx = 30 m	Δx = 100 m	Δx = 250 m	Δx = 500 m
Δt = 300 s	289	28.9	8.7	3.47	1.74
Δt = 150 s	145	14.5	4.3	1.73	0.87
Δt = 60 s	57.8	5.78	1.73	0.69	0.35
Δt = 30 s	28.8	2.88	0.87	0.35	0.17
Δt = 10 s	9.6	0.96	0.29	0.115	0.058
Δt = 1 s	0.96	0.096	0.028	0.01	0.0058

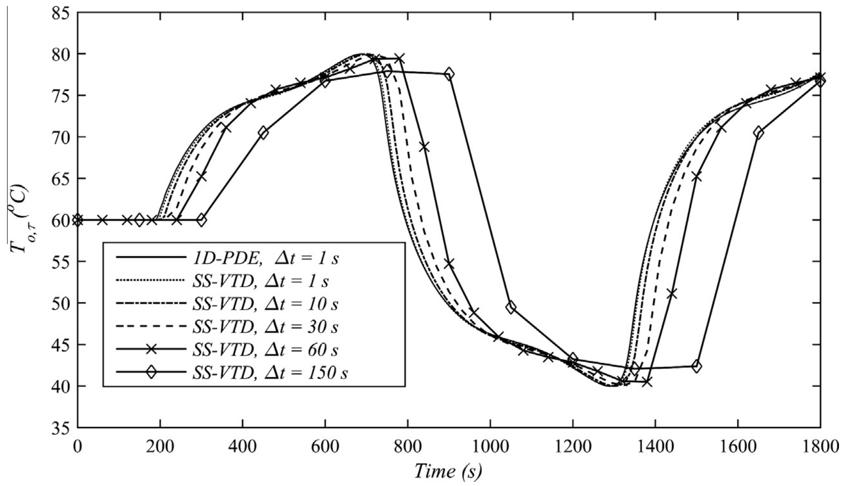

Fig. 8. Comparison of simulated pipe outlet temperature, $T_{o,\tau}$, for SS-VTD model using five different time steps and 1D-PDE model using a 1 s time step. Δx = 500 m for all scenarios.

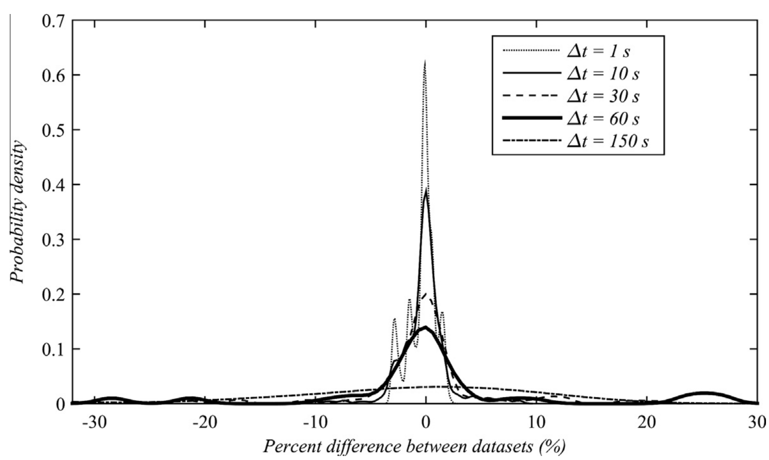

Fig. 9. PDFs representing the percent difference between the 1D-PDE dataset and the SS-VTD datasets.

Δt = 1 s is also shown in Fig. 8. An initial condition of $T_{o,\tau}$ equal to 60 °C is assumed at the start of the simulations, as indicated in Fig. 8. This condition is maintained for the time required for water to travel from the pipe inlet to the pipe outlet. The agreement between the 1D-PDE and SS-VTD datasets increases as the magnitude of the time step decreases.

The PDFs representing the percent difference between the 1D-PDE and SS-VTD datasets shown in Fig. 8 are depicted in Fig. 9. Fig. 9 shows a narrow distribution at Δt = 1 s that broadens as the time step increases to Δt = 150 s. The narrower the PDF in Fig. 9, the higher the degree of agreement between the SS-VTD dataset and the 1D-PDE dataset.

The standard deviations, σ, of the PDFs depicted in Fig. 9 are shown in Fig. 10 for all time steps considered. The smaller the value of σ, the more accurately the SS-VTD method replicates results produced via the 1D-PDE method.

The CPU simulation time, t_{CPU}, is used as a metric to quantify computational intensity. The CPU simulation time to compute the 1D-PDE dataset shown in Fig. 8 is 3120 s. The CPU simulation time to compute each of the SS-VTD model datasets is shown in Fig. 10. Fig. 10 shows that decreasing time step size causes an increase in computational intensity and a decrease in error.

In the second set of simulations, the impact of varying Δx while holding Δt constant is assessed. Simulations are conducted for all of the stable scenarios, as indicated in Table 3, and the results are shown in Fig. 11. The CFL stability limit is also plotted in Fig. 11. For each time step, σ remains relatively constant as a function of Δx.

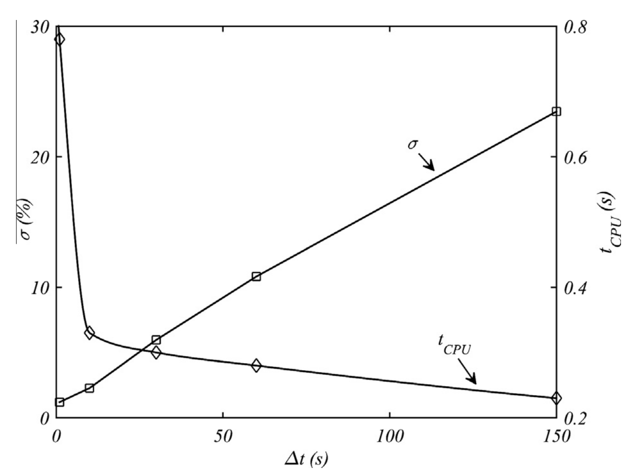

Fig. 10. Standard deviation, σ, of PDFs representing the percent difference between the SS-VTD datasets and the 1D-PDE dataset and CPU simulation time, t_{CPU}, for computing SS-VTD scenarios.

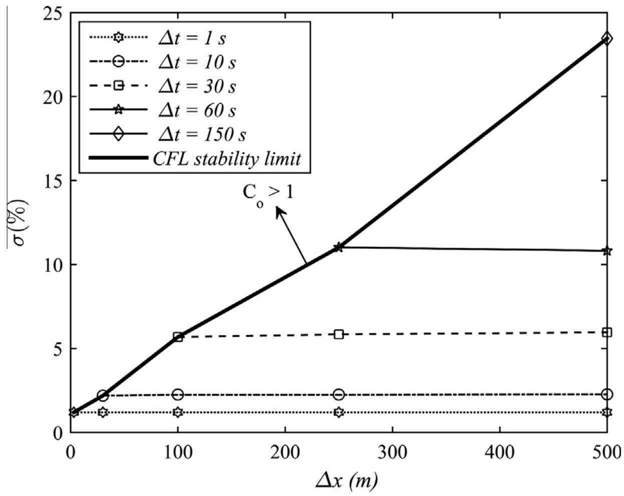

Fig. 11. Variation of standard deviation, σ, as a function of pipe segment length, Δx, for scenarios simulated at different time steps.

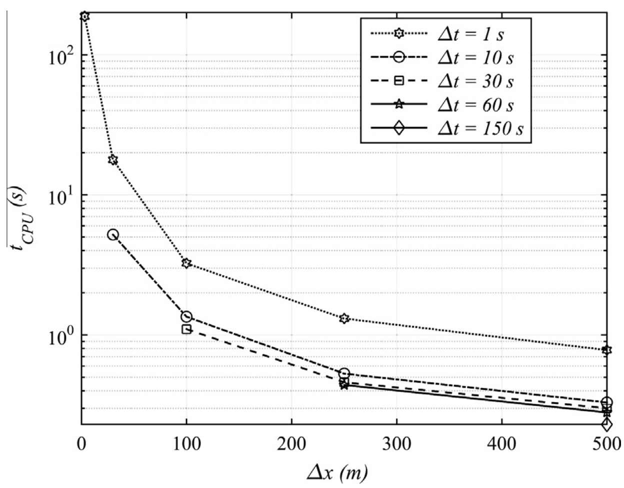

Fig. 12. Variation of CPU simulation time, t_{CPU}, as a function of pipe segment length, Δx, for scenarios simulated at different time steps.

Fig. 12 shows the calculated values of t_{CPU} for the fifteen scenarios that fall in the simulation stability domain in Table 3. As in Fig. 11, scenarios in Fig. 12 are demarcated by time step size and are plotted as a function of Δx. For each time step considered in Fig. 12, t_{CPU} increases as Δx decreases.

4. Discussion

Relative to the 1D-PDE model, the benefit of using the SS-VTD model with respect to computational intensity is significant. When compared with the 1D-PDE model at the same fixed time step of 1 s (see Fig. 8), the CPU simulation time of the SS-VTD model is approximately 4000 times shorter. This benefit increases as larger time steps are used in the SS-VTD model, but at the cost of increased error. With respect to reproducibility of results, the SS-VTD model is nearly equivalent to the 1D-PDE model at the same fixed time step of 1 s since the standard deviation of the PDF representing the percent difference between model datasets is small (approximately 1.2%), as shown in Fig. 9.

The impact of pipe segment length, Δx, on the error of the SS-VTD model is minimal. As shown in Fig. 11, reducing Δx from 500 m to 3 m causes no observable change in the standard deviation. This result is not surprising as the total thermal resistance per unit length of pipe, R', is assumed to be constant as a function of distance in both the 1D-PDE and SS-VTD models considered. Assuming constant R' in the SS-VTD model can provide satisfactory results for small DH grids, as demonstrated by the Saanich DE grid model. However, significant error may arise when modeling larger DH grids, since thermal interactions between the pipe and the soil surface can vary considerably with distance. Further studies using the SS-VTD method to model large DH grids are required to confirm this hypothesis.

The impact of time step size, Δt, on the error and computational intensity of the SS-VTD model is significant. As shown in Fig. 10, reducing Δt from 150 s to 10 s causes a decrease in standard deviation, from 23.5% to 2.3%. Corresponding to this decrease in standard deviation is a relatively small increase in CPU simulation time, from 0.23 s to 0.33 s. Between Δt = 10 s and Δt = 1 s, however, there is a significant increase in CPU simulation time, from 0.33 s to 0.78 s. The decrease in error, from Δt = 10 s to Δt = 1 s, in Fig. 10, on the other hand, is less significant as the standard deviation decreases only from 2.3% to 1.2%. This relatively small gain in accuracy comes with a high computational cost. To select an appropriate value of Δt for simulating DH grids composed of numerous interconnected pipes, a trade-off between error and computational intensity must be considered. When constant R' is assumed in the SS-VTD model, computational intensity can be minimized significantly if Δx is set to its maximum value for each pipe in the network. As shown in Fig. 12, increasing Δx from 3 m to 500 m causes a decrease in CPU simulation time for all time step sizes considered.

The results from the current study outline the benefits and limitations of the SS-VTD model with respect to error and computational intensity, in comparison to the 1D-PDE model over a range of simulation scenarios. The methods proposed for selecting stable simulation parameters (*i.e.* Δx and Δt) in Section 2.3 as well as the trends observed in the results section over the range of scenarios considered are applicable to all DH grid studies that use the SS-VTD model.

The global DH market is expected to grow considerably in years to come largely due to the growing importance of energy sustainability [37]. Variable speed systems will likely play an important role in this market due to the high energy and cost savings associated with variable speed pumping technology [38,7]. The SS-VTD model is shown to be an effective tool for simulating variable flow DH grids with low error and computational intensity. Potential uses of the model include the design and operational optimization of DH grids [39].

5. Conclusions

The steady state variable transport delay (SS-VTD) model is presented as well as a methodology describing its use for simulating DH grids containing variable flows. Measured data from the Saanich district energy grid has been used to validate the model experimentally. To assess the error and computational intensity of the SS-VTD model, fifteen scenarios describing variable flow in a buried pipe were simulated over a range of time step sizes, Δt, and pipe segment lengths, Δx. For each scenario, the simulated pipe outlet temperatures and CPU simulation time were compared with values obtained using the one-dimensional partial differential equation (1D-PDE) model. Under certain conditions, the SS-VTD model is shown to produce values that are nearly equivalent to those obtained with the 1D-PDE model at significantly lower computational intensity. Reductions in error relative to the 1D-PDE model are shown to occur in the SS-VTD model as Δt is decreased at fixed Δx. No reductions in error, however, are shown to occur as Δx is decreased at fixed Δt. In all scenarios, decreasing Δx and/or Δt results in greater computational intensity. The results of the study bring to light the importance of assessing the trade-offs between error and computational intensity before selecting suitable values of Δx and Δt for a particular pipe flow problem. The SS-VTD model's ability to handle variable transport delays makes it a valuable tool for simulating variable speed pumping systems, a common addition in today's modern DH grids.

Acknowledgments

The authors would like to thank the Natural Sciences and Engineering Research Council (NSERC) of Canada for their financial support and DEC Design Mechanical Consultants Ltd. (Vancouver, Canada) for their technical support in completing this study. The authors also appreciate the assistance provided by the City of Saanich in supplying operational data for the Saanich district energy system.

References

[1] Danish Board of District Heating. District Heating History 2014. <http://dbdh.dk/district-heating-history/>.
[2] King M, Bradford B. Planning, development & delivery – strategies; 2013.
[3] Rezaie B, Rosen M. District heating and cooling: review of technology and potential enhancements. Appl Energy 2012;93:2–10. http://dx.doi.org/10.1016/j.apenergy.2011.04.020.
[4] International Energy Agency. Cogeneration and District Energy – Sustainable energy technologies for today and tomorrow. Paris; 2009.
[5] Nyboer J, Murphy R, Melton N, Wolinetz M. District energy inventory for Canada, 2013. Simon Fraser University, Burnaby, BC: Canadian Industrial Energy End-Use Data and Analysis Centre; 2014.
[6] 4DH Research Centre. Appendix B: project description – strategic research centre for 4th generation district heating technologies and systems. Denmark; 2014.
[7] Yan A, Zhao J, An Q, Zhao Y, Li H, Huang YJ. Hydraulic performance of a new district heating system with distributed variable speed pumps. Appl Energy 2013;112:876–85. http://dx.doi.org/10.1016/j.apenergy.2013.06.031.
[8] US Department of Energy. Variable speed pumping – a guide to successful applications. Washington, D.C.: U.S. Department of Energy Industrial Technologies Program; 2004.
[9] Grosswindhager S, Voigt A, Kozek M. Efficient physical modelling of district heating networks. Model Simul Calgary A 2011.
[10] Zhang F, Yeddanapudi M. Modeling and simulation of time-varying delays. Mathworks.
[11] Gabrielaitiene I, Bohm B, Sunden B. Dynamic temperature simulation in district heating systems in Denmark regarding pronounced transient behaviour. J Environ Manage 2011;17:79–87.
[12] Gabrielaitiene I, Bøhm B, Sunden B. Modelling temperature dynamics of a district heating system in Naestved, Denmark—a case study. Energy Convers Manage 2007;48:78–86. http://dx.doi.org/10.1016/j.enconman.2006.05.011.
[13] Gabrielaitiene I, Kacianauskas R, Sunden B. Application of the finite element method for modelling of district heating networks. vol. 9. University of Ljubljana: Digital Library of Construction Informatics and Information Technology in Civil Engineering and Construction; 2001.
[14] Gabrielaitiene I, Kacianauskas R, Sunden B. Thermo-hydraulic finite element modelling of district heating network by the uncoupled approach. J Civ Eng Manage 2012;9:153–62.
[15] Stevanovic VD, Zivkovic B, Prica S, Maslovaric B, Karamarkovic V, Trkulja V. Prediction of thermal transients in district heating systems. Energy Convers Manage 2009;50:2167–73. http://dx.doi.org/10.1016/j.enconman.2009.04.034.
[16] Li H, Svendsen S. Energy and exergy analysis of low temperature district heating network. Energy 2012;45:237–46. http://dx.doi.org/10.1016/j.energy.2012.03.056.
[17] Haiyan L, Valdimarsson P. District heating modelling and simulation. In: Thirty fourth Work. Geotherm. Reserv. Eng. Stanford; 2009. p. 10.
[18] Hassine I Ben, Eicker U. Control aspects of decentralized solar thermal integration into district heating networks. In: Proc 2nd int conf sol heat cool build ind (SHC 2013). Vol. 48; 2014. p. 1055–64. http://dx.doi.org/10.1016/j.egypro.2014.02.120.
[19] Hassine BI, Eicker U. Simulation and optimization of the district heating network in Scharnhauser park. In: Proc. 2nd polygeneration conf., Tarragona; 2011.
[20] Sener AC. Modelling of Balcova geothermal district heating system, Turkey, vol. 13. Reykjavik, Iceland: The United Nations University, Geothermal Training Programme; 2002.
[21] Liu X, Wu J, Jenkins N, Bagdanavicius A. Combined analysis of electricity and heat networks. Appl Energy 2015:1–13. http://dx.doi.org/10.1016/j.apenergy.2015.01.102.
[22] Palsson H. Methods for planning and operating decentralized combined heat and power plants. Technical University of Denmark; 2000.
[23] Palsson H. Analysis of numerical methods for simulating temperature dynamics in district heating pipes. In: 6th Int. symp. dist. heat. cool. simul., Reykjavic; 1997.
[24] Heller A. Demand modelling for central heating systems. vol. 8. Lyngby, Denmark: Department of Buildings and Energy, Technical University of Denmark; 2000.
[25] Kicsiny R, Nagy J, Szalóki C. Extended ordinary differential equation models for solar heating systems with pipes. Appl Energy 2014;129:166–76. http://dx.doi.org/10.1016/j.apenergy.2014.04.108.
[26] Incropera FP, DeWitt DP, Bergman TL, Lavine AS. Fundamentals of heat and mass transfer, vol. 6th. John Wiley & Sons; 2007. http://dx.doi.org/10.1016/j.applthermaleng.2011.03.022.
[27] Cengel YA, Cimbala JM. Fluid mechanics – fundamentals and applications, vol. 1. New York: McGraw Hill; 2006.
[28] Ben Hassine I, Eicker U. Impact of load structure variation and solar thermal energy integration on an existing district heating network. Comb Spec Issues ECP 2011 IMPRES 2010 2013; 50: 1437–46. http://dx.doi.org/10.1016/j.applthermaleng.2011.12.037.
[29] Dıaz G, Sen M, Yang KT. Effect of delay in thermal systems with long ducts. Int J Therm Sci 2004;43:249–54. http://dx.doi.org/10.1016/j.ijthermalsci.2003.07.004.
[30] Liu X, Mancarella P. Modelling, assessment and Sankey diagrams of integrated electricity-heat-gas networks in multi-vector district energy systems. Appl Energy 2015. http://dx.doi.org/10.1016/j.apenergy.2015.08.089.
[31] Mathworks. Variable time delay, variable transport delay 2014; 2014.
[32] Mathworks. Simulink – Simulation and model-based design 2014. <http://www.mathworks.com/products/simulink/>.
[33] Shah Timothy, Beckstead C. Saanich Peninsula: Wastewater heat recovery; 2012.
[34] Urecon. Urecon Pre-Insulated Standard Wall, ASTM A53 Grade B Steel Core Pipe 2015. <http://www.urecon.com/documents/documents_steel.html>.
[35] F-3500 Series, Insertion Electromagnetic Flow Meter, Onicon Incorporated 2015:2. <http://photos.state.gov/libraries/uae/323264/spare-parts/0520-13f3500catalog-sheet-05-14.pdf>.
[36] The Mathworks Inc., Partial Differential Equation Toolbox – User's Guide; 2007.
[37] District Heating and Cooling Market – Global Industry Analysis, Size, Share, Trends, Growth and Forecoast 2015 – 2023. Transpar Mark Res 2014. <http://www.transparencymarketresearch.com/district-heating-cooling-market.html>.
[38] Sarbu I, Valea E. Energy savings potential for pumping water in district heating stations. Sustainability 2015;7:5705–19. http://dx.doi.org/10.3390/su7055705.
[39] Prato A Pini, Strobino F, Broccardo M, Parodi Giusino L. Integrated management of cogeneration plants and district heating networks. Appl Energy 2012:10. http://dx.doi.org/10.1016/j.apenergy.2012.02.038.

Appendix C:

Coupled electrical-thermal grids to accommodate high penetrations of renewable energy in an isolated system

Duquette J, Wild P, Rowe A. Coupled electrical-thermal grids to accomodate high penetrations of renewable energy in an isolated system. Renewable Energy 2016; *Submitted*.

Coupled electrical-thermal grids to accommodate high penetrations of renewable energy in an isolated system

Jean Duquette[a], Peter Wild[b], Andrew Rowe[c]

[a] Corresponding author, email: duquette@uvic.ca, phone: +1 250 853-3180

[b] email: pwild@uvic.ca, phone: +1 250 721-8901

[c] email: arowe@uvic.ca, phone: +1 250 721-8920

Institute for Integrated Energy Systems

Department of Mechanical Engineering

University of Victoria

PO Box 1700, Stn. CSC, Victoria, BC

V8W 2Y2, Canada

Abstract

A coupled electrical-thermal grid is an integrated energy system in which distributed electrical and heating loads are linked at one or more central generation points via both an electrical grid and a district heating grid. In this work, an assessment is conducted of the impacts associated with converting a conventional isolated energy system to one of two configurations. The first configuration consists of an uncoupled electrical grid with wave power integration and building-based heating systems. The second configuration consists of a coupled electrical-thermal grid with wave power integration and a centralized electric boiler plant. A high temporal resolution model calculates district heating grid losses, fossil fuel consumption, and CO_2 emissions for the case of an isolated community on the west coast of Vancouver Island. Results show that fossil fuel consumption and CO_2 emissions in the coupled grid are lower by up to 47% relative to the uncoupled grid. Additionally, wave energy utilization is greater by up to 1.5 times in the coupled grid, demonstrating the gains in overall efficiency that can be achieved when an electric boiler plant is used to convert excess wave power to heat.

Keywords

District heating, simulation, wave energy, heat loss, CHP, coupled electrical-thermal grid

Nomenclature

Symbols

$\eta_{propane}$	Propane heater thermal efficiency (%)
$\eta_{elec,heat}$	Electrical heater thermal efficiency (%)
COP_{GSHP}	Ground source heat pump coefficient of performance
L_{elec}	Community electrical heating and appliance load (kW)
E_{wave}	Available wave energy (kW)
G_{elec}	Electricity generation from powerhouse (kW)
$E_{wave,gen}$	Wave energy integration in the energy system (kW)
$E_{wave,excess}$	Excess wave energy (kW)
G_{small}	Installed capacity of small diesel generator (kW)
G_{medium}	Installed capacity of medium diesel generator (kW)
G_{large}	Installed capacity of large diesel generator (kW)
$G_{\min}$	Minimum allowable diesel plant output (kW)
$\delta_{pl,\min}$	Minimum allowable generator part load (%)
Q_{CHP}	Heat generation from the CHP plant (kW)
Q_{Be}	Heat generation from the electric boiler plant (kW)
Q_{Bd}	Heat generation from the diesel boiler plant (kW)
$Q_{propane}$	Heat generation from building-based propane heaters (kW)
Q_{excess}	Excess heat generation (kW)
$L_{heat,ph}$	Powerhouse heating load (kW)
L_{heat}	Community heating load (kW)

η_{Be}	Electric boiler plant thermal efficiency (%)
η_{Bd}	Diesel boiler plant thermal efficiency (%)
$\eta_{propane}$	Building-based propane heater thermal efficiency (%)
$r_{heat\_to\_fuel}$	CHP plant heat to fuel ratio (%)
f_G	Diesel generator fuel consumption (kW)
$f_{G,spin}$	Diesel generator fuel consumption when generator is 'spinning' (kW)
$f_{G,\mathrm{FL}}$	Diesel generator fuel consumption at full load (kW)
$f_{propane}$	Building-based propane heater fuel consumption (kW)
f_{Bd}	Diesel boiler plant fuel consumption (kW)
η_G	Diesel generator electrical efficiency (%)
$\eta_{G,\max}$	Diesel generator electrical efficiency at full load (%)
r_{spin}	Spinning fuel ratio (%)
e_{diesel}	Diesel CO_2 emission factor ($kgCO_2$/kWh)
$e_{propane}$	Propane CO_2 emission factor ($kgCO_2$/kWh)
k_{pipe}	Steel pipe thermal conductivity (W/mK)
k_{ins}	Foam insulation thermal conductivity (W/mK)
k_{casing}	Polyethylene casing thermal conductivity (W/mK)
ε_{pipe}	Steel pipe inner wall absolute roughness coefficient (m)
η_{pump}	Average pump efficiency (%)
T_{supply}	District heating grid supply temperature (°C)

ΔT_{HEX}	Temperature differential across consumer heat exchanger (°C)
d	Pipe burial depth (m)
k_{soil}	Soil thermal conductivity (W/mK)
$\dot{m}$	Mass flow rate (kg/s)
Q_{peak}	Peak heating load (kW)
c_p	Specific heat capacity (kJ/kgK)
$L_{heat\_ph\_a}$	Annual powerhouse heating load (MWh)
L_{heat_a}	Annual community heating load (MWh)
Q_{CHP_a}	Annual heat generation from the diesel CHP plant (MWh)
Q_{Be_a}	Annual heat generation from the electric boiler plant (MWh)
Q_{CHP+Be_a}	Total annual heat generation from the diesel CHP and electric boiler plants (MWh)
r_{elec_gen}	Electrical generation ratio (%)
r_{heat_gen}	Heat generation ratio (%)
r_{WEU}	Wave energy utilization ratio (%)

Abbreviations

HPVG	High penetration variable generation
DH	District heating
CHP	Combined heat and power
PV	Photovoltaic
SS-VTD	Steady state – variable transport delay

GSHP	Ground source heat pump
WEC	Wave energy converter
FO	Full occupancy
LO	Limited occupancy
DL	Dump load
VG	Variable displacement generator
GCU	Grid control unit
RME	Resolute marine energy
WEP	Wave energy penetration
B	Building
C	Building cluster
P	Pump
CT	Cooling tower
CFL	Courant-Friedrichs-Levy
SWAN	Simulating waves near shore

1 Introduction

High penetration variable generation (HPVG) systems are electrical power systems that are capable of accommodating instantaneous penetrations of variable renewable sources such as wind, wave, and solar at levels exceeding roughly 25% of the instantaneous demand [1,2]. HPVG systems typically have lower emissions than conventional fossil fuel based power systems [3] but can be difficult to control due to the intermittent nature of renewable generation which can affect grid stability, safety, and reliability [4].

One technique for balancing supply and demand in HPVG systems is to couple electrical and thermal grids [5–7]. A coupled electrical-thermal grid is an integrated energy system in which distributed electrical and heating loads are linked at one or more central generation points via both an electrical grid and a district heating (DH) grid. Typical generation plants in coupled electrical-thermal grids include combined heat and power (CHP), electric boilers, and heat pumps [8,9]. Excess variable renewable generation that would otherwise be curtailed or dumped in an uncoupled grid is converted to hot water using electric boilers and/or heat pumps in a coupled electrical-thermal grid. The hot water produced can either be used for meeting instantaneous heating demands or sent to thermal storage tanks for future use [10].

Model-based studies have investigated the impacts of power-to-heat technologies, such as heat pumps, in coupled electrical-thermal grids for integrating high levels of variable renewable generation [11–17]. Hedegaard and Münster [11] modeled the Danish energy system in 2030 with a wind energy penetration of approximately 60% to assess the feasibility of using heat pumps and thermal storage on a large scale to support wind power integration. They demonstrated that heat pumps and thermal storage can reduce system costs, CO_2 emissions, and peak/reserve capacity requirements in the energy system. Li et al. [14] developed an energy model of a Chinese city comprising an interconnected electrical and thermal grid to identify optimal dispatch strategies for both a wind farm coupled to a heat pump plant, and a combined heat and power plant. This study showed that, relative to the case where thermal and electrical grids are operating independently, coupling electrical and thermal grids can lead to reductions in daily wind curtailment and network heat loss of up to 50% and 27%, respectively. Pensini et al. [16] constructed an energy model of the North-Eastern United States to assess the impacts of using excess electricity for heating in an energy system with a high penetration of wind and solar energy. Their analysis considered both heat pumps coupled to thermal storage in district heating grids, and electric resistance heaters coupled to high temperature thermal storage in individual buildings. They found that heat pumps are more cost-effective than electrical resistance heaters and that CO_2 emission reductions of up to 97% in the heating sector are possible, relative to the reference energy system.

Model-based studies have also investigated the impacts of electric boilers in coupled electrical-thermal grids for integrating high levels of variable renewable generation. Böttger et al. [18] modeled the German energy system for the years 2012 and 2025 to assess the impacts of integrating 1000 MW of electric boiler capacity in district heating grids for accommodating wind and solar photovoltaic (PV) energy sources. This study demonstrates that when wind and solar PV penetrations of 23% and 54% are considered, CO_2 emission reductions of 0.4 and 1.8 million tons, and power generation cost reductions of up to 65 and 158 million Euros are possible for the 2012 and 2025 energy systems, respectively. Blarke [19] compared electric boilers and heat pumps for balancing excess wind generation in the Danish energy system for the years 2003 to 2010. Heat and power generation from existing CHP plants and wind energy penetrations were fixed in his analysis, as was the total thermal storage capacity. This study showed that both electric boilers and heat pumps are capable of providing consistent improvements regarding the intermittency-friendliness of the energy system relative to the reference case, however, heat pumps are able to do so in a more cost-effective manner.

As described above, the majority of the coupled HPVG literature focuses on the impacts of integrating renewable energy on total CO_2 emissions for a fixed renewable energy penetration scenario. The majority of these studies are conducted using hourly resolution models in which DH grid distribution losses are assumed to be constant. No studies have been identified that analyze a coupled HPVG electrical-thermal grid using a high temporal resolution model that is capable of calculating DH grid distribution losses. Nor do any studies examine a range of different renewable energy penetration scenarios.

The primary objective of this study is to assess the impacts of renewable energy integration in a coupled HPVG electrical-thermal grid over a range of renewable energy penetration scenarios using a high temporal resolution model that calculates DH grid distribution losses (*i.e.* heat losses and electrical pumping requirements), fossil fuel consumption, and CO_2 emissions. A secondary objective is to assess the impacts of DH grid distribution losses on the total thermal load that must be supplied at the central generation plant (*i.e.* the powerhouse) in the coupled HPVG system. DH grid distribution losses are calculated using a steady state - variable transport delay (SS-VTD) model [20].

2 Methodology

The energy system of the Hot Springs Cove community, located on the west coast of Vancouver Island, Canada is used as the case study in the analysis. The population of Hot Springs Cove varies from approximately 50 to 80 from winter to summer, respectively. There are 44 buildings in the community: 37 residential buildings and 7 non-residential buildings [21]. Non-residential buildings include a school, band office, health centre, lodge, communications building, water treatment plant, and a powerhouse. The community is not grid connected and derives all of its annual electrical energy needs from a diesel generator plant. Wave energy integration is considered in the current study as the wave climate near Hot Springs Cove is favorable for wave energy development [22].

Models are constructed in the Matlab/Simulink™ environment corresponding to three scenarios: a reference scenario, a wave energy scenario and a DH-wave energy scenario. A description of each of these scenarios is provided in Section 2.2. The wave energy and DH-wave energy scenarios are the key scenarios for comparison in the current study as these represent uncoupled and coupled electrical-thermal grids, respectively, and include variable renewable generation. Electrical load data from 2011 is used in all scenarios as this is the most recent year for which hourly electrical load data is available for the community. Heating load data is calculated for 2011 based on data obtained from [21].

2.1 The Hot Springs Cove energy model

Matlab/Simulink™ is used to model the Hot Springs Cove energy system. Table 1 summarizes annual electrical and heating loads by building type and end-use conversion technology in the Hot Springs Cove community [21]. End-use conversion technologies include electrical heaters, propane heaters, and a ground source heat pump. Building types include residential, commercial, and a school. Residential buildings are subdivided into full and limited occupancy buildings. The total annual electricity generation in the community is comprised of the sum of the annual non-heating electrical load and the annual heating load supplied by electrical heaters and the GSHP, shown in Table 1. Electricity is supplied by a central diesel generator plant which comprises three generator units of varying size. Electrical resistance heating is the primary heating source in the existing community, whereas propane heating is the secondary heating source. Heating in the school is primarily supplied via a ground source heat pump. Although wood is also used for heating in Hot Springs Cove, it is not considered in the model as it is a small component and a reliable estimate could not be found regarding its annual usage. Both annual electrical and heating loads are aggregated, respectively, in the Hot Springs Cove energy model.

Table 1: Annual non-heating electrical load and annual heating load by building type and end-use conversion technology in Hot Springs Cove community for 2011. FO, LO, $\eta_{propane}$, $\eta_{elec,heat}$, GSHP, and COP_{GSHP} refer to full occupancy, limited occupancy, propane heater thermal efficiency, electrical heater thermal efficiency, ground source heat pump, and ground source heat pump coefficient of performance, respectively.

Building type	Number of buildings	Annual non-heating electrical load (MWh)	Annual heating load (MWh)		
		[a] Electrical appliances	[a,b] Electrical heaters $\eta_{elec,heat}$ = 100%	[a] Propane heaters $\eta_{propane}$ = [d] 80%	[a,c] GSHP COP_{GSHP} = [e] 3
Residential - FO	14	79	225	98	0
Residential - LO	23	37	107	47	0
School	1	59	56	37	112
Commercial	5	38	108	47	0
Total	43	213	496	229	112

[a] Calculated based on data obtained from [21]. Temporal load distributions are estimated as described in Supplementary materials - Section S.1.

[b] Includes GSHP electrical compressor load

[c] Includes heat transferred from low temperature source (does not include GSHP electrical compressor load)

[d] Based on [21]

[e] Based on [23]

2.2 Scenarios

As noted earlier, three scenarios are modeled: a reference scenario, a wave energy scenario, and a DH-wave energy scenario. The following sub-sections describe each of these scenarios.

2.2.1 Reference scenario

The reference scenario represents the community in the year 2011. A schematic of the reference scenario showing buildings B1 to B44 is shown in Figure 1. B1 is the powerhouse which comprises the diesel generator plant which supplies electricity to all buildings in the community. All buildings have an electrical and auxiliary heating load, and an electrical appliance load. The auxiliary heating load is met entirely using propane heaters in all buildings except the school which also uses a ground source heat pump.

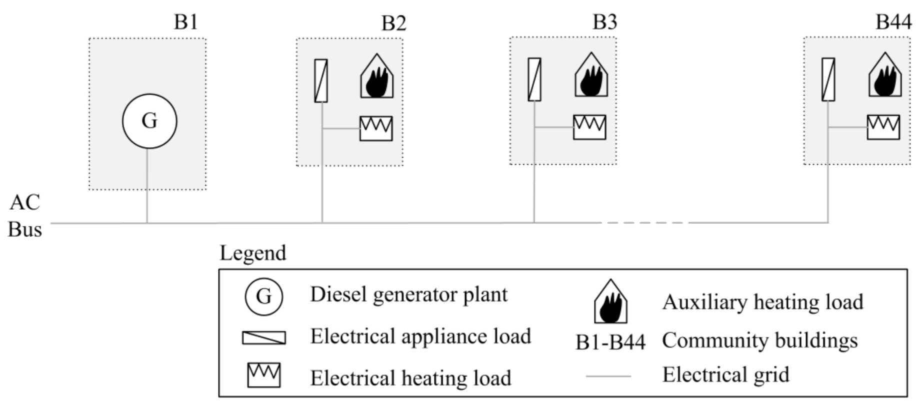

Figure 1: Schematic of reference scenario.

2.2.2 Wave energy scenario

The wave energy scenario represents the uncoupled community electrical-thermal grid with wave energy integration. In addition to the components shown in Figure 1, the wave energy scenario includes a wave energy converter (WEC) plant and a dump load, as shown in Figure 2. The dump load is used to dissipate excess wave energy that cannot be used in the energy system.

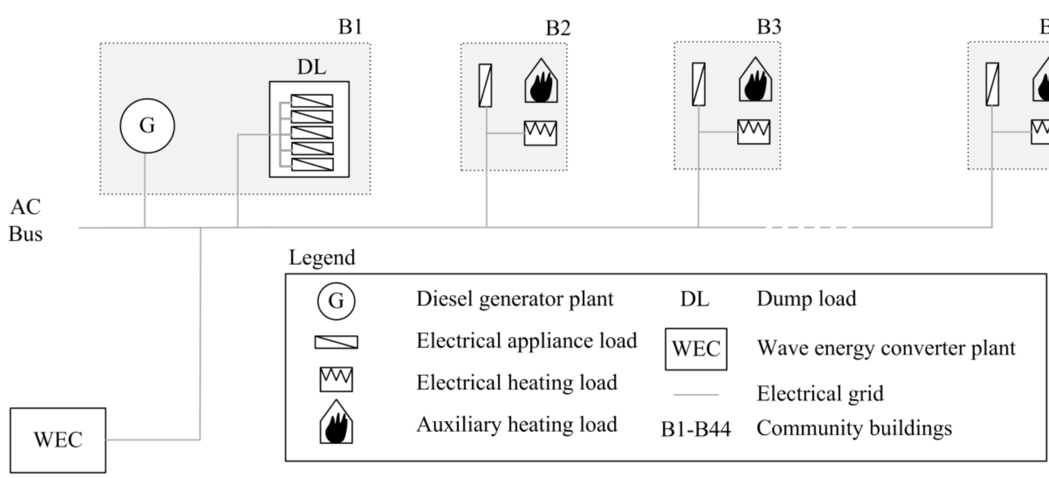

Figure 2: Schematic of wave energy scenario.

The WEC plant is based on the resolute marine energy (RME) SurgeWEC™ system. The RME WEC is a hydraulic power take off system with a rated capacity of 50 kW. The average annual wave-to-mechanical and mechanical-to-electrical efficiency of the device at the Hot Springs Cove site are approximately 40% and 50%, respectively [24]. The WEC is assumed to be operational when the average electrical power output for a given sea state is greater or equal to 25% of the WEC's rated electrical output. Below this threshold, the WEC is disabled. Details surrounding the operation of the RME WEC can be found in [25].

Wave energy penetration varies from 0-45% in the wave energy scenario. Wave energy penetration (WEP) is defined as

$$\mathrm{WEP} = \frac{\text{Annual electrical energy generation derived from wave energy}}{\text{Annual fossil fuel consumption in the reference year}} \quad . \qquad (1)$$

The total annual fossil fuel consumption in the reference year is calculated using the higher heating value of fuel and is obtained from the reference scenario. Figure 3 shows the annual wave power duration curve corresponding to a WEP of approximately 4%. The annual wave power duration curve for a given WEP is generated by arranging the annual available wave energy distribution (see Supplemental Section S.2) in descending order of magnitude, rather than chronologically, over a 1-year period.

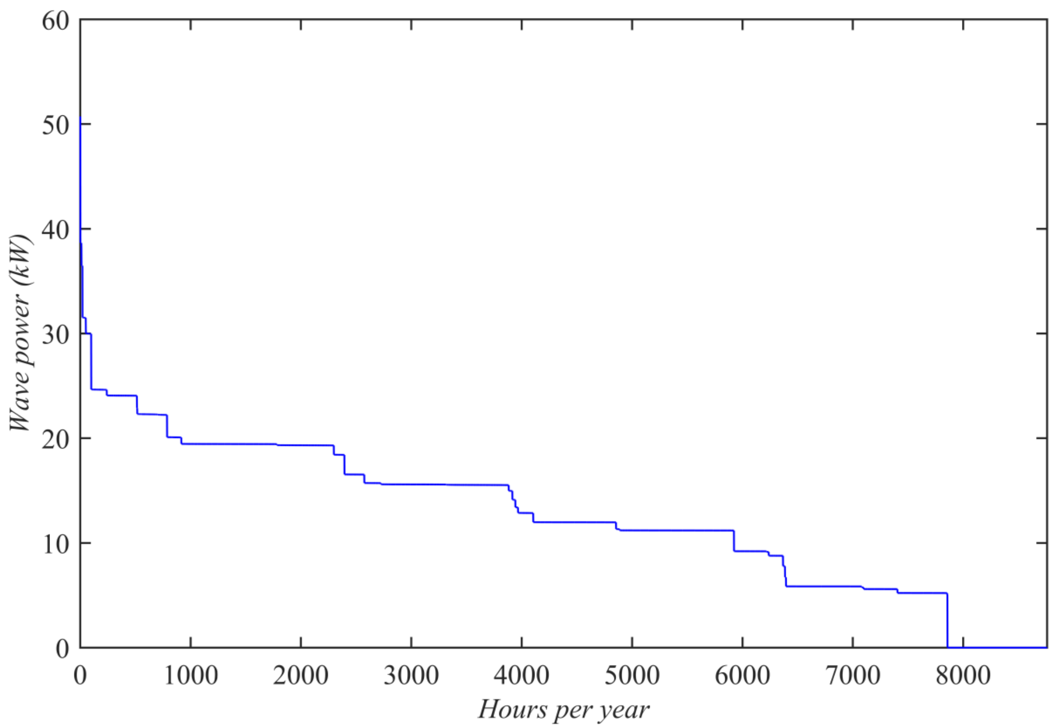

Figure 3: Annual wave power duration curve corresponding to a wave energy penetration of approximately 4%.

2.2.3 DH-wave energy scenario

The DH-wave energy scenario represents the coupled community electrical-thermal grid with wave energy integration. Powerhouse components include a diesel CHP plant, a diesel boiler plant, an electric boiler plant, a cooling tower, and a number of heat exchangers and variable speed pumps, as shown in Figure 4. The diesel CHP plant comprises three generator units of varying size. Pumping energy requirements for circulating water in the powerhouse pipes, pumps, heat exchangers, boilers, and cooling tower are not considered.

The electrical and thermal grids are coupled in the DH-wave energy scenario as wave energy is used to meet electrical loads directly, via the electrical grid, and heating loads indirectly, via the electric boiler plant. Figure 4 shows the electrical and thermal grid connections between the WEC plant, the powerhouse (C1), and the individual building clusters

(C2 – C16). Building clusters are defined as groups of buildings that are in close proximity to one another. Clusters are used instead of individual buildings in the DH grid model to minimize the computational intensity of the DH-wave energy scenario. The DH grid model is described in Section 2.4.

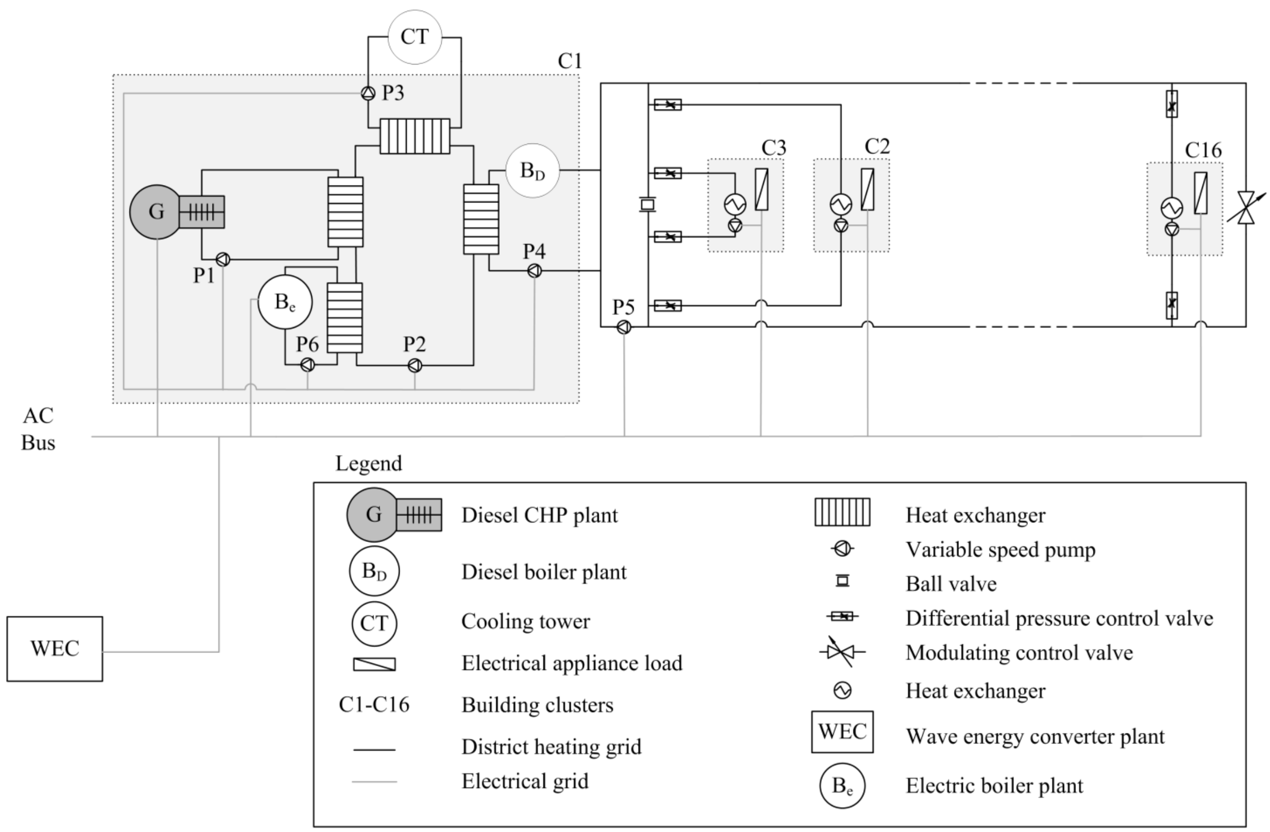

Figure 4: Schematic of DH-wave energy scenario.

The DH-wave energy scenario also differs from the wave energy scenario in that the annual building heating loads are not aggregated and are met entirely using the diesel CHP plant, the electric boiler plant and the diesel boiler plant via the DH grid using heat exchangers with an assumed efficiency of 1. Building cluster loads, end-use conversion technologies, and assumed efficiencies are listed in Table A. 1 of the Appendix. The ratio of useful heat generation to primary fuel energy consumed in the CHP plant (*i.e.* heat to fuel ratio) is 40% [26] . The diesel

CHP plant comprises a small, a medium and a large generator unit. Installed capacities corresponding to these units are listed in Table 2. Also shown in Table 2 are the installed capacities of the generator units considered in the reference and wave energy scenarios.

Table 2: Diesel plant generation unit installed capacity by size and scenario.

		Unit installed capacity (kW)		
Scenario	Diesel plant type	Small	Medium	Large
Reference	Generator	[a] 75	[a] 115	[a] 220
Wave energy	Generator	[a] 75	[a] 115	[a] 220
DH-wave energy	CHP	[b] 20	[b] 50	[b] 150

[a] Based on [21]

[b] Calculated (see Supplementary materials - Section S.4)

The Simulink® software is used to conduct time series simulations on the three scenarios described in Section 2.2 using an explicit fixed step continuous solver based on Euler's method [27]. Simulations are carried out over a one year period using 30 second time steps. A time step of 30 seconds is used as it is the largest simulation time step that can be used in the DH grid model without violating the Courant-Friedrichs-Levy (CFL) stability criterion [20].

2.3 Scenario dispatch strategy

2.3.1 Electrical dispatch

A technical dispatch strategy is used to allocate electricity generation at each 30 second time step for a period of one year for all scenarios with the objective of minimizing fossil fuel consumption. For the reference scenario, the diesel generator plant is used to meet the community electrical heating and appliance load. For the wave energy and DH-wave energy scenarios, the WEC plant is dispatched first if wave energy is available, followed by the diesel plant to make up the electrical balance. Only one of the three diesel units located in the diesel plant is dispatched at any given time. Available wave energy can be used to meet up to 100% of the community electrical heating and appliance load. Wave energy that cannot be accommodated in the electrical system (excess wave energy) is either sent to the dump load (wave energy scenario) to be dissipated into the environment or to the electric boiler plant (DH-wave energy scenario) to be converted to useful heat.

A detailed description of the electrical dispatch algorithm used in this study is provided in Section A.1 of the Appendix.

2.3.2 Heat dispatch

Total heat generation in the reference and wave energy scenarios is supplied via building-based electrical heaters, propane heaters, and a ground source heat pump. The technical dispatch strategy used to meet the building-based electrical heating load in these scenarios is described in Section 2.3.1. Building-based propane and ground source heat pump heating loads in these scenarios are met on demand.

Total heat generation in the DH-wave energy scenario is supplied via the powerhouse, which includes a diesel CHP plant, an electric boiler plant, a diesel boiler plant, and a number of pumps, as shown in Figure 4. A technical dispatch strategy is used to allocate heat generation in the powerhouse at each 30 second time step for a period of 1 year for the DH-wave energy scenario with the objective of minimizing fossil fuel consumption. If heat is available from the diesel CHP and/or electric boiler plants, these plants are dispatched first, followed by the diesel boiler plant to make up the heat balance. Excess heat generation from these plants is sent to the cooling tower to be dissipated into the environment. The amount of heat available from the diesel CHP plant is based on the amount of fossil fuel the plant consumes (see Supplementary materials - Section S.5). The amount of heat available from the electric boiler plant is based on the amount of excess wave energy that is available. Heat is generated at the powerhouse to supply the community heating load and overcome heat losses in the DH grid. DH grid heat losses are calculated using the DH grid model (see Section 2.4).

A detailed description of the heat dispatch algorithm used in this study is provided in Section A.2 of the Appendix.

2.4 The DH grid model

Using the building clustering method, heating loads from the 44 buildings located in the community are reduced to 16. Figure 5 shows the geographical layout of the 16 building clusters, labeled as C1-C16, which comprise the DH grid model. A full description of the building clustering method can be obtained from Ref. [28].

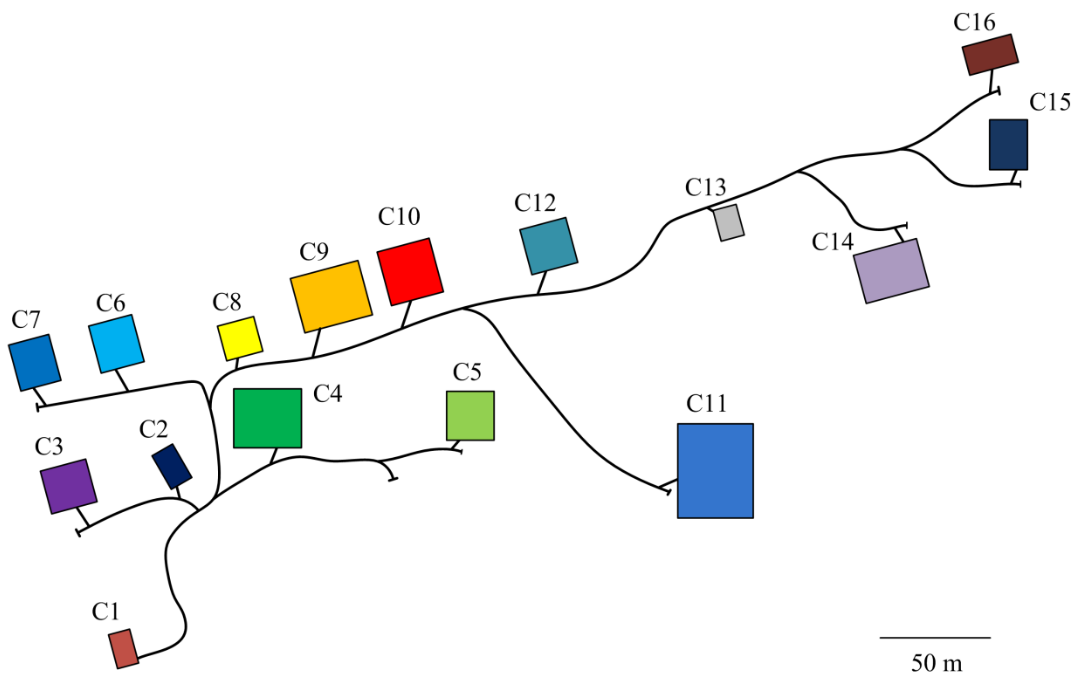

Figure 5: Geographical layout of the 16 building clusters considered the DH grid model. C1 represents the powerhouse.

The DH grid is modeled as a system of interconnected pipes which delivers heat from the powerhouse to individual building clusters, as shown in Figure 4. The DH grid includes a primary variable speed pump, shown as P5 in Figure 4, for circulating hot water in the system and a modulating control valve. Each building cluster shown in Figure 4 comprises an electrical appliance load, a heat exchanger, and a variable speed pump for circulating hot water from the DH grid to the building cluster. Additionally, differential pressure control valves are used for maintaining a hydraulic balance throughout the DH grid.

The DH grid operates as a supply-return, variable flow system. The main variable speed circulation pump, P5, is pressure controlled and varies its speed in order to maintain a set point pressure differential across the modulating control valve. Cluster-based variable speed pumps on the other hand, are temperature controlled and vary their speed in order to maintain a set point temperature differential across the DH side of the heat exchanger.

The DH grid is modeled using the steady state - variable transport delay (SS-VTD) model. The SS-VTD model is a load driven pipe flow model that allows rapid computation of grid heat losses, grid pumping energy requirements, and pipe outlet temperatures. The model also tracks time delays in the pipes as the flow rate varies. A thorough description and validation of the SS-VTD model is provided in Ref. [20].

All pipes in the DH grid are assumed to be made of steel, and are surrounded by a layer of foam insulation and a polyethylene casing. The soil surface temperature varies with time in the DH grid model and is assumed to be equal to the outside air temperature in the reference year. Table 3 shows a breakdown of select input parameters, utilized in the DH grid model. Pipe parameters, shown in Table 3, are based on standard specifications for commercially available insulated steel pipe [29]. Other fixed inputs in the model include the pipe burial depth (d), the DH grid supply temperature (T_{supply}), the temperature differential across the district heating side of the consumer heat exchanger (ΔT_{HEX}), and the average pumping efficiency (

η_{pump}). A T_{supply} value of 70°C is assumed in the model to minimize ground heat losses. The method used for sizing individual pipes in the DH grid is described in Supplementary materials - Section S.6.

Table 3: Input parameters assumed in the DH grid model.

Parameter name	Symbol	Value
Steel pipe thermal conductivity	k_{pipe}	[a] 43 W/mK
Foam insulation thermal conductivity	k_{ins}	[a] 0.025 W/mK
Polyethylene casing thermal conductivity	k_{casing}	[a] 0.45 W/mK
Steel pipe inner wall absolute roughness coefficient	ε_{pipe}	[a] 4.5e-5 m
Average pump efficiency	η_{pump}	[b] 85%
District heating grid supply temperature	T_{supply}	[b] 70°C
Temperature differential across DH side of consumer heat exchanger	ΔT_{HEX}	[b] 30°C
Pipe burial depth	d	[b] 1 m
Soil thermal conductivity	k_{soil}	[b] 0.6 W/mK

[a] Based on [29]

[b] Based on data from existing DH grids operating on Vancouver Island

2.5 Model validation

The model is validated to verify that the reference scenario is representative of the 2011 Hot Springs Cove electrical system. The total documented diesel generator plant output for the reference year is compared with the calculated output in the reference scenario. As the percent difference between the values is less than 2%, the reference scenario is considered to be an acceptable basis for comparison in the study.

3 Results

Figure 6 shows the annual heat generation from the diesel CHP plant (Q_{CHP_a}), the annual heat generation from the electric boiler plant (Q_{Be_a}), and the total annual heat generation from both plants combined (Q_{CHP+Be_a}) as a function of wave energy penetration (WEP) in the DH-wave energy scenario. As shown in Figure 6, increasing WEP from 0% to 45% causes a decrease in the annual heat generation from the diesel CHP plant from 330 MWh to 80 MWh. This decrease is caused by higher levels of wave energy displacing CHP plant electrical generation which in turn causes the CHP plant to run less frequently and generate less heat. Corresponding to this decrease is an increase in the annual heat generation from the electric boiler plant from 0 MWh to 1122 MWh. This increase is directly proportional to the increase in WEP. When considering both the CHP plant and the electric boiler plant combined, increasing WEP from 0% to 4% causes a decrease in the total annual heat generation from 330 MWh to 236 MWh, respectively, followed by a gradual increase to 1202 MWh as WEP increases to 45%.

Figure 6 also shows the annual powerhouse heating load ($L_{heat\_ph\_a}$) and the annual community heating load (L_{heat_a}). Both of these values are constant as WEP increases in the DH-wave energy scenario and are equal to 938 MWh and 837 MWh, respectively. The former is greater than the latter as heat losses occur in the DH grid.

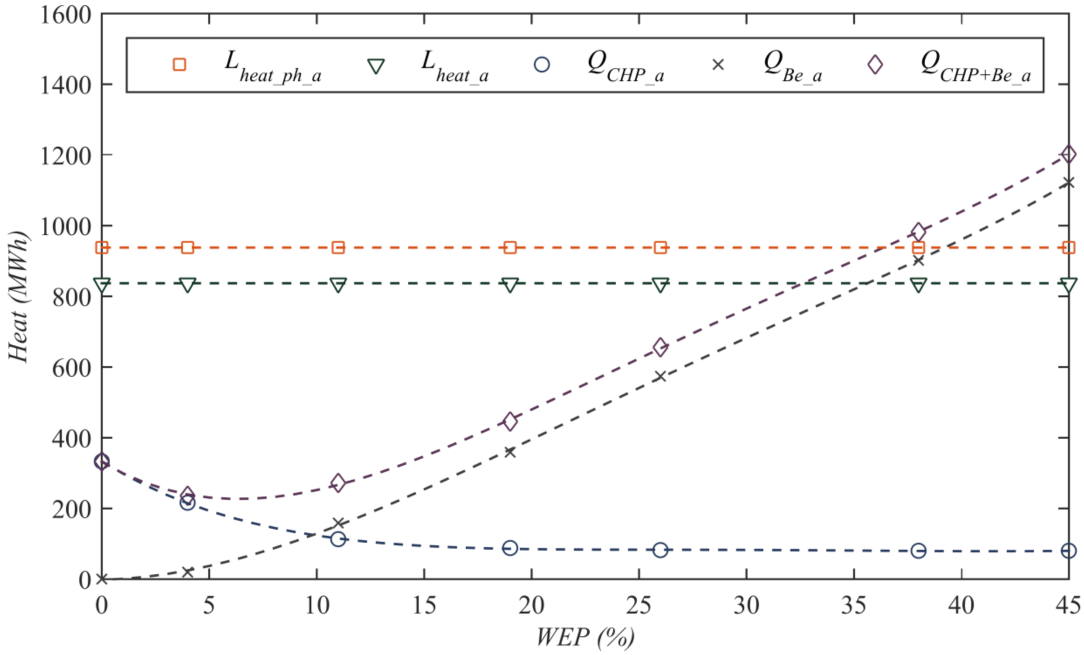

Figure 6: Annual powerhouse heating load ($L_{heat\_ph\_a}$), annual community heating load (L_{heat_a}); and annual heat generation from the diesel CHP plant (Q_{CHP_a}), annual heat generation from the electric boiler plant (Q_{Be_a}), and total annual heat generation from both plants combined (Q_{CHP+Be_a}) as a function of wave energy penetration (WEP) in the DH-wave energy scenario.

DH grid heat losses vary throughout the year, as shown by the annual heat loss ratio duration curve depicted in Figure 7 (*a*). This curve is created by dividing the DH grid heat loss by the powerhouse heating load at each time step in a one year period and then ordering the resulting values from largest to smallest magnitude. Figure 7 (*a*) shows that the heat loss ratio in the DH-wave energy scenario varies between approximately 7% and 21% for over 98% of the year and between approximately 21% and 25% for the remainder of the year.

Electrical pumping requirements in the DH grid vary throughout the year, as shown by the annual pump loss ratio duration curve depicted in Figure 7 (*b*). This curve is created by dividing the DH grid electrical pump load by the powerhouse heating load at each time step in a one year period and then ordering the resulting values from largest to smallest magnitude.

Figure 7 (*b*) shows that the pump loss ratio in the DH-wave energy scenario varies between approximately 0.1% and 0.3% for over 98% of the year and between approximately 0.3% and 0.8% for the remainder of the year.

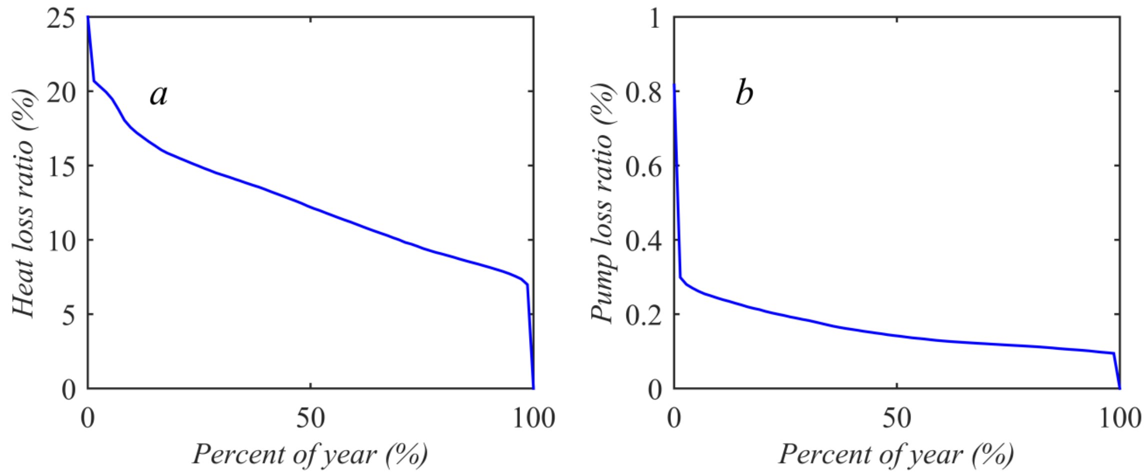

Figure 7: Annual duration curves of (*a*) heat loss ratio and (*b*) pump loss ratio in the DH-wave energy scenario.

Figure 8 shows the electrical and heat generation ratios for the wave energy scenario and the DH-wave energy scenario as a function of WEP. The electrical generation ratio (r_{elec_gen}) is defined as

$$r_{elec\_gen} = \frac{\text{Annual useful electrical energy generation derived from wave energy}}{\text{Annual electrical energy generation at the powerhouse}} , \qquad (2)$$

where useful electrical energy represents energy that is used to do work and/or generate heat in the community. The heat generation ratio (r_{heat_gen}) is defined as

$$r_{heat\_gen} = \frac{\text{Annual useful heat generation derived from CHP and electric boiler plants}}{\text{Annual heat generation at the powerhouse}} , \qquad (3)$$

where useful heat represents energy that is used to meet heating loads in the community. As the electrical generation ratio increases, more electrical energy derived from wave energy displaces generation from the diesel generator plant (wave energy scenario) or the diesel CHP plant (DH-wave energy scenario). As the heat generation ratio increases, more heat derived from the diesel CHP plant and the electric boiler plant displaces generation from the diesel boiler plant in the DH-wave energy scenario. The electrical generation ratio is greater in the DH-wave energy scenario than in the wave energy scenario. This is due to the reduced electrical energy generation requirement at the powerhouse as DH services displace electrical heating services. Unutilized electrical energy generation derived from wave energy (wave energy scenario), and heat generation derived from the diesel CHP plant and the electric boiler plant (DH-wave energy scenario) are dissipated via the dump load and cooling tower, respectively.

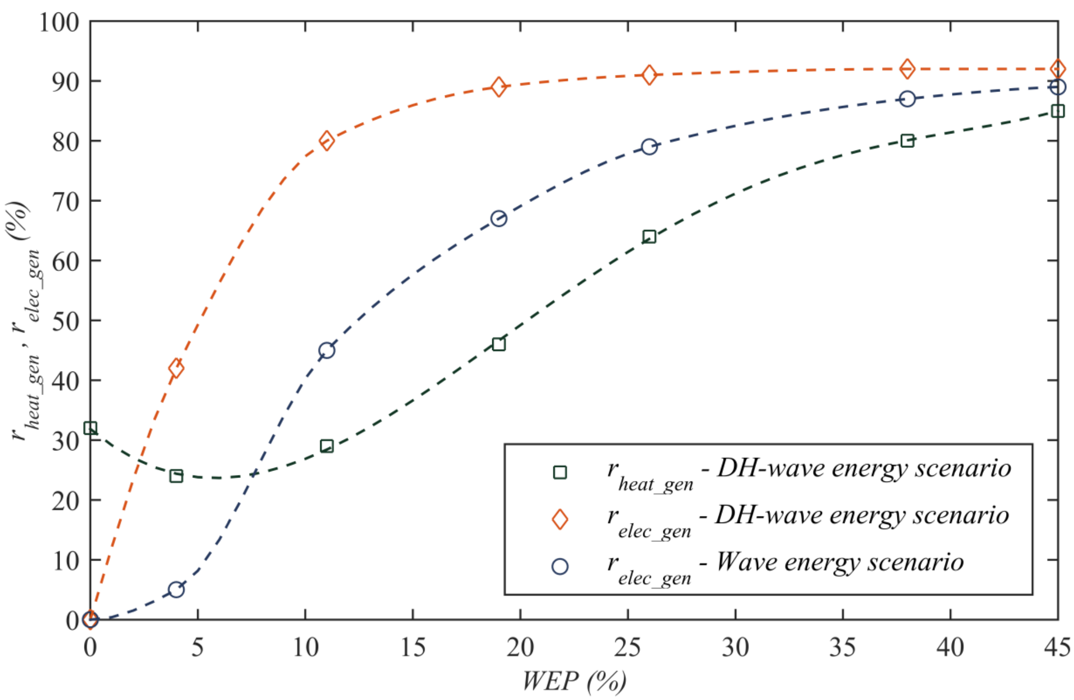

Figure 8: Heat generation ratio (r_{heat_gen}) and electrical generation ratio (r_{elec_gen}) as a function of wave energy penetration (WEP) in the wave energy and DH-wave energy scenarios.

Figure 9 shows the wave energy utilization ratio as a function of WEP for both the wave energy scenario and the DH-wave energy scenario. The wave energy utilization ratio (r_{WEU}) is defined as

$$r_{WEU} = \frac{\text{Annual useful electrical energy generation derived from wave energy}}{\text{Annual electrical energy generation derived from wave energy}} \tag{4}$$

As shown in Figure 9, increasing WEP causes the wave energy utilization ratio to decrease for both the wave energy scenario and the DH-wave energy scenario. As this ratio decreases, a smaller percentage of the annual electrical energy derived from wave energy is converted to useful work and a higher percentage is dissipated via the dump load (wave energy scenario) or cooling tower (DH-wave energy scenario). The wave energy utilization ratio is greater in the DH-wave energy scenario than in the wave energy scenario as the energy system efficiency is greater. In addition to contributing to electricity production, electrical energy derived from wave energy in the DH-wave energy scenario is used to generate heat via the electric boiler plant. Figure 9 shows that at a WEP set point of 45%, the wave energy utilization ratio is 48% and 72% in the wave energy scenario and DH-wave energy scenario, respectively. This difference corresponds to an increase in the wave energy utilization ratio of approximately 1.5 times, relative to the wave energy scenario.

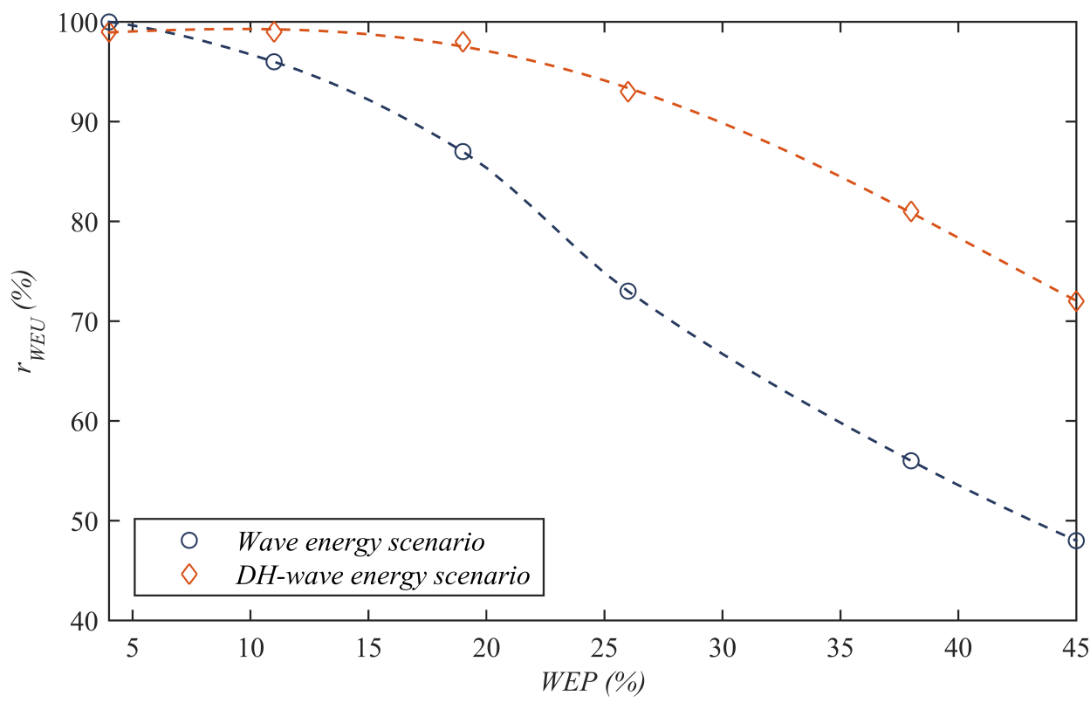

Figure 9: Wave energy utilization ratio (r_{WEU}) as a function of wave energy penetration (WEP) in the wave energy and DH-wave energy scenarios.

Fossil fuel consumption and CO_2 emissions are calculated for the reference, wave energy, and DH-wave energy scenarios and plotted as a function of WEP in Figures 10 and 11.

As shown in Figure 10, increasing WEP from 0% to 45% in the wave energy and DH-wave energy scenarios causes an overall decrease in fossil fuel consumption of approximately 60% and 77%, respectively, and is primarily due to higher levels of wave energy displacing diesel plant generation at the powerhouse, as demonstrated by the electrical and heat generation ratios in Figure 8. Figure 10 also shows that, relative to the wave energy scenario, fossil fuel consumption in the DH-wave energy scenario is lower by up to 47% over the range of WEP set points analyzed. This effect is due to the increase in overall system efficiency from adding the diesel CHP plant, electric boiler plant, and diesel boiler plant; and displacing electrical heating services with DH services.

As shown in Figure 11, increasing WEP from 0% to 45% in the wave energy and DH-wave energy scenarios causes an overall decrease in CO_2 emissions of approximately 60% and 77%, respectively. As in Figure 10, this decrease is primarily due to higher levels of wave energy displacing diesel plant generation at the powerhouse. Figure 11 also shows that the CO_2 emissions are lower in the DH-wave energy scenario than in the wave energy scenario for all WEP set points analyzed. As in Figure 10, this effect is due to the increase in overall system efficiency from adding the diesel CHP plant, electric boiler plant, and diesel boiler plant; and displacing electrical heating services with DH services. CO_2 emission reductions are also lower by approximately 0.5% on average relative to the corresponding fossil fuel consumption reductions depicted in Figure 10. This effect is due the high efficiency centralized diesel boiler plant in the DH-wave energy scenario displacing individual building propane heaters in the wave energy scenario.

Also shown in Figures 10 and 11 are two additional scenarios which comprise wave energy data from the year 2014. In 2014, annual wave energy output was higher than any other year between 2004 and 2015. In 2011 (*i.e.* the reference year) annual wave energy output was lower than any other year between 2004 and 2015. The annual wave energy output in 2014 is approximately 30% greater than in 2011. Figure 10 shows that relative to the reference year scenarios, fossil fuel consumption in the 2014 wave energy and DH-wave energy scenarios is lower by up to 9% and 21%, respectively, over the range of WEP set points analyzed. CO_2 emissions for the 2014 scenarios, shown in Figure 11, are approximately lower by these same amounts, respectively.

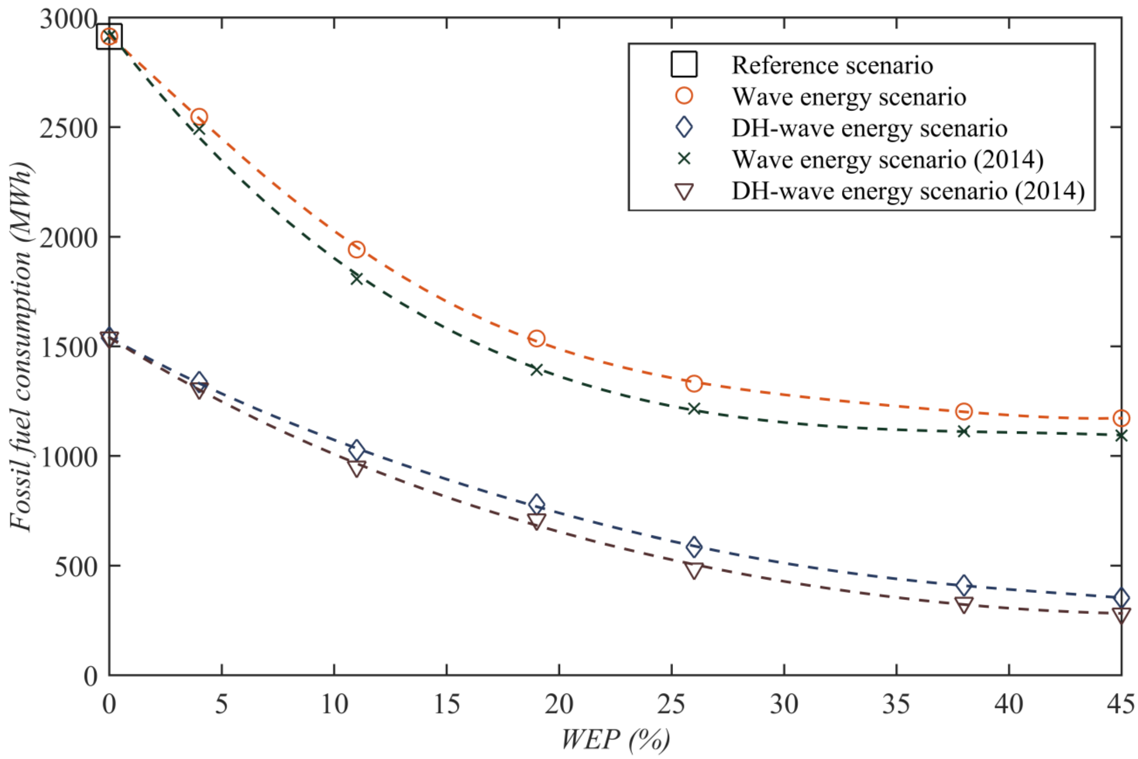

Figure 10: Fossil fuel consumption as a function of WEP in reference, wave energy, and DH-wave energy scenarios. Scenarios comprising wave energy data from the year 2014 are also shown for comparison.

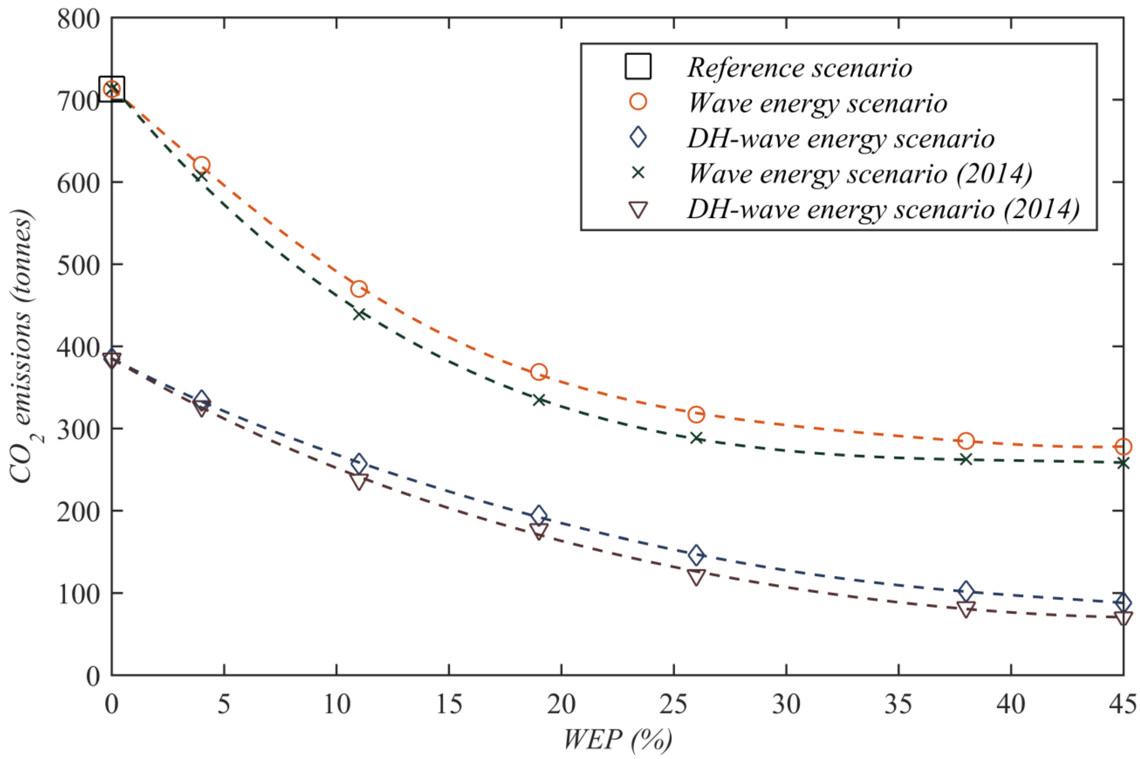

Figure 11: CO_2 emissions as a function of WEP in reference, wave energy, and DH-wave energy scenarios. Scenarios comprising wave energy data from the year 2014 are also shown for comparison.

4 Discussion

The current study demonstrates that there are clear advantages to integrating wave energy in a coupled HPVG electrical-thermal grid relative to an uncoupled HPVG grid. From a system efficiency standpoint, the coupled grid is superior to the uncoupled grid due to greater amounts of wave energy displacing total electrical and thermal generation in the system, as shown by the electrical and heat generation ratios in Figure 8, and greater amounts of wave energy being utilized, as shown by the wave energy utilization ratio in Figure 9. Lower fossil fuel consumption and CO_2 emissions are also associated with the coupled HPVG grid, as shown in Figures 10 and 11.

This study also demonstrates the impacts of DH grid heat losses and electrical pumping requirements on the total thermal load that must be supplied at the powerhouse in the coupled HPVG system, as shown in Figure 6. These impacts are assessed using a high temporal resolution pipe flow model (*i.e.* the SS-VTD model [20]). Using this model, the average annual DH grid heat loss in the Hot Springs Cove DH grid is found to be approximately 12% of the annual powerhouse heating load. This value is obtained by taking the average of the annual heat loss ratio dataset depicted in Figure 7 (a). Similarly, the average annual electrical pumping requirement is found to be equal to approximately 0.2% of the annual powerhouse heating load, and is obtained by taking the average of the annual pump loss ratio dataset depicted in Figure 7 (b). The main benefit associated with this model is its ability to accurately predict the thermal load that must be supplied at the powerhouse. If a pipe flow model were not used, heat losses and electrical pumping requirements would need to be assumed. Making such assumptions can lead to erroneous results as these values vary considerably from one DH grid to another. For example, a report by Nussbaumer and Thalmann [30] on DH grids operating in IEA countries shows average annual heat losses for fifty individual systems with similar supply temperatures (~70°C – 90°C) and different lengths to vary between approximately 5% and 20% of the annual DH grid heating load . The same study shows average annual electrical pumping requirements for nine DH grids to vary between 0.1% and 1.2% of the annual DH grid heating load.

A limitation of the current study is that it remains unclear how coupled and uncoupled HPVG grids compare from an economic standpoint. Additional consideration of capital costs and lifetimes for system components is needed to assess the economic viability of the coupled HPVG system. A second limitation of the study is that the analysis is conducted using a DH grid model comprising a number of fixed input parameters such as the supply temperature, the thermal conductivity of pipe materials and soil, the pipe burial depth, the grid size, and the pumping control method. Varying one or more of these parameters may have a significant impact on the grid distribution losses and hence on the thermal generation mix in coupled HPVG electrical-thermal grids.

Although this work focuses on wave energy integration in coupled HPVG electrical-thermal grids, the findings from the study may also be broadly applicable to other similar systems comprising intermittent variable renewable generation sources such as wind and solar energy.

5 Conclusions

A model of the 2011 Hot Springs Cove reference energy system was constructed in the Matlab/Simulink™ environment. Three scenarios: a reference scenario, a wave energy scenario, and a DH-wave energy scenario were analyzed. The wave and DH-wave energy scenarios are representative of uncoupled and coupled electrical-thermal grids, respectively. A technical dispatch was conducted on the scenarios with the objective of minimizing total fossil fuel consumption. To increase the accuracy of the DH-wave energy scenario, a high temporal resolution pipe flow model (*i.e.* the SS-VTD model) was used to calculate heat losses and electrical pumping requirements in the DH grid. On an annual basis, these parameters were found to account for approximately 12% and 0.2% of the total heat supplied to the DH grid.

Fossil fuel consumption and CO_2 emissions in the coupled grid were found to be lower by up to 47% relative to the uncoupled grid over the range of wave energy penetration (WEP) set points analyzed. Additionally, an increase in the wave energy utilization ratio of up to 1.5 times was found to occur in the coupled grid relative to the uncoupled grid, demonstrating the gains in overall system efficiency that can be achieved when utilizing an electric boiler plant to convert excess wave power to heat. The results of this study are applicable to other jurisdictions with significant installed thermal power capacity who are considering transitioning to a higher efficiency, low carbon energy system.

As the economics of coupled HPVG electrical-thermal grids were not covered, the subject remains a topic for future research. Other potential areas for future work include assessing the impacts of hot water storage, building demand side management measures, alternative power to heat technologies (*e.g.* heat pumps), and spatial variation of heating loads in coupled HPVG electrical-thermal grids.

6 Acknowledgements

The authors would like to thank the Natural Sciences and Engineering Research Council (NSERC) of Canada for their financial support and the West Coast Wave Initiative (WCWI) for their technical support in generating wave energy data. The authors are also grateful to Resolute Marine Energy (Boston, Massachusetts), Pulse Energy (Vancouver, British Columbia), BC Hydro (Vancouver, British Columbia), and the Hot Springs Cove community for their assistance in providing data.

Appendix

A.1 Electrical dispatch algorithm

Figure A. 1 of the Appendix shows the electrical dispatch algorithm which is repeated at each 30 second time step for a year. The algorithm comprises the following three steps:

1) Calculate diesel plant electricity generation (G_{elec});

2) Calculate wave energy integration in the energy system ($E_{wave,\mathrm{gen}}$) and excess wave energy ($E_{wave,\mathrm{excess}}$);

3) Select diesel generator unit to dispatch. If G_{elec} is equal to zero, the small generator is dispatched in 'spinning' mode. Dispatching the generator in 'spinning' mode is used as a precautionary measure for ensuring safe and reliable operation of the electrical grid [31]. The generator produces no power while in 'spinning' mode.

Scenario input data, depicted in the 'Scenario input data' box in Figure A. 1, is comprised of 30 second time step distributions of the community electrical heating and appliance load (L_{elec}) and available wave energy (E_{wave}). Other scenario inputs include installed capacities of the three diesel units (G_{small}, G_{medium}, and G_{large}), and the minimum allowable diesel plant output ($G_{\min}$). Installed capacities of the diesel generator units (reference and wave energy scenarios) or the diesel CHP units (DH-wave energy scenario) are set as described in Table 2. The minimum allowable diesel plant output is also set and is defined by

$$G_{\min} = G_{small} \times \delta_{pl,\min} \tag{5}$$

where $\delta_{pl,\min}$ represents the minimum allowable generator part load (see Supplementary materials - Section S.5). Installed capacities vary by scenario. E_{wave} distributions vary in the wave energy and DH-wave energy scenarios, respectively, over the wave energy penetration range specified in Section 2.2.2.

Scenario output data from the technical dispatch are shown in the 'Scenario output data' box in Figure A. 1.

A.2 Heat dispatch algorithm

Figure A. 2 of the Appendix shows the heat dispatch algorithm which is repeated at each 30 second time step for a year. The algorithm comprises the following four steps:

1) Select operating mode (*i.e.* on or off) for powerhouse pump P4;
2) Calculate diesel CHP plant heat generation (Q_{CHP}) and select operating mode for powerhouse pump P1;
3) Calculate electric boiler plant heat generation (Q_{Be}) and select operating mode for powerhouse pump P6;
4) Calculate diesel boiler plant heat generation (Q_{Bd}) and excess heat generation (Q_{excess}), and select operating mode for powerhouse pumps P2 and P3.

Scenario input data, depicted in the 'Input data' box in Figure A. 2, is comprised of 30 second time step distributions of the powerhouse heating load ($L_{heat,ph}$), excess wave energy ($E_{wave,excess}$), and generator fuel consumption (f_G) ; and fixed values for the heat to fuel ratio ($r_{heat\_to\_fuel}$), and the electric boiler efficiency (η_{Be}). $E_{wave,excess}$ distributions vary in the DH-wave energy scenario over the wave energy penetration range specified in Section 2.2.2.

Scenario output data from the technical dispatch are shown in the 'Output data' box in Figure A. 2.

Table A. 1: Annual and peak heating loads, and annual electrical loads by building cluster and end-use conversion technology for DH-wave energy scenario. η_{Be} , η_{Bd} , and $r_{heat\_to\_fuel}$ refer to the electric boiler plant thermal efficiency, the diesel boiler plant thermal efficiency, and the CHP plant heat to fuel ratio, respectively.

	[a] Annual heating load (MWh)	[a] Peak heating load (kW)	[a] Annual electrical load (MWh)

Building cluster	Electric boiler plant (η_{Be} = 100%), Diesel boiler plant (η_{Bd} = [b] 90%), CHP plant ($r_{heat\_to\_fuel}$ = [c] 40%)		Electrical appliances
2	27	7	7
3	51	13	13
4	72	18	18
5	27	7	7
6	52	13	13
7	52	13	13
8	28	7	7
9	69	17	17
10	76	19	17
11	233	55	65
12	26	7	6
13	22	5	5
14	38	10	9
15	36	9	9
16	28	8	7
Total	837	207	213

[a] Calculated based on data obtained from [21]. Temporal load distributions are estimated as described in Supplementary materials - Section S.1. Annual building cluster heating loads are estimated as described in Supplementary materials - Section S.3)
[b] Based on [32]

[c] Based on [26]

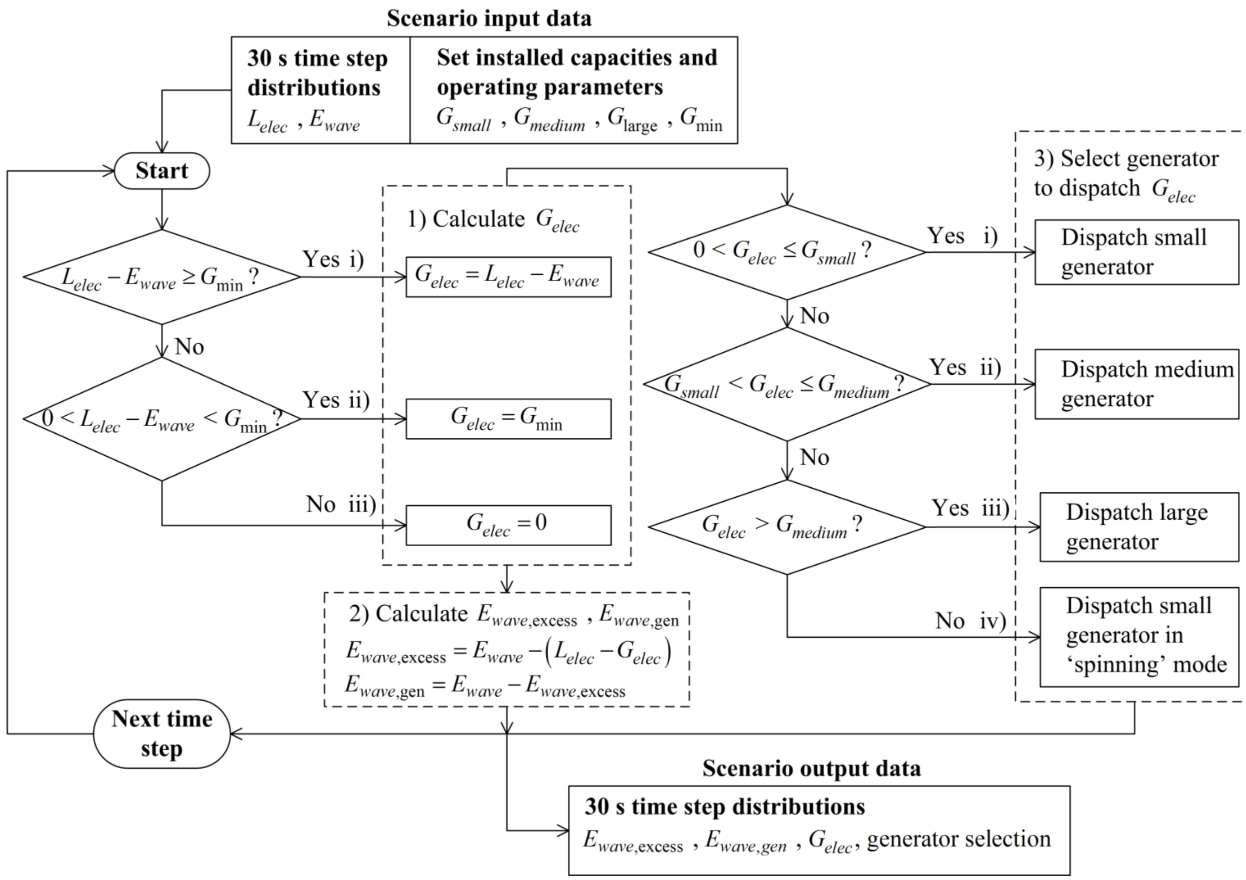

Figure A. 1: Electrical dispatch algorithm for selecting generator and calculating diesel plant electricity generation (G_{elec}), excess wave energy, ($E_{wave,excess}$), and wave energy integration in the energy system ($E_{wave,gen}$) at each 30 s time step. Inputs include the community electrical heating and appliance load (L_{elec}**),** the available wave energy (E_{wave}), set installed capacities of diesel plant units (G_{small} , G_{medium} , and G_{large}), and the minimum allowable diesel plant output (G_{min}).

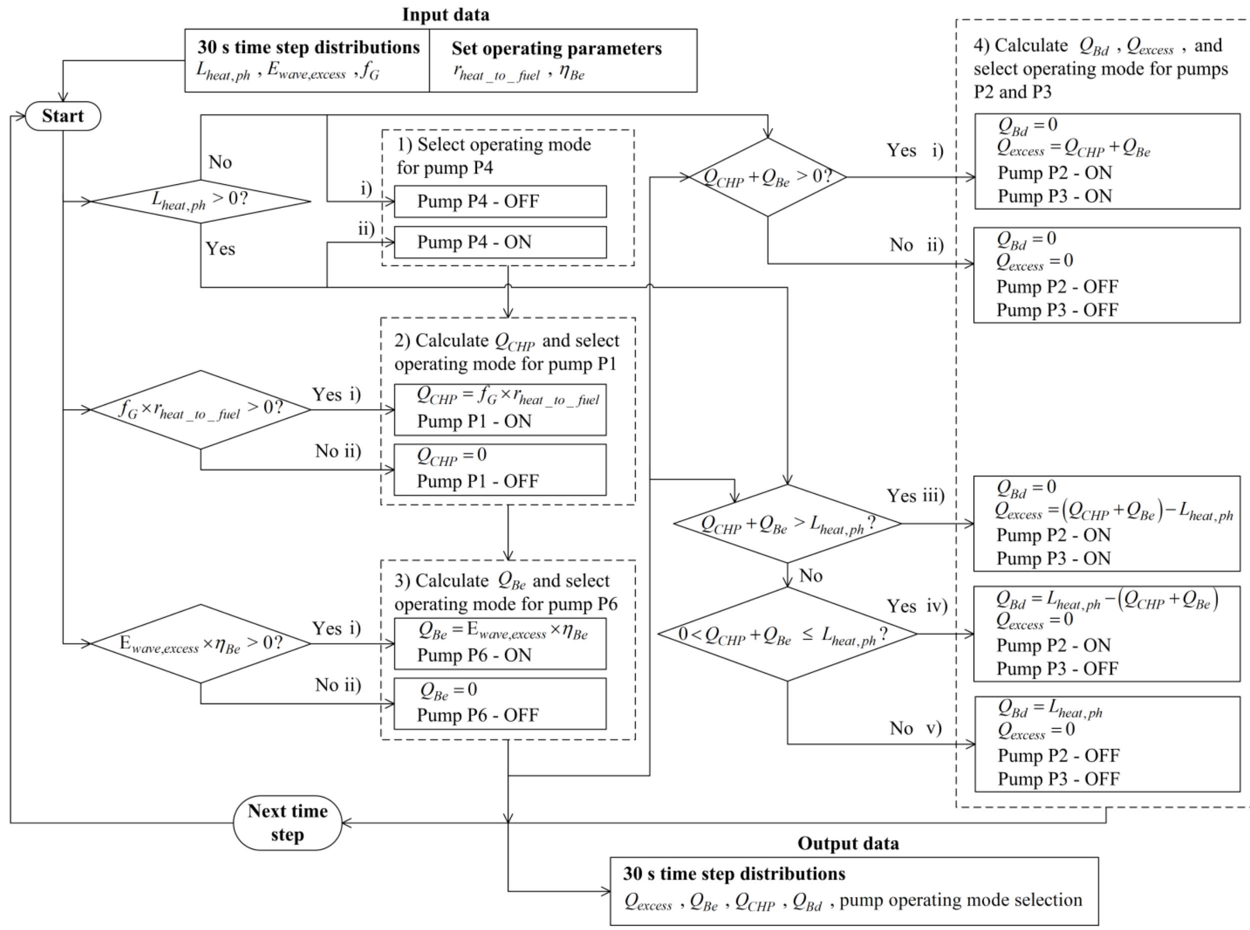

Figure A. 2: Heat dispatch algorithm for calculating heat generation from the diesel CHP plant (Q_{CHP}), heat generation from the electric boiler plant (Q_{Be}), heat generation from the diesel boiler plant (Q_{Bd}), and excess heat generation (Q_{excess}) at each 30 s time step in the DH-wave energy scenario. Inputs include the powerhouse heating load ($L_{heat,ph}$), the excess wave energy ($E_{wave,excess}$), the fossil fuel consumption of the diesel plant (f_G), the heat to fuel ratio of the diesel CHP plant ($r_{heat\_to\_fuel}$), and the electrical boiler plant thermal efficiency (η_{Be}).

References

[1] Makarov Y et. al. Analysis Methodology for Balancing Authority Cooperation in High Penetration of Variable Generation. 2010.

[2] Silva V, Lopez-Botet-Zulueta M, Wang Y. Impact of high penetration of variable renewable generation on frequency dynamics in the continental Europe interconnected system. IET Renew Power Gener 2016;10:10–6. doi:10.1049/iet-rpg.2015.0141.

[3] Mills A, Wiser R. Changes in the Economic Value of Variable Generation at High Penetration Levels : A Pilot Case Study of California. 2012.

[4] Makarov Y V, Member S, Du P, Kintner-meyer MCW, Jin C, Illian HF. Sizing Energy Storage to Accommodate High Penetration of Variable Energy Resources. IEEE Trans Sustain Energy 2012;3:34–40.

[5] Liu X, Wu J, Jenkins N, Bagdanavicius A. Combined analysis of electricity and heat networks. Appl Energy 2015:1–13. doi:10.1016/ j.apenergy.2015.01.102.

[6] Grønnegaard M, Miguel J, Zugno M, Engberg T, Madsen H. Economic valuation of heat pumps and electric boilers in the Danish energy system. Appl Energy 2015. doi:10.1016/j.apenergy.2015.08.115.

[7] Wang H, Yin W, Abdollahi E, Lahdelma R, Jiao W. Modelling and optimization of CHP based district heating system with renewable energy production and energy storage. Appl Energy 2015;159:401–21. doi:10.1016/j.apenergy.2015.09.020.

[8] Lund H, Werner S, Wiltshire R, Svendsen S, Eric J, Hvelplund F, et al. 4th Generation District Heating (4GDH) Integrating smart thermal grids into future sustainable energy systems. Energy 2014;68:1–11. doi:10.1016/j.energy.2014.02.089.

[9] Kusch W, Schmidla T, Stadler I. Consequences for district heating and natural gas grids when aiming towards 100 % electricity supply with renewables. Energy 2012;48:153–9. doi:10.1016/j.energy.2012.06.054.

[10] Bachmaier A, Narmsara S, Eggers J, Herkel S. Spatial Distribution of Thermal Energy Storage Systems in Urban Areas Connected to District Heating for Grid Balancing. Energy Procedia 2015;73:3–11. doi:10.1016/j.egypro.2015.07.549.

[11] Hedegaard K, Münster M. Influence of individual heat pumps on wind power integration – Energy system investments and operation. Energy Convers Manag 2013;75:673–84. doi:10.1016/j.enconman.2013.08.015.

[12] Hedegaard K, Mathiesen BV, Lund H, Heiselberg P. Wind power integration using individual heat pumps – Analysis of different heat storage options. Energy 2012;47:284–

93. doi:10.1016/j.energy.2012.09.030.

[13] Østergaard PA. Wind power integration in Aalborg Municipality using compression heat pumps and geothermal absorption heat pumps. Energy 2013;49:502–8. doi:10.1016/j.energy.2012.11.030.

[14] Li J, Fang J, Zeng Q, Chen Z. Optimal operation of the integrated electrical and heating systems to accommodate the intermittent renewable sources. Appl Energy 2015. doi:10.1016/j.apenergy.2015.10.054.

[15] Yang Y, Wu K, Long H, Gao J, Yan X, Kato T, et al. Integrated electricity and heating demand-side management for wind power integration in China. Energy 2014;78:235–46. doi:10.1016/j.energy.2014.10.008.

[16] Pensini A, Rasmussen CN, Kempton W. Economic analysis of using excess renewable electricity to displace heating fuels. Appl Energy 2014;131:530–43. doi:10.1016/j.apenergy.2014.04.111.

[17] Zwaenepoel B, Vansteenbrugge J, Vandoorn TL, Van Eetvelde G, Vandevelde L. Ancillary services for the electrical grid by waste heat. Appl Therm Eng 2014;70:1–6. doi:10.1016/j.applthermaleng.2014.04.010.

[18] Böttger D, Götz M, Theofilidi M, Bruckner T. Control power provision with power-to-heat plants in systems with high shares of renewable energy sources – An illustrative analysis for Germany based on the use of electric boilers in district heating grids. Energy 2015;82:157–67. doi:10.1016/j.energy.2015.01.022.

[19] Blarke MB. Towards an intermittency-friendly energy system: Comparing electric boilers and heat pumps in distributed cogeneration. Appl Energy 2012;91:349–65. doi:10.1016/j.apenergy.2011.09.038.

[20] Duquette J, Rowe A, Wild P. Thermal performance of a steady state physical pipe model for simulating district heating grids with variable flow. Appl Energy 2016;178:383–93. doi:10.1016/j.apenergy.2016.06.092.

[21] Van Dijk G, Crompton J. COMMUNITY ELECTRICITY PLAN FOR REFUGE COVE.

2013.

[22] Hiles CE, Buckham BJ, Wild P, Robertson B. Wave energy resources near Hot Springs Cove , Canada. Renew Energy 2014;71:598–608. doi:10.1016/j.renene.2014.06.020.

[23] Centre CET. RETScreen ® International CLEAN ENERGY PROJECT ANALYSIS : Ground source heat pump project analysis. 2005.

[24] Reavis C, Zuckerman E. Resolute Marine Energy : Power in Waves. 2013.

[25] Bailey H, Ortiz JP, Robertson B, Buckham BJ, Nicoll RS. A METHODOLOGY FOR WAVE-TO-WIRE WEC SIMULATIONS. Proc. 2nd Mar. Energy Technol. Symp., 2014, p. 1–15.

[26] Nyboer J, Groves S, Centre A. A review of Existing Cogeneration Facilities In Canada. 2012.

[27] Mathworks. Simulink - Simulation and model-based design 2014. http://www.mathworks.com/products/simulink/.

[28] Canmet Energy Technology Centre. RETScreen Software - Online User Manual - Combined Heat & Power Project Model. Natural Resources Canada; 2005.

[29] Urecon. Urecon Pre-Insulated Standard Wall, ASTM A53 Grade B Steel Core Pipe 2015. http://www.urecon.com/documents/documents_steel.html.

[30] Eidgenossenschaft S, Nussbaumer T, Thalmann S, Nussbaumer T, Thalmann S. Status Report on District Heating Systems in IEA Countries. 2014.

[31] Hunter R, Elliot G. Wind-Diesel Systems - A guide to the technology and its implementation. New York: Cambridge University Press; 1994.

[32] Canmet Energy Technology Centre. RETScreen Software Online User Manual ®: Biomass Heating. 2005.

Appendix D: Supplementary materials

S.1 Estimation of heating and electrical load distributions

S.1.1 Heating

Heating load distributions for Hot Springs Cove (*i.e.* electrical, propane, GSHP, building cluster heating load distributions) are estimated using a three-step approach, as follows:

1) Generate normalized hourly space and water heating load distributions using the method described in Ref. [1].

   Distributions are normalized such that the area under the curve is equal to 1, respectively. The normalized hourly space heating load distribution is calculated using an annual heating degree day distribution and an average daily space heating schedule. The heating degree day distribution is estimated based on hourly recorded outdoor temperatures for Hot Springs Cove for the reference year [2]. The average daily space heating schedule is acquired from Ref. [3]. Building heating systems are assumed to be operational year round in the calculation. The normalized hourly water heating load distribution is calculated using a constant annual water heating distribution and an average daily water heating schedule. A constant annual water heating distribution is used as total daily water heating loads are assumed to be equal for all days of the year. The average daily water heating schedule is acquired from Ref. [4].

2) Scale normalized hourly space and water heating load distributions by setting the area under the curves equal to the total annual space and water heating load, respectively.

   Total annual space and water heating loads for electrical, propane, and GSHP heating technologies, and individual building clusters are calculated by applying the total annual water heating to space heating load ratio to the total annual heating loads, shown in Table 1 of the manuscript. The total annual water heating to space heating load ratio is equivalent to 1.3:3 in Hot Springs Cove [5]. For example, based on a total annual heating load of 496 MWh for electrical heaters (see Table 1 of the manuscript), the total annual electrical water and space heating loads are 150 MWh and 346 MWh, respectively.

3) Combine hourly space and water heating load distributions into a unique hourly heating load distribution.

4) Convert hourly heating load distribution to 30 second resolution by assuming constant load for all inter-hourly time steps.

S.1.2 Electrical (non-heating)

Non-heating electrical load distributions for Hot Springs Cove are estimated using a two-step approach, as follows:

1) Subtract hourly electrical heating load distribution, calculated in Supplementary Section S.1.1, from the hourly reference electrical generation distribution.

   The hourly reference electrical generation distribution is based on hourly recorded diesel generator plant loads from two separate datasets: a reference year

(2011) dataset [6] and a dataset for the year 2014 [7]. The 2014 dataset is used to fill in missing data gaps in the reference year dataset. As the 2014 dataset is larger on average than the reference year dataset, the 2014 data is multiplied by the mean dataset ratio which is expressed as

$$\text{Mean dataset ratio} = \frac{\text{Mean of 2011 dataset}}{\text{Mean of 2014 dataset}} \approx 0.75\,.$$

2) Convert hourly electrical load distribution to 30 second resolution by assuming constant load for all inter-hourly time steps.

S.2 Estimation of annual available wave energy distribution

Available wave energy (E_{wave}) is defined as electricity that is generated by the WEC plant. The annual E_{wave} distribution for a single WEC at the Hot Springs Cove site is estimated by conducting a time series numerical simulation of the RME WEC model, using wave resource data as an input. Time series wave resource data for Hot Springs Cove for the reference year is estimated using the simulating waves near shore (SWAN) model [8]. The SWAN model hindcasts wave conditions for the 10 year period from 2006 to 2015. Using this model, wave conditions at a specific site within a 410 000 km^2 area off the coast of Vancouver island can be predicted with a relatively high degree of accuracy [9]. Details surrounding the RME WEC model and the SWAN model are described in Ref. [10].

The annual E_{wave} distribution for an array comprising multiple WECs, is estimated using a stochastic model of WEC array power [11]. The stochastic model is able to predict the electrical power output for arrays comprising multiple WECs based on the electrical power output time series from a single WEC simulation.

Annual E_{wave} distributions are generated at a time resolution of 30 seconds.

S.3 Estimation of annual building cluster heating loads

Annual heating loads for individual building clusters are calculated by summing the annual heating loads of the buildings which constitute each cluster. The annual heating load of an individual building is calculated by multiplying the total annual heating load of all buildings of the same type (*e.g.* all commercial buildings), shown in Table 1 of the manuscript, by the ground floor area ratio of the building. The ground floor area ratio is defined as the ground floor area of a building of a given type divided by the total ground floor area of all buildings of the same type, as shown in Supplementary Table S. 3. Table S. 3 shows the estimated ground floor area ranges used to classify buildings by building type, the number of buildings of each type falling within each range, and the total ground floor area of all buildings of each type. The ground floor area of each building in Hot Springs Cove is estimated from a satellite image of the community.

Table S. 3: Building ground floor area (GFA) ranges used to classify buildings by building type. FO and LO refer to full occupancy and limited occupancy, respectively.

Building type	[a] Building GFA range (m^2)	[a] Number of buildings	[b] Total GFA (m^2)
Residential - LO	< 150	23	2755
Residential - FO	150 – 200	14	2328
Commercial	200 – 1000	5	1689
School	> 1000	1	1323

[a] Based on [5]

[b] Calculated

S.4 Sizing of diesel CHP plant

The total annual electrical requirement from the powerhouse in the DH-wave energy scenario is approximately 3.3 times smaller than in the reference and wave energy scenarios since electrical heating is not considered in the former. Thus, a smaller diesel plant is needed in the DH-wave energy scenario. The diesel CHP plant in the DH-wave energy scenario is sized based on data obtained from the hourly reference electrical generation duration curve. The hourly reference electrical generation duration curve is constructed by arranging data from the hourly reference electrical generation distribution (see Supplementary Section S.1.2) in descending order of magnitude, rather than chronologically. The sizing approach is described as follows:

1) Using the hourly reference electrical generation duration curve and the installed capacities of the three diesel plant generators in the reference and wave energy scenarios, determine the following parameters:
    a) The ratio of the large diesel generator installed capacity to the peak electrical generation. The peak electrical generation in the hourly reference electrical generation duration curve is approximately 166 kW.
    b) The number of hours the diesel plant operates at a power level below that of the medium diesel generator installed capacity.
    c) The number of hours the diesel plant operates at a power level below that of the small diesel generator installed capacity.

2) Construct the hourly electrical generation duration curve for the DH-wave energy scenario and from it determine the three CHP generator unit installed capacities that correspond to the parameters identified in Step 1. The peak electrical generation in the hourly electrical generation duration curve for the DH-wave energy scenario is approximately 113 kW.

S.5 Calculation of fossil fuel consumption and CO_2 emissions

Fuel consumption from the diesel generator plant (f_G) at each time step is expressed as

$$f_G = \frac{G_{elec}}{\eta_G} \tag{1}$$

where η_G represents the generator electrical efficiency, which varies as a function of the generator part load (δ_{pl}), as shown in Figure S.5. The generator efficiency curve, depicted in Figure S.5, is obtained from Ref. [12].

If the diesel generator plant is in 'spinning' mode, fuel consumption is calculated as

$$f_G = \frac{G_{elec}}{\eta_{G,\max}}\left(r_{spin}\right) \tag{2}$$

where $\eta_{G,\max}$ and r_{spin} represent the generator electrical efficiency at full load and the spinning fuel ratio, respectively. The spinning fuel ratio is given by the following expression:

$$r_{spin} = \frac{f_{G,spin}}{f_{G,\mathrm{FL}}} \tag{3}$$

where $f_{G,spin}$ and $f_{G,\mathrm{FL}}$ represent the fuel consumption when the generator is 'spinning' and when it is at full load, respectively. Values for $\eta_{G,\max}$ and r_{spin} are shown in Table S.5.

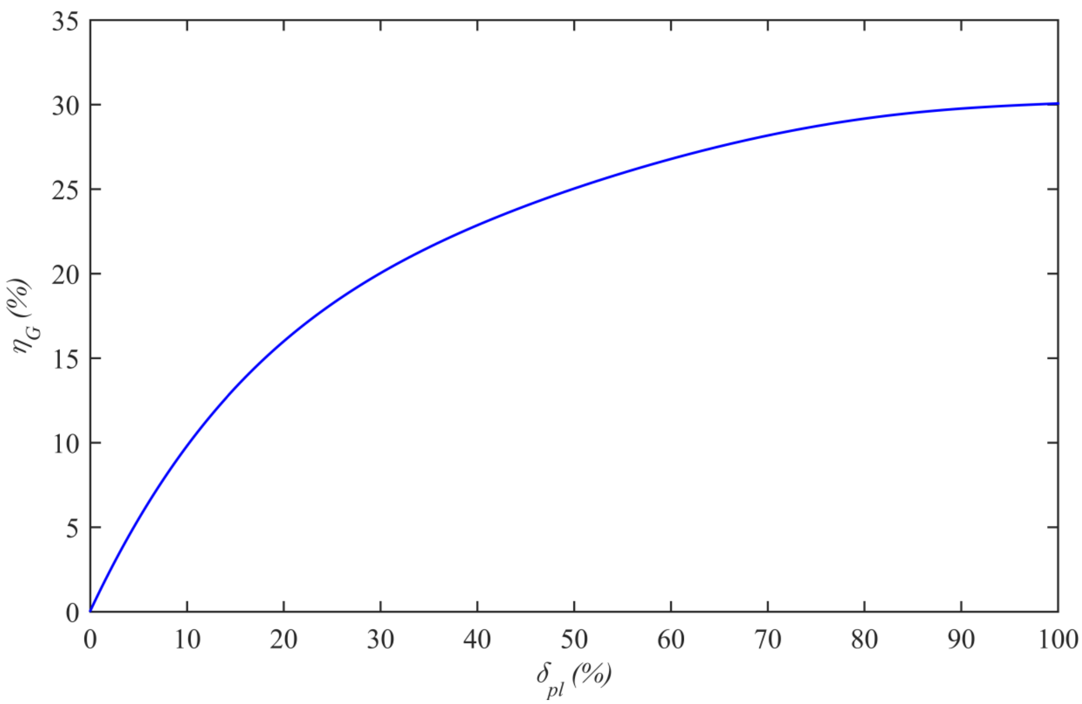

Figure S.5: Electrical efficiency curve for generation units in the diesel generator plant (reference and wave energy scenarios) and the CHP plant (DH-wave energy scenario) [12].

Fuel consumption from the building-based propane heaters ($f_{propane}$) at each time step in the reference and wave energy scenarios is expressed as

$$f_{propane} = \frac{Q_{propane}}{\eta_{propane}} \tag{4}$$

where $Q_{propane}$ and $\eta_{propane}$ represent heat generation from the propane heaters and the propane heater thermal efficiency, respectively.

Fuel consumption from the diesel boiler plant (f_{Bd}) at each time step in the DH-wave energy scenario is expressed as

$$f_{Bd} = \frac{Q_{Bd}}{\eta_{Bd}} \quad (5)$$

where Q_{Bd} and η_{Bd} represent heat generation from the diesel boiler plant and the diesel boiler plant thermal efficiency (see Table A. 1 of the Appendix), respectively.

CO_2 emissions for all scenarios are calculated by multiplying the fuel consumption of fuel consuming equipment, in units of kWh, by their respective CO_2 emission factors, shown in Table S.5.

Table S.5: Parameters used for calculating fossil fuel consumption and CO_2 emissions.

Parameter name	Symbol	Value
Minimum diesel generator part load	$\delta_{pl,\min}$	[a] 25%
Diesel generator electrical efficiency at full load	$\eta_{G,\max}$	[b] 30%
Diesel generator spinning fuel ratio	r_{spin}	[c] 25%
Diesel CO_2 emission factor	e_{diesel}	[d] 0.25kgCO_2/kWh
Propane CO_2 emission factor	$e_{propane}$	[d] 0.214kgCO_2/kWh

[a] Based on [13]
[b] Based on [12]
[c] Based on [14]
[d] Based on [15]

S.6 Sizing of DH grid pipes

A simplified method is used to size the pipes in the DH grid model. The method, which is described in Ref. [16], is summarized as follows:

1) Calculate the peak heating load for all building clusters, respectively (see Table A. 1 of the Appendix);
2) For each cluster, calculate the mass flow rate, $\dot{m}$, required for meeting the peak heating load using the following expression:

$$\dot{m} = \frac{Q_{peak}}{c_p \Delta T_{HEX}} \tag{6}$$

where Q_{peak}, c_p, and ΔT_{HEX} represent the peak heating load, specific heat capacity, and the temperature differential across the district heating side of the cluster heat exchanger, shown in Table 3 of the manuscript, respectively.

3) For each pipe connecting to a cluster, determine the smallest internal diameter that satisfies the condition that head loss due to friction cannot exceed 20 mm H_2O per meter of pipe. Head losses in the pipes are calculated using the Darcy – Weisbach equation [17].
4) Working upstream towards the powerhouse, repeat step 3 for all pipes entering a pipe junction. The mass flow rate entering a pipe junction is assumed to be equal to the sum of the mass flow rates leaving the pipe junction.

All DH pipes are oversized by a factor of 20% to allow for future expansion of the system.

References - Supplementary Materials

[1] Duquette J, Wild P, Rowe A. The potential benefits of widespread combined heat and power based district energy networks in the province of Ontario. Energy 2014;67:41–51. doi:10.1016/j.energy.2013.12.038.

[2] Environment Canada. Weather office - Historical weather - Estevan Point 2011. http://climate.weather.gc.ca/.

[3] Bouchelle MP, Parker DS, Anello MT, Richardson KM. Factors Influencing Space Heat and Heat Pump Efficiency from a Large-Scale Residential Monitoring Study. Proc. 2000 Summer Study Energy Effic. Build. Am. Counc. an Energy-Efficient Econ., vol. Washington, 2000.

[4] Masiello JA, Parker DS. Factors Influencing Water Heating Energy Use and Peak Demand in a Large Scale Residential Monitoring Study. 2001.

[5] Van Dijk G, Crompton J. COMMUNITY ELECTRICITY PLAN FOR REFUGE COVE. 2013.

[6] Pulse Energy. Hot Springs Cove hourly generation dataset - 2011. n.d.

[7] Pulse Energy. Hot Springs Cove hourly generation dataset - 2014. n.d.

[8] Robertson BRD, Hiles CE, Buckham BJ. Characterizing the near shore wave energy resource on the west coast of Vancouver Island , Canada. Renew Energy 2014;71:665–78. doi:10.1016/j.renene.2014.06.006.

[9] Robertson B, Hiles C, Luzko E, Buckham B. Quantifying the Wave Energy Resource and Farm Siting Opportunities for Western Canada. Int. Conf. Ocean energy, 2014.

[10] Bailey H, Ortiz JP, Robertson B, Buckham BJ, Nicoll RS. A METHODOLOGY FOR WAVE-TO-WIRE WEC SIMULATIONS. Proc. 2nd Mar. Energy Technol.

Symp., 2014, p. 1–15.

[11] Bailey H, Robertson B, Ortiz J, Buckham B. Stochastic Methods to Predict WEC Array Power for Grid Integration. Eur. wave tidal energy Conf., 2015.

[12] HOMER Energy. The HOMER Microgrid Software 2014. http://www.homerenergy.com/.

[13] Ibrahim H, Dimitrova M, Dutil Y, Rousse D, Ilinca A. Wind-Diesel hybrid system : energy storage system selection method. 12th Int. Conf. Energy Storage, 2012, p. 1–10.

[14] Hunter R, Elliot G. Wind-Diesel Systems - A guide to the technology and its implementation. New York: Cambridge University Press; 1994.

[15] UK Department for environment food & rural affairs. Guidelines for company reporting on greenhouse gas emissions - fuel conversion factors. 2005.

[16] Canmet Energy Technology Centre. RETScreen Software Online User Manual ®: Biomass Heating. 2005.

[17] Cengel YA, Cimbala JM. Fluid Mechanics - Fundamentals and Applications. vol. 1. New York: McGraw Hill; 2006.